INFORMATION TO USERS

This manuscript has been reproduced from the microfilm master. UMI films the text directly from the original or copy submitted. Thus, some thesis and dissertation copies are in typewriter face, while others may be from any type of computer printer.

The quality of this reproduction is dependent upon the quality of the copy submitted. Broken or indistinct print, colored or poor quality illustrations and photographs, print bleedthrough, substandard margins, and improper alignment can adversely affect reproduction.

In the unlikely event that the author did not send UMI a complete manuscript and there are missing pages, these will be noted. Also, if unauthorized copyright material had to be removed, a note will indicate the deletion.

Oversize materials (e.g., maps, drawings, charts) are reproduced by sectioning the original, beginning at the upper left-hand corner and continuing from left to right in equal sections with small overlaps.

Photographs included in the original manuscript have been reproduced xerographically in this copy. Higher quality 6" x 9" black and white photographic prints are available for any photographs or illustrations appearing in this copy for an additional charge. Contact UMI directly to order.

Bell & Howell Information and Learning
300 North Zeeb Road, Ann Arbor, MI 48106-1346 USA
800-521-0600

UNIVERSITY OF OKLAHOMA

GRADUATE COLLEGE

ANISOTROPIC EFFECTS UPON AMPLITUDE-VS-OFFSET RESPONSE IN REALISTIC EARTH MODELS

A Dissertation

SUBMITTED TO THE GRADUATE FACULTY

in partial fulfillment of the requirements for the

degree of

Doctor of Philosophy

By

HE CHEN
Norman, Oklahoma
2000

ANISOTROPIC EFFECTS UPON AMPLITUDE-VS-OFFSET RESPONSE
IN REALISTIC EARTH MODELS

A Dissertation APPROVED FOR THE
SCHOOL OF GEOLOGY AND GEOPHYSICS

BY

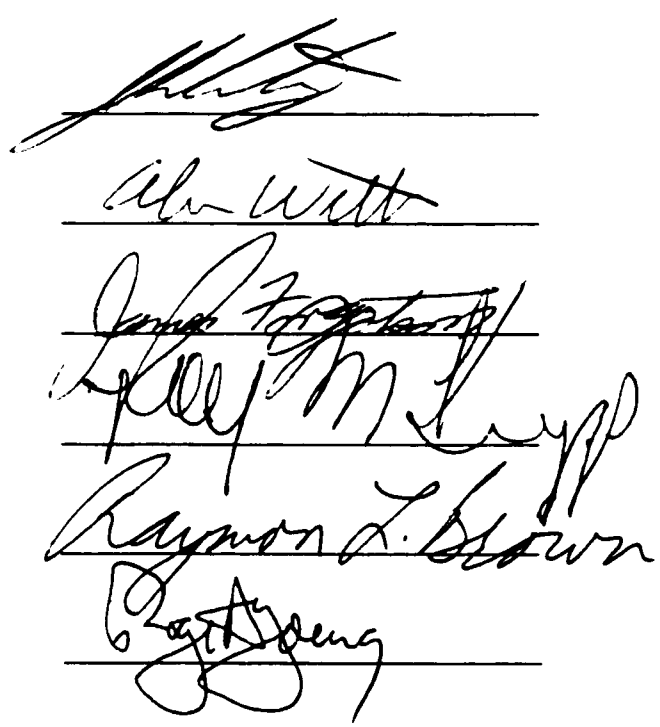

Dedicate to my father Jingda Chen

Acknowledgements

I would like to take this opportunity to express my sincere thanks and appreciation to following people for their support throughout this entire study.

First of all, I would like to thank Dr. John Castagna, my research advisor and graduate committee chairman, for his encouragement and guidance for this research. His knowledge and intelligent thoughts enlightened me in the little known world of anisotropy. His professional skills and spirit inspired me throughout the entire study. I am also grateful to him for providing me an excellent working environment in which I was able to focus totally on the research. Dr. Castagna is not only my academic advisor, but also a mentor for my personal development. In the past fours years, he taught me very important skills on personal communication, teamwork, peer cooperation and self-planning from which I would benefit for the rest of my entire life.

I would like to thank Dr. Ray Brown of Oklahoma Geological Survey, a member of my graduate committee, for his time and patience in helping me to understand some key mathematical and physical concepts. Some ideas for my programs were originated from our numerous long discussions.

I would also like to thank Dr. Bill Lamb of Institute of Exploration and Development Geoscience for many insightful comments and direction toward a better solution. His sound knowledge and deep understanding of seismic geophysics and strong programming skills is always a valuable resource of mine.

Thanks Dr. Antonio Ramos of Institute of Exploration and Development Geoscience for many great comments and helping me understand some subtle aspect of Anisotropy.

Thanks to Dr. Roger Young of Department of Geology and Geophysics, a member of my graduate committee, for your excellent lectures on exploration seismology that I enjoyed most during my study in the university and that helped me build a strong basis for this research.

I also want to thank the other members of my graduate committee - Dr. Allen Witten, Dr. James Forgotson of Department of Geology and Geophysics and Dr. Roy Knapp of Department of Petroleum Engineering –who all played an important role in defining this thesis.

I would like to thank Institute of Exploration and Development Geosciences for their long time financial support to this research. I also would like to thank the Department of Energy for their financial support to this thesis work under project DE-AC26-99BC15212.

I gratefully acknowledge the assistance provided by staff in the School of Geology and Geophysics, Ms Donna Montogomery. I also deeply appreciate the friendly and enjoyable environment made possible by everyone in the department.

Finally I would like to thank my wife, Lijuan, for enduring the hard time during the writing of this paper and her help in editing of the paper. Her love, patience and support is the source of force that drove me forward through the entire work.

TABLE OF CONTENTS

List of Tables

List of Figures

Abstract

This thesis investigates some of the effects of anisotropy upon seismic exploration for oil and gas. In particular, the effects of anisotropy upon amplitude versus offset (AVO) and seismic interpretation are examined.

The AVO studies were accomplished by developing two reflection coefficient programs. The first program computes the reflection across a boundary between two transversely isotropic media with vertical axes of symmetry (VTI). Although the equations for this program have been published, this thesis corrects important typographical errors in the published paper. The second program computes the reflection across the boundary of two arbitrary anisotropic media. The computer implementation published here was developed specifically for this thesis work.

The VTI reflection coefficient program is used to evaluate several approximate reflection coefficient formulas. A method of using three parameter cross-plotting is developed that can be used to consider the role of anisotropy in AVO studies and improve the accuracy of the interpretation.

The derivation and computation of the reflection coefficient for general anisotropic media is described along with software written to implement the computation. This program is then used to compare the reflection response over a fractured reservoir model with a single set of fractures with the response over a reservoir with two fracture sets. The results clearly indicate that shear waves show the greatest potential for exploration of fractured reservoirs using AVO methods.

A case history AVO study is applied to data collected in the Gulf of Mexico to identify the important parameters for a bright reflector using published empirical relationships between parameters. Inversions for V_p/V_s are found to be dependent on assured anisotropic parameters.

Finally, ray tracing through simple anisotropic models is used to evaluate the effects of anisotropy upon seismic processing. The results indicate that by ignoring anisotropy, a number of processing artifacts can be produced that will mislead the interpreter.

Chapter 1

Introduction

Reflection and transmission of plane waves at a plane boundary between two media are one of the most fundamental problems in wave propagation. One significant application of reflection-coefficient studies is analysis of amplitude variations with offset (AVO).

In the past 15 years, AVO analysis, utilizing an isotropic earth model, has been widely used as a hydrocarbon indicator in the oil industry. However, subsurface formations are invariably anisotropic. It is intuitively obvious that the angular dependence of elastic wave velocities should modify the reflection and transmission coefficients (Wright, 1984, 1987; Thomsen, 1993). By ignoring the existence of anisotropy, the conventional isotropic AVO techniques may be erroneous.

Seismic anisotropy is one of the major problems facing the new frontiers of exploration for oil and gas. This dissertation addresses important problems where seismic anisotropy needs to be taken into account.

1.1 Typical problem from the real world

Two typical anisotropy-related reservoir reflections can be easily recognized as described below:

1) Most reservoirs are surrounded by shales, which are usually highly anisotropic. During some shallow, surface-to-borehole field tests, it was found that the

near-surface shales behave approximately like transversely isotropic solids with a vertical axis of symmetry (VTI) (Robertson et, al., 1983).

2) Some reservoirs are naturally fractured. Laboratory measurements have shown that parallel fractures and aligned cracks can cause significant azimuthally velocity anisotropy (Nur, 1971; Hudson, 1981). In simple situations, this kind of model can be treated as a transversely isotropic medium with a horizontal axis of rotational symmetry (HTI).

Under each condition above, the anomaly 'signature' of hydrocarbons on AVO can be seriously distorted by the effect of the anisotropy.

1.2 Solution Approach

Theoretical and laboratory studies (Thomsen, 1986; Vernik, 1992; Tsvankin, 1996) have shown that other anisotropic effects, such as non-hyperbolic moveout, higher attenuation, also exist in the data processing and interpretation. When seismic waves pass through an anisotropic rock, the anisotropy may influence or change the characteristics of the waves. For example, the traveltime may increase, the AVO responses may change, the recorded seismic traces may have less high frequency content, and the travel time and AVO trends may display azimuthal variations.

The underlying hypothesis of this dissertation is that anisotropy exists in the real world, and it is significant, observable, and measurable. Through an understanding of anisotropic effects on seismic wave propagation and data processing, interpretation and analysis can be improved.

Conventional AVO analysis is based on approximate isotropic reflection coefficients. Under certain kinds of anisotropic conditions, it has been modified using Thomsen's anisotropic parameters (Banik, 1987; Thomsen, 1993; Ruger, 1997; and Wei, 1993). These reflection approximations simplify the dependence of the reflection response upon the parameters. However, they may introduce larger errors beyond a certain range of incident angles. The exact solution for reflection coefficients at interfaces of anisotropic media is very complicated, but it is useful, and sometimes necessary. Other anisotropic effects, such as non-hyperbolic moveout, and higher attenuation, also exist in the data processing and interpretation.

1.3 Major Accomplishments

The objective of this research is to theoretically study the anisotropic effects on amplitude-versus-offset (AVO).

My approaches can be summed up as follows:

1) Study and rederive the exact reflection coefficient for VTI case following Daley and Hron's (1979) derivation. Correct printing errors in the publication, program it and verify the output using energy flux method.

2) Compare the exact reflection coefficients with some existing approximate coefficients. It is important to realize which approximation is more accurate at different boundary conditions.

3) Study AVO crossplotting using exact P-P reflection coefficients under VTI condition. An improved approximation is given in this dissertation that better accounts for the TI elastic properties across the reflecting boundary.

4) Program ray-tracing through VTI models, and study the anisotropic effects on the stacked sections. The result shows false AVO anomalies on far-trace stacked sections which can be misinterpreted as persuasive hydrocarbon indicators.

5) Study and derive the exact reflection coefficient for general anisotropic case using Rokhlin's (1986) method, and make a numerical program to compute the coefficients.

6) Application of the anisotropic AVO study on synthetic fractured models and real data.

With this research work, I wish to synthesize fundamental theoretical tools to provide a basis for dealing with the anisotropic effects on AVO.

1.4 Thesis Outlines

This dissertation is organized as follows:

Chapter 2 provides an overview of the physical principles that leads to the boundary conditions under the supposition of a rigid contact between the media. As a first step to study the anisotropic AVO, this chapter also gives a review on the reflection and transmission coefficients and the AVO analysis in isotropic media. Finally, it introduces the notations of anisotropic medium which is used throughout the thesis.

The theoretical background of AVO analysis is the study of the change of the reflection coefficients as a function of angle of incidence upon the reflector. Chapter 3 rederives the exact reflection and transmission coefficients for transverse isotropic media with vertical symmetry axes (VTI), and corrects some mistakes that are in the published literature on this topic. Then, some popular reflection coefficient

approximations are discussed and comparison studies are made between the exact and approximate reflection coefficients.

AVO interpretation can be facilitated by crossplotting AVO intercept (A), gradient (B) and curvature (C) terms. However, this popular technique is challenged by the existence of anisotropy. In chapter 4, the effects of transverse anisotropy on angle dependent reflectivity is discussed. Recognition of anisotropic behavior on AVO crossplots can help avoid AVO interpretation errors. Empirical corrections that result in more accurate crossplot interpretation are also introduced for specific circumstances.

Chapter 5 discusses the anisotropic effects on full and partial stacks. Non-hyperbolic moveout resulting from localized variations in anisotropy can create many misleading artifacts such as apparent faults, folds, channels, flat spots, dim spots, bright spots, and AVO anomalies on fully and partially stacked seismic sections.

In current exploration practice, it sometime requires an AVO study over a general anisotropic model, e.g., a model with multiple aligned sets of fracture. In Chapter 6, a numerical solution of the reflection-transmission problem for general anisotropic media is presented. For programming purpose, detailed algorithm and basic equations are all given for each steps. Some numerical problems that can occur during computation are also discussed.

Finally, one of the conclusions in this thesis is that the exact reflection coefficients and the corresponding AVO analysis methods are very significant for the modern seismic exploration. As application of these useful tools, Chapter 7 presents a synthetic azimuthal AVO study over fractured models. Chapter 8 shows a case study on

extraction of some petrophysics parameters of a reservoir by using the exact AVO trend.

Chapter 2

Principles and Notations

In this chapter, I review the AVO principles in isotropic media and the anisotropic notations and terminology which will be used through out the dissertation.

Reflection and transmission of plane waves at a plane boundary between two elastic isotropic media is one of the most fundamental problems in wave propagation. An exact solution for this problem was given by Zoeppritz (1911). Then, because the solution is so complex algebraically, many later attempts were made to find approximate expressions that give a more intuitive picture of the reflection coefficient (e.g., Shuey, 1985).

Since Ostrander (1982,1984) demonstrated that the variation in P-wave reflection coefficient versus angle of incidence is controlled by the contrast in Poisson's ratio across the reflection plane, the technique of AVO analysis has been used extensively in the seismic exploration for hydrocarbon-bearing reservoirs (Castagna and Buckus, 1993, Fatti et al., 1994, Rutherford and Williams, 1989). However, most of the previous AVO analysis work implicitly assumes that rocks are isotropic, which is often invalid. Anisotropic effects on AVO have been considered by many authors (e.g., Banik, 1984, Thomsen, 1986, Ruger, 1995 Tsvankin, 1996).

2.1 Basic characteristics and notations of isotropic media

In a linear elastic system, the stress tensor τ_{ij}, strain tensor ε_{kl} and elastic stiffness tensor c_{ijkl} Satisfy the generalized Hooke's law:

$$\tau_{ij} = c_{ijkl}\varepsilon_{kl} \qquad i,j,k,l = 1,\ 2,\ 3 \qquad \text{.....(2.1)}$$

Because stress and strain are symmetric and each has only six independent components, equation (2.1) can be written as:

$$\tau_I = c_{IJ}\varepsilon_J \qquad I,J = 1,\ 2,\ \ldots,\ 6 \qquad \text{.....(2.2)}$$

where ij or kl is mapped into I or J according to the following rule (Auld, 1973):

ij or kl:	11	22	33	23 = 32	31 = 13	12 = 21	
I or J:	1	2	3	4	5	6	.....(2.3)

Here, C_{IJ} is a 6X6 symmetric matrix which can have at most 21 independent elements. This notation for the elastic stiffness is used in both the engineering and the geophysical literature.

Two different types of body waves propagate in isotropic media. They are P (compressional) waves and S (shear) waves. P-waves cause the medium to alternatively undergo compression and rarefaction, and S-waves generate a transverse particle motion.

One of the important characteristics of an isotropic medium is that its stiffness matrix C_{ij} can be written in the following simple form by using the notation of Love (1934):

$$C = \begin{bmatrix} C_{33} & (C_{33}-C_{44}) & (C_{33}-C_{44}) & & & \\ & C_{33} & (C_{33}-C_{44}) & & & \\ & & C_{33} & & & \\ & & & C_{44} & & \\ & & & & C_{44} & \\ & & & & & C_{44} \end{bmatrix} \quad \text{.....(2.4)}$$

The above 6x6 matrix is symmetric. Only the non-zero components in the upper triangle are shown. Notice that it has only two independent parameters:

$$C_{33} = \lambda + 2\mu \quad \text{.....(2.5)}$$

and

$$C_{44} = \mu \quad \text{.....(2.6)}$$

where λ and μ are Lame parameters

Poisson's ratio is another important elastic constant in AVO analysis for isotropic media. Poisson's ratio σ is related to Vp/Vs by:

$$\sigma = \frac{\frac{1}{2}\left(\frac{V_P}{V_S}\right)^2 - 1}{\left(\frac{V_P}{V_S}\right)^2 - 1} \quad \text{.....(2.7)}$$

2.2 AVO analysis on isotropic media

Conventional AVO analysis is based on approximate isotropic reflection coefficients of Shuey's (1985):

$$R_{pp}^{iso}(\theta) = R_0 + \left[A_0 + \frac{\Delta\sigma}{(1-\sigma)^2} \right] \sin^2\theta + \frac{1}{2}\frac{\Delta\alpha}{\alpha_0}\tan^2\theta \sin^2\theta \qquad \text{.....(2.8)}$$

in which

$$R_0 = \frac{1}{2}\left(\frac{\Delta\alpha}{\alpha_0} + \frac{\Delta\rho}{\rho} \right) \qquad \text{.....(2.9)}$$

$$A_0 = -2\left(1 - \frac{\Delta\sigma}{1-\sigma}\right) R_0 - \frac{1}{2}\frac{1-3\sigma}{1-\sigma}\frac{\Delta\alpha}{\alpha_0} \qquad \text{.....(2.10)}$$

where θ is the incident angle, α_0 is the average *P*-wave velocity across the interface, and σ is the average Poisson's ratio. The parameter differences across the boundary are: $\Delta\alpha=\alpha_2-\alpha_1$, $\Delta\rho=\rho_2-\rho_1$, and $\Delta\sigma=\sigma_2-\sigma_1$.

This equation can be written in the form:

$$R(\theta) = A + B\sin^2\theta + C\sin^2\theta\tan^2\theta \qquad \text{.....(2.11)}$$

As discussed in more detail in Castagna and Backus (1993), the main advantage of this representation is that each term is responsible for a different angular range. The coefficient A is the normal-incidence reflection coefficient, while B describes the initial slope of the reflection-coefficient curve. The "curvature term" C becomes important when the incidence angle is larger (>20°).

Rutherford and Williams (1989) suggested a classification of 3 types of gas-sand reflections based on their AVO characteristics, which was complimented by a 4th type of sand discussed by Castagna et at (1997). Castagna et al (1998) also built up a

framework for standard isotropic AVO interpretation utilizing crossplots of Shuey's coefficients in equation (2.11).

2.3 Existance of anisotropy

Over the past 20 years, numerous laboratory experiments indicate that many rocks are anisotropic (e.g., Thomsen, 1986, Levin, 1979, etc.). For example, shales are ususlly anisotropic. Here, anisotropy is defined as the variation of seismic velocity depending on the direction in which it is measured (Sheriff, 1991). Further studies also show that, when a layered sequence of different media is probed with an elastic wave of wavelength much longer than the typical layer thickness, the wave propagates as though it were in a homogeneous, but anisotropic medium (Backus, 1962).

Phase velocity and group velocity are important concepts for anisotropic media. The phase velocity is the velocity perpendicular to a surface of constant phase in an anisotropic medium. The group velocity is the velocity with which the energy in a wavetrain travels (Sheriff, 1991). The phase velocity (V_p) and group velocity (V_g) are related by:

$$V_p = V_g \cdot \mathrm{n} \qquad \text{.....(2.12)}$$

where n is a unit vector along the wave normal.

The relationship between ray angle and phase angle is illustrated in Figure 2.1. The wave vector points in the direction of maximum rate of increase in phase. At any location the wave vector is perpendicular to the wave front. The ray vector, however, points from the source to the wave front, which is the direction of energy propagation.

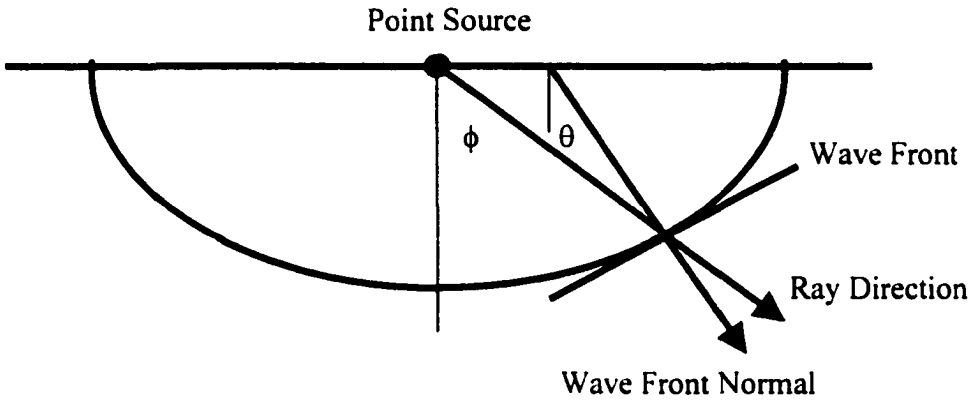

Figure 2.1 The relationship between phase angle and group angle

In an anisotropic medium, the wave front is not spherical, and the phase angle θ is usually different from the ray angle ϕ except in the symmetry planes.

The formula to calculate the ray angle ϕ, given by Berryman (1979), is:

$$\tan\phi(\theta) = \frac{\tan\theta + \frac{1}{v}\frac{dv}{d\theta}}{1 - \frac{\tan\theta}{v}\frac{dv}{d\theta}} \qquad \text{.....(2.13)}$$

Regarding anisotropy associated with lithology, laboratory measurements suggests that many shales have significant intrinsic anisotropy, which is caused mainly from a laminated/lenticular texture of clay aggregates (Vernik and Liu, 1997). Vernik (1992) also noticed that kerogen has a dramatic effect on anisotropy even in

microcrack-free shales. The experimental data of Hornby (1995) indicates that some shales may exhibit a much stronger SV-wave anisotropy than P-wave anisotropy.

During shallow, surface-to-borehole field tests, it has been found that the near-surface shales behave approximately like transversely isotropic solids with a vertical axis of symmetry (Robertson et, al., 1983). Thomsen (1986) further suggested that transverse isotropy, the simplest anisotropic case, can be applied broadly in geophysical exploration circumstances. In this case, the sedimentary rock has one distinct symmetry axis (usually perpendicular to bedding), while the other two directions are equivalent to each other forming a plane of isotropy.

2.4 Characteristics of transverse anisotropy and Thomsen's parameters

Using the notation of Love (1934), the stiffness tensor C in transversely isotropic media can be expressed as follows:

$$C = \begin{bmatrix} C_{11} & (C_{11}-2C_{66}) & C_{13} & & & \\ & C_{11} & C_{13} & & & \\ & & C_{33} & & & \\ & & & C_{44} & & \\ & & & & C_{66} & \\ & & & & & C_{66} \end{bmatrix} \qquad \text{.....(2.14)}$$

The matrix is symmetric, and has five independent components among the twelve nonzero components; ie., C_{11}, C_{13} ,C_{33} ,C_{44}, and C_{66}.

For weak anisotropy, Thomsen's parameters (1986), as functions of the five elastic components, are:

$$V_{P0} = \sqrt{\frac{C_{33}}{\rho}} \quad \text{.....(2.15)}$$

$$V_{S0} = \sqrt{\frac{C_{44}}{\rho}} \quad \text{.....(2.16)}$$

$$\varepsilon = \frac{C_{11} - C_{33}}{2C_{33}} \quad \text{.....(2.17)}$$

$$\gamma = \frac{C_{66} - C_{44}}{2C_{44}} \quad \text{.....(2.18)}$$

and

$$\delta = \frac{(C_{13} + C_{44})^2 - (C_{33} - C_{44})^2}{2C_{33}(C_{33} - C_{44})} \quad \text{.....(2.19)}$$

V_{P0} is the vertical P-wave velocity. V_{S0} is the vertical SH-wave velocity. The physical meaning of ε and γ in weak anisotropic media are P-wave and SH-wave anisotropy, respectively. Banik (1987) explained the physical meaning of δ by introducing SV-wave anisotropy defined as below:

$$\varepsilon_v = \frac{\beta_{45} - \beta}{\beta} \quad \text{.....(2.20)}$$

where, β is the vertical SV-wave phase velocity, and β_{45} is the SV-wave phase velocity at an angle of 45 degrees to the axis of symmetry. Then, δ can be expressed as:

$$\delta \equiv \varepsilon - \varepsilon_v \frac{4\beta^2}{\alpha^2} \quad \text{.....(2.21)}$$

As Banik (1987) noticed, this equation indicates that δ is the relative competitiveness between P-wave ε and the SV-wave anisotropy ε_s.

Using Thomsen's (1986) anisotropic parameters, the phase velocities of P-, SV-, and SH-wave can be expressed as follows:

$$V_p(\theta) = \alpha_0\left(1 + \delta \sin^2\theta \cos^2\theta + \varepsilon \sin^4\theta\right) \quad \text{.....(2.22)}$$

$$V_v(\theta) = \beta_0\left(1 + \frac{\alpha_0^2}{\beta_0^2}(\varepsilon - \delta)\sin^2\theta \cos^2\theta\right) \quad \text{.....(2.23)}$$

and

$$V_{sh}(\theta) = \beta_0\left(1 + \gamma \sin^2\theta\right) \quad \text{.....(2.24)}$$

where α_0 is the vertical P-wave velocity, β_0 is the vertical S-wave velocity, Notice the anisotropic notations separate the influence of the anisotropy from the "isotropic" quantities, i.e., P- and S-wave phase velocities along the symmetry axis.

2.5 Anisotropic effect on AVO

Anisotropy affects AVO in a number of ways.

2.5.1. Reflection coefficient

A direct influence upon AVO can result from the anisotropic effects on the reflection coefficients. When the media across an interface are anisotropic, incident and reflected waves have directionally-dependent wave speeds and can no longer be thought

of as purely longitudinally or transversely polarized. In addition, the direction of the wave normal, the particle movement and the energy flux do not coincide with each other. Using continuity of stress and displacement at the anisotropic interface, a theoretical derivation of the exact solution for reflection and transmission coefficients, of VTI and general anisotropic media, will be given in following chapters.

2.5.2. Energy Radiation Patterns

According to Tsvankin (1995), AVO signatures (e.g., AVO gradient) can be significantly distorted by the redistribution of energy along the wavefront of the wave travelling down to the reflector and back up to the surface. Significant anisotropy above the target horizon may be rather typical of sand-shale sequences commonly encountered in AVO analysis.

2.5.3. Polarization vector

Tsvankin (1996) also pointed out that the deviations of the polarization vector from its "isotropic" direction may cause distortions of radiation patterns in anisotropic media. Helbig and Schoenberg (1987) showed that for "abnormal" media that have negative $C_{13}+C_{44}$, the P-wave polarization vector can even become perpendicular to the phase-velocity vector. Thus, the polarization vector can have an indirect influence on AVO analysis.

2.5.4. Normal Moveout

Velocity anisotropy may significantly enhance deviations from hyperbolic moveout (Tsvankin et. al., 1994). The nonhyperbolic moveout cannot be removed by using conventional first-order isotropic processing software. In terms of AVO analysis on near and far stacked sections, a model study has shown that this anisotropic nonhyperbolic effect may produce strong AVO anomalies for reasonable anisotropic values (Chen et. al., 2000).

Chapter 3

Exact and Approximate P-wave Reflection in VTI Media

The behavior of elastic waves in anisotropic media is much more complicated than in isotropic media. In this chapter, First, the exact reflection coefficients are derived for the simplest anisotropic model – a transversely isotropic homogeneous medium with a vertical symmetry axis. This part of the chapter corrects some typophial errors that are in the published literature on this topic. Then, some popular reflection coefficient approximations are analyzed, and the comparison studies are made between the exact and approximate reflection coefficients.

3.1 Exact reflection and transmission coefficients in VTI media

In order to understand AVO in VTI media, the exact solution for the VTI reflection and transmission coefficients, assuming an incident P-wave, are rederived using Daley and Hron's mathod and notations. The final form of the solution is verified as it is in the literature (see equation (17) of Daley and Hron (1977), Page 668). However, many typographical errors have been found in the published solutions and the corrected version is given placing '*' next to corrected equations.

3.1.1 Wave-fields in VTI media

To be consistent with Daley (1977), Figure 3.1 shows an incident quasi-P wave and its 4 reflected and transmitted quasi-P and quasi-SV waves with the same notations

from Daley. The positive polarization directions are also defined as shown in Figure 3.1. The sign convention of the positive direction is that the horizontal polarization component points in the direction of horizontal slowness (Aki and Richard, 1980). As described by Daley (1977), all relevant displacement vectors are assigned an integral value, v, between 0 – 4, with: v = 0 for the incident quasi-P wave; v = 1 for the reflected quasi-P wave; v = 2 for the transmitted quasi-P wave; v = 3 for the reflected quasi-SV wave; v = 4 for the transmitted quasi-SV wave.

For a given angular frequency ω, the particle displacement vector of the (unit amplitude) plane wave incident in the [X, Z] plane can be written as:

$$U_0 = \begin{pmatrix} l_1 \sin\theta_1 \\ -m_1 \cos\theta_1 \end{pmatrix} e^{-i\omega\left(t - \frac{\sin\theta_1}{V_{p1}}x + \frac{\cos\theta_1}{V_{p1}}z\right)} \qquad \text{.....(3.1)}$$

where l, m denote components of the polarization vector projected onto a coordinate system fixed with the ray. Positive Z is in the direction of ray propagation and positive X is such that $\mathbf{X}\times\mathbf{Y}=\mathbf{Z}$. V_p is the phase velocity of the P wave. The generated wave modes are:

$$\begin{cases} U_1 = R_{11}\begin{pmatrix} l_1 \sin\theta_1 \\ m_1 \cos\theta_1 \end{pmatrix} e^{-i\omega\left(t - \frac{\sin\theta_1}{V_{p1}}x - \frac{\cos\theta_1}{V_{p1}}z\right)} \\ U_2 = R_{12}\begin{pmatrix} l_2 \sin\theta_2 \\ -m_2 \cos\theta_2 \end{pmatrix} e^{-i\omega\left(t - \frac{\sin\theta_2}{V_{p2}}x + \frac{\cos\theta_{21}}{V_{p2}}z\right)} \\ U_3 = R_{13}\begin{pmatrix} l_3 \sin\theta_3 \\ -m_3 \cos\theta_3 \end{pmatrix} e^{-i\omega\left(t - \frac{\sin\theta_1}{V_{s1}}x - \frac{\cos\theta_1}{V_{s1}}z\right)} \\ U_4 = R_{14}\begin{pmatrix} l_4 \sin\theta_4 \\ m_4 \cos\theta_4 \end{pmatrix} e^{-i\omega\left(t - \frac{\sin\theta_4}{V_{s4}}x + \frac{\cos\theta_4}{V_{s4}}z\right)} \end{cases} \qquad \text{.....(3.2)}$$

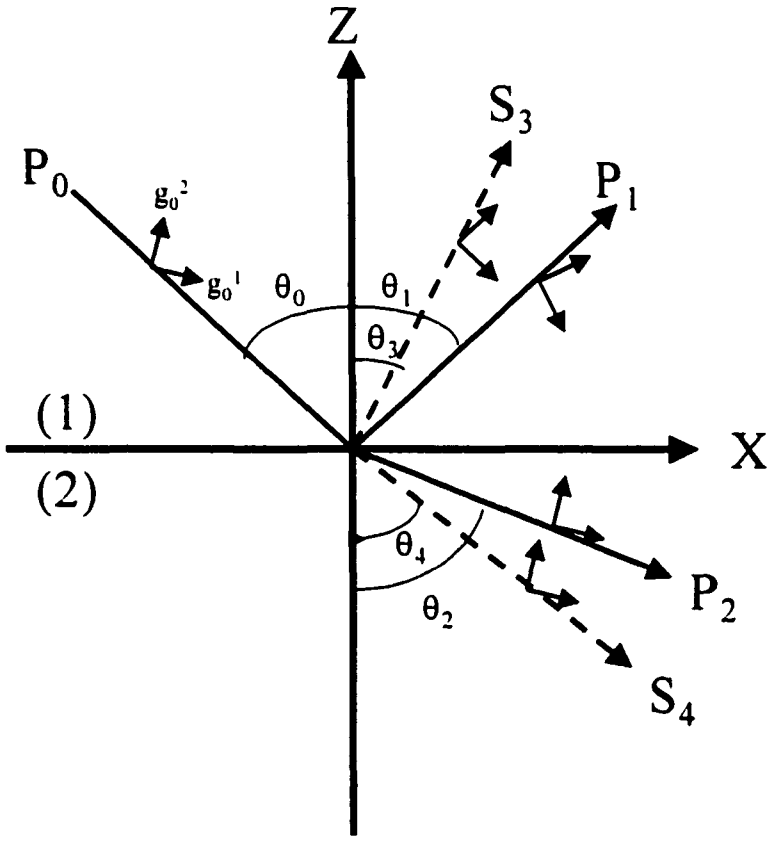

Figure 3.1 Geometry of wave –front normals and displacement vectors of incidence P-wave and all four reflected and transmitted P-waves and SV-waves at the interface of two VTI layers

Here, R_{11}, R_{12}, R_{13}, R_{14} denote the amplitudes of the scattered wave modes and V_s is the phase velocity of SV wave.

As noticed, the phase velocities V_p and V_s, and polarization vectors, l and m for each wave in the above expressions are functions of the medium and the phase angle.

3.1.2 Phase velocity and polarization in VTI medium

The equations of motion in an elastic medium in Cartesian coordinates, neglecting body forces are:

$$\rho \ddot{u}_j = \frac{\partial}{\partial x_i}\left\{c_{ijkl}\frac{\partial u_k}{\partial x_l}\right\} \qquad (i, j = 1,\ 2,\ 3) \qquad \text{.....(3.3)}$$

where, u_j is the displacement vector component; c_{ijkl} is elastic stiffness tensor; ρ is density. The double dot over the u_j represents the 2nd order time derivative of the displacement (particle acceleration).

One of the solutions of equation (3.3) can be expressed in the form:

$$u_l = U_l e^{-i\omega\left(t-\frac{n_k x_k}{V}\right)} \qquad \text{.....(3.4)}$$

where U_j is vector amplitude component of the wave, V is phase velocity, n_k is the directional cosine of the wave-front normal. Substitution (3.3) into the equations of motion (3.1) yields the Christoffel equation form as:

$$\left(\Gamma_{ik} - \delta_{ik}\right)U_k = 0 \qquad \text{.....(3.5)}$$

where Γ_{ik} is the Christoffel matrix: $\Gamma_{ik}= (c_{ijkl}/\rho)s_i\, s_l = a_{ijkl}s_i\, s_l$. It is a 3X3 matrix determined only by the direction of plane wave propagation and the elastic constants of the medium. The slowness vector component s_i at a given point and direction (specified by the normal component of $\mathbf{n}_i$) are related to the phase velocity by the relation:

$$s_i = \frac{n_i}{V} \qquad \text{.....(3.6)}$$

Since the strain energy is positive definite, Γ_{ik} is positive definite. Thus, the three eigenvalues of Γ_{ik} are all positive. Each eigenvalue corresponds to a quasi-P and the other two quasi-shear waves. Using the Voigt notation (See eq. (2.3)) to transform a_{ijkl} to A_{mn}, the Christoffel equation (3.5) can be written as a function of the horizontal slowness p_1 and vertical slowness s_3 (with $s_1^2 + s_3^2 = 1/V^2$) as:

$$\det\begin{pmatrix} s_1^2A_{11} + s_3^2A_{55} - \lambda & 0 & s_1s_3(A_{13} + A_{55}) \\ 0 & s_1^2A_{66} + s_3^2A55 - \lambda & 0 \\ s_1s_3(A_{13} + A_{55}) & 0 & s_1^2A_{55} + s_3^2A_{33} - \lambda \end{pmatrix} = 0 \qquad \text{.....(3.7)}$$

The solution of equation (3.7) yields the three eigenvalues:

$$\begin{cases} \lambda_1 = \frac{1}{2}\left\{K + \sqrt{K^2 - 4L}\right\}^* \\ \lambda_2 = \frac{1}{2}\left\{K - \sqrt{K^2 - 4L}\right\}^* \\ \lambda_3 = s_1^2A_{66} + s_3^2A_{55} \end{cases} \qquad \text{.....(3.8)}$$

where

$$K = (A_{11} + A_{55})s_1^2 + (A_{33} + A_{55})s_3^2$$

$$L = 4\left[(A_{11}s_1^2 + A_{55}s_3^2)(A_{55}s_1^2 + A_{33}s_3^2) - (A_{13} + A_{55})^2 s_1^2 s_3^2\right]$$

Substitution of (3.6) into (3.8) (with the eigenvalues equal to 1) yields the phase velocities of the quasi-P and quasi-SV waves:

$$V_P = \sqrt{\frac{1}{2}\left[A_{33} + A_{55} + (A_{11} - A_{33})Y + Q\right]} \quad \text{.....(3.9)}$$

$$V_{SV} = \sqrt{\frac{1}{2}\left[A_{33} + A_{55} + (A_{11} - A_{33})Y - Q\right]} \quad \text{.....(3.10)}$$

where

$$Y = \sin^2\theta$$

$$Q = \left\{(A_{13} - A_{55})^2 + 2A_1 Y + A_2 Y^2\right\}^{1/2} \quad *$$

$$A_1 = 2(A_{13} + A_{55})^2 - (A_{13} - A_{55})(A_{11} + A_{33} - 2A_{55})$$

$$A_2 = (A_{11} + A_{33} - 2A_{55})^2 - 4(A_{13} + A_{55})$$

The quasi-P and quasi-SV polarization (normalized eigenvectors in equation (3.5)) can be obtained by substituting the phase velocities back into the Christofel equation (3.5):

$$\begin{cases} l = \left\{\dfrac{\left[(Q - A_{33} + A_{55})/\sin^2\theta\right] + \left[A_{11} + A_{33} + 2A_{55}\right]}{2Q}\right\} \\ m = \left\{\dfrac{\left[(Q - A_{11} + A_{55})/\cos^2\theta\right] + \left[A_{11} + A_{33} - 2A_{55}\right]}{2Q}\right\} \end{cases} \quad \text{.....(3.11)}$$

3.1.3. Boundary conditions

Without energy loss, the reflection and transmission coefficients of a plane-wave at an interface between two media, isotropic or anisotropic, are computed using the two physical principles (Aki and Richard, 1980):

1) The displacement amplitudes in the two media are equal at the boundary. In other words, the media are in welded contact. This condition is also referred to as "kinematic" boundary conditions.

2) The sum of the tractions acting on the boundary have to be zero. Expanding the traction in terms of the stresses, this assumption leads to the required continuity of normal and shear components of stress across the boundary. This condition is also referred to as "dynamic" boundary conditions.

Thus, the continuity of the x component of displacement yields:

$$\sum_{v=1}^{2} P_{nv} m_v \cos\theta_v - \sum_{v=3}^{4} s_{nv} l_v \sin\theta_v = P_{n0} m_0 \cos\theta_0 - \sum_{v=3}^{4} S_{nv} m_v \cos\theta_v + \sum_{v=0}^{2} (-1)^{\delta_{v0}} \rho_{nv} l_v \sin\theta_v \quad \text{.....(3.12)}$$

Continuity of the z component of displacement yields:

$$\sum_{v=1}^{2} (-1)^v P_{nv} l_v \sin\theta_v + \sum_{v=3}^{4} (-1)^v s_{nv} m_v \cos\theta_v = P_{n0} l_0 \sin\theta_0 - \sum_{v=3}^{4} (-1)^v S_{nv} l_v \sin\theta_v - \sum_{v=0}^{2} (-1)^{\delta_{v0}+v} \rho_{nv} m_v \cos\theta_v \quad \text{.....(3.13)}$$

Continuity of shear stress:

$$\sum_{v=1}^{2}\frac{C_{55}^{(v)}\left(l_v+m_v\right)\sin 2\theta_v P_{nv}}{2V_v}+\sum_{v=3}^{4}\frac{C_{55}^{(v)}\left(m_v\cos^2\theta_v-l_v\sin^2\theta_v\right)s_{nv}}{V_v}$$

$$=\frac{C_{55}^{(0)}\left(l_0+m_0\right)\sin 2\theta_0 P_{n0}}{2V_0}+\sum_{v=0}^{2}\left[\frac{(-1)^{1+\delta_{v0}}C_{55}^{(v)}\left(m_v\cos^2\theta_v-l_v\sin^2\theta_v\right)\rho_{nv}}{V_n}\right.$$

$$\left.-(-1)^{v+\delta_{v0}}C_{55}^{(v)}\left(\frac{\partial\left(P_x\right)_{n-1,v}}{\partial z}+\frac{\partial\left(P_z\right)_{n-1,v}}{\partial x}\right)\right]-\sum_{v=3}^{4}\left\{\frac{C_{55}^{(v)}\left(l_v+m_v\right)\sin 2\theta_v S_{nv}}{2V_v}\right.$$

$$\left.+(-1)^{v}C_{55}^{(v)}\left(\frac{\partial\left(S_x\right)_{n-1,v}}{\partial z}+\frac{\partial\left(S_z\right)_{n-1,v}}{\partial x}\right)\right\} \qquad \text{.....(3.14)}$$

Continuity of normal stress:

$$\sum_{v=1}^{2}(-1)^{v}\frac{\left[l_vC_{13}^{(v)}+\left(m_vC_{33}^{(v)}-l_vC_{13}^{(v)}\right)\cos^2\theta_v\right]P_{nv}}{V_v}-\sum_{v=3}^{4}(-1)^{v}\frac{\left(l_vC_{33}^{(v)}-m_vC_{13}^{(v)}\sin 2\theta_v s_{nv}\right)}{2V_v}$$

$$=\frac{\left[l_0C_{13}^{(0)}+\left(m_0C_{33}^{(0)}-l_0C_{33}^{(0)}\right)\cos^2\theta_0\right]P_{n0}}{V_0}+\sum_{v=0}^{2}(-1)^{v+\delta_{v0}}\left\{C_{13}^{(v)}\frac{\partial\left(P_x\right)_{n-1,v}}{\partial z}\right.$$

$$\left.+C_{33}^{(v)}\frac{\partial\left(P_z\right)_{n-1,v}}{\partial z}+\frac{\left(l_vC_{33}^{(v)}-m_vC_{13}^{(v)}\right)\sin 2\theta_v\rho_{nv}}{2V_v}\right\}+\sum_{v=3}^{4}(-1)^{v}\left\{C_{13}^{(v)}\frac{\partial\left(S_x\right)_{n-1,v}}{\partial x}\right.$$

$$\left.+C_{33}^{(v)}\frac{\partial\left(S_z\right)_{n-1,v}}{\partial z}-\frac{\left[l_vC_{13}^{(v)}+\left(m_vC_{33}^{(v)}-l_vC_{13}^{(v)}\right)\cos^2\theta v\right]S_{nv}}{V_v}\right\} \qquad \text{.....(3.15)}$$

Equation (3.12) – (3.15) represent the continuity of displacement and stress requirements used to find the reflection coefficient between VTI media (Daley, 1977)

3.1.4 Algebraic expression of reflection coefficients

Let $\sin\theta_1 = x$, and follow the Daley's variable notations as follow:

$$
\begin{cases}
V_1/V_2 = n, \\
V_3/V_1 = k_1, \\
V_4/V_2 = k_2 \\
P = \cos\theta_1 = \left(1 - x^2\right)^{1/2} \\
Q = \cos\theta_2 = \left(1 - x^2/n^2\right)^{1/2} \quad * \\
S = \cos\theta_3 = \left(1 - k_1^2 x^2\right)^{1/2} \quad * \\
R = \cos\theta_4 = \left(1 - k_2^2 x^2/n^2\right)^{1/2} \\
C_{55}^{*0} = C_{55}^{*(1)} = C_{55}^{*(3)} = \beta_1 \\
C_{55}^{*(2)} = C_{55}^{*(4)} = \beta_2 \\
l_3 C_{33}^{*(3)} - m_3 C_{13}^{*(3)} = \delta_1 \\
l_4 C_{33}^{*(4)} - m_4 C_{13}^{*(4)} = \delta \\
\dfrac{V_1}{V_3}\dfrac{1}{l_1 + m_1}\left(m_3 \cos^2\theta_3 - l_3 \sin^2\theta_3\right) = \omega_1 \\
\dfrac{V_1}{V_4}\dfrac{1}{l_1 + m_1}\left(m_4 \cos^2\theta_4 - l_4 \sin^2\theta_4\right) = \omega_2 \\
l_1 C_{13}^{*(1)} + \left(m_1 C_{33}^{*(1)} - l_1 C_{13}^{*(1)}\right)\cos^2\theta_1 = \varepsilon_1 \\
\dfrac{V_1}{V_2}\left\{l_2 C_{13}^{*(2)} + \left(m_2 C_{33}^{*(2)} - l_2 C_{13}^{*(2)} \cos^2\theta_2\right)\right\} = \varepsilon_2 \\
\dfrac{l_2 + m_2}{l_1 + m_1} = l
\end{cases}
\qquad \text{.....(3.16)}
$$

Substitution of (3.16) back into the equations (3.12) ~ (3.15) yields the four linear equations below (written in matrix form):

$$\begin{bmatrix} x & \frac{m_3}{l_1}Q & \frac{-l_2}{l_1}\frac{x}{n} & \frac{-m_4}{l_1}R \\ P & \frac{-l_3}{m_1}k_1x & \frac{m_2}{m_1}S & \frac{-l_4k_2x}{m_1n} \\ \beta_1xP & \beta_1\omega_1 & \beta_2lxS & \beta_2\omega_2 \\ -\varepsilon_1 & \delta_1xQ & \varepsilon_2 & -\delta_2xR \end{bmatrix} \begin{bmatrix} R_{11} \\ R_{13} \\ R_{12} \\ R_{14} \end{bmatrix} = \begin{bmatrix} -x \\ P \\ \beta_1xP \\ \varepsilon_1 \end{bmatrix} \quad \text{.....(3.17)}$$

where R_{11} is the P-wave reflection coefficient, R_{12} is the P-wave transmission coefficient, R_{13} is the SV-wave reflection coefficient, R_{14} is the SV-wave transmission coefficient. Using Cramer's method, the solution of (3.17) can be written as:

$$\begin{cases} R_{11} = \dfrac{-E_1 + E_2 + E_3 + E_4 - E_5 - E_6}{D} \\ R_{12} = \dfrac{E_7 + E_8}{D} \\ R_{13} = \dfrac{E_9 + E_{10}}{D} \\ R_{14} = \dfrac{E_{11} + E_{12}}{D} \end{cases} \quad \text{.....(3.18)}$$

where E_1 ~ E_{12} and D are given explicitly as follows:

$$
\begin{cases}
E_1 = T_1 T_2 x^2 \\
E_2 = T_3 T_4 PQ \\
E_3 = T_5 T_6 PR \\
E_4 = T_7 T_8 x^2 PQRS \\
E_5 = T_9 T_{10} QS \\
E_6 = T_{11} T_{12} RS \\
E_7 = 2T_5 T_{11} PR \\
E_8 = 2T_3 T_{10} PQ \quad * \\
E_9 = -2xT_7 T_{11} PRS \\
E_{10} = -2xT_1 T_3 P \\
E_{11} = -2xT_7 T_{10} PQS \\
E_{12} = 2xT_1 T_5 P \\
D = E_1 + E_2 + E_3 + E_4 + E_5 + E_6 \qquad \text{.....(3.19)}
\end{cases}
$$

and

$$
\begin{cases}
T_1 = \varepsilon_2 - \dfrac{\varepsilon_1 l_2}{n l_1} \\
T_2 = \beta_2 \varpi_2 k_1 \dfrac{l_3}{m_1} - \beta_1 \dfrac{\varpi_1 k_2 l_4}{n m_1} \\
T_3 = \beta_2 \varpi_2 + \beta_1 \dfrac{k_2 x^2 l_4}{n m_1} \\
T_4 = \varepsilon_2 \dfrac{m_3}{l_1} + \dfrac{\delta_1 x^2 l^2}{n l_1} \\
T_5 = \beta_1 \left(\varpi_1 + k_1 x^2 \dfrac{l_3}{m_1} \right) \\
T_6 = \varepsilon_2 \dfrac{m_4}{l_1} + \dfrac{\delta_2 x^2}{n} \dfrac{l_2}{l_1} \\
T_7 = \beta_2 l - \beta_1 \dfrac{m_2}{m_1} \\
T_8 = \delta_2 \dfrac{m_3}{l_1} - \delta_1 \dfrac{m_4}{l_1} \\
T_9 = \beta_2 \left(\varpi_2 \dfrac{m_1}{m_2} + \dfrac{k_2 x^2 l l_4}{n m_1} \right) \\
T_{10} = \varepsilon_1 \dfrac{m_3}{m_1} + \delta_1 x^2 \\
T_{11} = \varepsilon_1 \dfrac{m_4}{m_1} + \delta_2 x^2 \\
T_{12} = \beta_2 \dfrac{k_1 x^2 l l_3}{m_1} + \dfrac{\beta_1 \varpi_1 m_2}{m_1}
\end{cases}
\qquad \text{.....(3.20)}
$$

A FORTRAN90 subroutine (See Appendix I) was written to calculate the exact reflection coefficients for reflected P-wave and SV-waves when provided a P-wave incident upon a boundary between two TI media. Using Daley's model parameters shown in Table 3.1 (Daley, 1979, p.36), Figure 3.2 shows the P and SV reflection coefficients and transmission coefficients when a P-wave is incident. The angle of incidence refers to the group angle of the incident P-wave. The basic shapes of the curves in Figure 3.2 agree with those published in Daley's (1979) work (compare Daley's figure 3 to figure 6). The results in this thesis plotted have a finer sampling of the incidence angles than Daley's and yield a more detailed version of the curves shown in Daley and Hron (1979).

For a plane wave incident on the boundary between two VTI media, the energy of the incident wave is distributed between all the reflected and refracted phases. An energy-flux method was used in order to verify conservation of energy for the reflection and transmission coefficients.

It should be noted Thomsen's definition for the anisotropic parameter ε is used here:

$$\varepsilon = \frac{C_{11} - C_{33}}{C_{33}} \times 100\% = \frac{v_p^2(\pi/2) - \alpha_0^2}{\alpha_0^2} \times 100\% \qquad \text{.....(3.21)}$$

where, C_{11} and C_{33} are the elastic tensors on horizontal and vertical direction. $v_p(\pi/2)$ and α_0 are the horizontal and vertical P-wave phase velocity respectively.

This definition is different from Daley's (1979):

$$\varepsilon = \frac{v_p(\pi/2) - \alpha_0}{\alpha_0} \times 100\% \qquad \text{.....(3.22)}$$

Thus, a different set of anisotropy parameter ε (0%, 5.48%, 11%, 16.53%, 21.32%) is listed here corresponding to Daley's ε (0%, 5%, 10%, 15%, 20%) for the five models.

Table 3.1 Daley's model parameters

Curve No.	$V_{p1}(90^0)$ (m/s)	α_{01} (m/s)	β_{01} (m/s)	ρ_1 (g/cm^3)	$V_{p2}(90^0)$ (m/s)	α_{02} (m/s)	β_{02} (m/s)	ρ_2 (g/cm^3)	A_1 (%)	ε_1 (%)
1	2310	2310	1330	2.04	3360	3060	1770	2.21	0	0
2	2370	2250	1330	2.04	3360	3060	1770	2.21	5	5.48
3	2430	2200	1330	2.04	3360	3060	1770	2.21	10	11
4	2480	2150	1330	2.04	3360	3060	1770	2.21	15	16.53
5	2520	2110	1330	2.04	3360	3060	1770	2.21	20	21.32

3.2 Approximations under VTI condition and their assumptions

By differentiating the exact expression for R_{11} (see equation (3.18)) and ignoring the high-order terms, much previous work (e.g., Banik; 1986, Ruger, 1995; Thomsen, 1993; etc.) has been done on P-wave reflection approximations.

The approximations have been applied widely for modeling of VTI media. These equations are important because they simplify the dependence of the reflection response upon the parameters. However, the approximations differ in their sensitivity to the elastic parameters and can yield different results for the same model. Therefore four

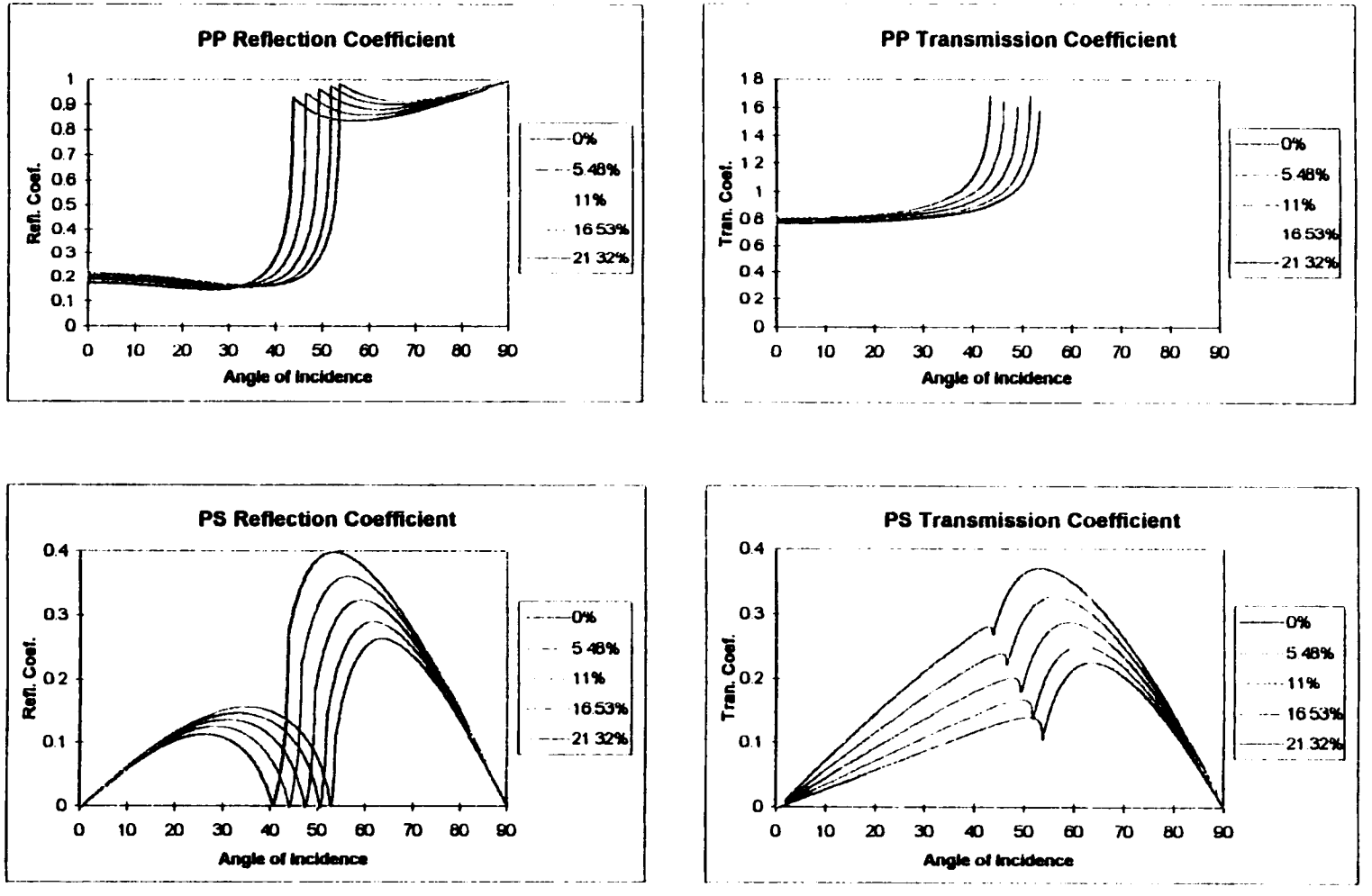

Figure 3.2 Reflection and transmission coefficients versus angle of incidence

approximations, which come from the work of Banik (1987), Thomsen (1993), Ruger (1997), and Chen (1995), are examined below.

For convenience in the comparison, all the equations are expressed using the same variables. Hence, the 4 approximations can be written in the original form:

Banik (1987):

$$R_{pp}(\theta) = \frac{1}{2}\left(\frac{\Delta\rho}{\rho} + \frac{\Delta\alpha}{\alpha_0}\right) - 2\frac{\beta_0^2}{\alpha_0^2}\left(\frac{\Delta\rho}{\rho} + 2\frac{\Delta\beta}{\beta_0}\right)\sin^2\theta + \frac{1}{2}\frac{\Delta\alpha}{\alpha_0}\tan^2\theta + \frac{\Delta\delta - 2\Delta\varepsilon}{2}\sin^2\theta \quad \text{.....(3.23)}$$

Chen (1995)

$$R_{pp}(\theta) = \frac{1}{2}\left(1 - 4\frac{\beta_0^2}{\alpha_0^2}\sin^2\theta\right)\frac{\Delta\rho}{\rho} + \frac{1}{2\cos^2\theta}\frac{\Delta\alpha}{\alpha_0} - \frac{4\beta_0^2}{\alpha_0^2}\sin^2\theta\frac{\Delta\beta}{\beta_0} + \frac{\sin^2\theta}{2}\Delta\delta \quad \text{.....(3.24)}$$

Thomsen (1993)

$$R_{pp}(\theta) = \frac{1}{2}\frac{\Delta Z_0}{Z_0} + \frac{1}{2}\left[\frac{\Delta\alpha}{\alpha_0} - \left(\frac{2\beta_0}{\alpha_0}\right)^2\frac{\Delta G_0}{G_0} + \Delta\delta\right]\sin^2\theta + \frac{1}{2}\left(\frac{\Delta\alpha}{\alpha_0} + \Delta\varepsilon - \Delta\delta\right)\sin^2\theta\tan^2\theta \quad \text{.....(3.25)}$$

Ruger (1995)

$$R_{pp}(\theta) = \frac{1}{2}\frac{\Delta Z_0}{Z_0} + \frac{1}{2}\left[\frac{\Delta\alpha}{\alpha_0} - \left(\frac{2\beta_0}{\alpha_0}\right)^2\frac{\Delta G_0}{G_0} + \Delta\delta\right]\sin^2\theta + \frac{1}{2}\left(\frac{\Delta\alpha}{\alpha_0} + \Delta\varepsilon\right)\sin^2\theta\tan^2\theta \quad \text{.....(3.26)}$$

where θ is the incident angle, α_0 is the *P*-wave vertical velocity, β_0 is the *SV*-wave vertical velocity, ρ is average density, $Z_0 = \rho\alpha_0$ is the average vertical *P*-wave impedance, and $G_0 = \rho\beta_0^2$ is the average vertical shear modulus. The difference between isotropic parameters across the boundary are: $\Delta\alpha = \alpha_2 - \alpha_1$, $\Delta\beta = \beta_2 - \beta_1$, $\Delta\rho = \rho_2 - \rho_1$, $\Delta Z = Z_2 - Z_1$, $\Delta G = G_2 - G_1$. The differences in anisotropy across the boundary are written as $\Delta\varepsilon = (\varepsilon_2 - \varepsilon_1)$, $\Delta\delta = (\delta_2 - \delta_1)$.

All the approximations discussed are valid under the following assumptions:

$$\begin{cases} \left|\dfrac{\Delta\alpha_0}{\alpha_0}\right| << 1 \\ \left|\dfrac{\Delta\beta_0}{\beta_0}\right| << 1 \\ \left|\dfrac{\Delta\rho}{\rho}\right| << 1 \\ |\varepsilon| << 1 \\ |\delta| << 1 \end{cases} \qquad \text{.....(3.27)}$$

Ignoring the terms that depend upon anisotropy (ε, δ), Thompsen and Ruger's results use the same set of isotropic parameters (eg. $\Delta Z_0/Z_0$, $\Delta G_0/G_0$) and the expressions are identical. On the other hand, the isotropic parts of Banik's and Chen's equations are identical, use another set of isotropic parameters (eg. $\Delta\rho/\rho$, $\Delta\beta_0/\beta_0$). The following approximation can be used to relate the work of Thompen and Ruger to that of Banik and Chen:

$$\begin{cases} \dfrac{\Delta Z_0}{Z_0} \approx \dfrac{\Delta \alpha_0}{\alpha_0} + \dfrac{\Delta \rho}{\rho} \\ \dfrac{\Delta G_0}{G_0} \approx \dfrac{2\Delta \beta_0}{\beta_0} + \dfrac{\Delta \rho}{\rho} \end{cases} \qquad \text{.....(3.28)}$$

Figure 3.3 shows that, when the contrast is small ($\Delta\alpha_0/\alpha_0 < 0.2$, $\Delta\beta_0/\beta_0 < 0.2$, and $\Delta\rho/\rho < 0.2$), the error of these transformation is negligible. This means, with small contrast isotropic models, Banik's and Chen's approximations should be almost the same as those described by Thomsen and Ruger.

When equations (3.28) for the $\Delta Z_0/Z_0$ and $\Delta G_0/G_0$ terms are substituted into Thomsen's and Ruger's approximations, the differences between the four approximations are seen to be in the anisotropic portions of the equations:

Banik (1986)

$$R_{11}(\theta) = \frac{1}{2}\left(1 - 4\frac{\beta_0^2}{\alpha_0^2}\sin^2\theta\right)\frac{\Delta\rho}{\rho_0} + \frac{1}{2\cos^2\theta}\frac{\Delta\alpha}{\alpha_0} - \frac{4\beta_0^2}{\alpha_0^2}\sin^2\theta\frac{\Delta\beta}{\beta_0} + \frac{\sin^2\theta}{2}\Delta\delta \qquad \text{.....(3.29)}$$

Thomsen (1993

$$R_{11}(\theta) = \frac{1}{2}\left(1 - 4\frac{\beta_0^2}{\alpha_0^2}\sin^2\theta\right)\frac{\Delta\rho}{\rho_0} + \frac{1}{2\cos^2\theta}\frac{\Delta\alpha}{\alpha_0} - \frac{4\beta_0^2}{\alpha_0^2}\sin^2\theta\frac{\Delta\beta}{\beta_0} + \frac{\sin^2\theta}{2}\Delta\delta + \frac{1}{2}(\Delta\varepsilon - \Delta\delta)\sin^2\theta\tan^2\theta \qquad \text{.....(3.30)}$$

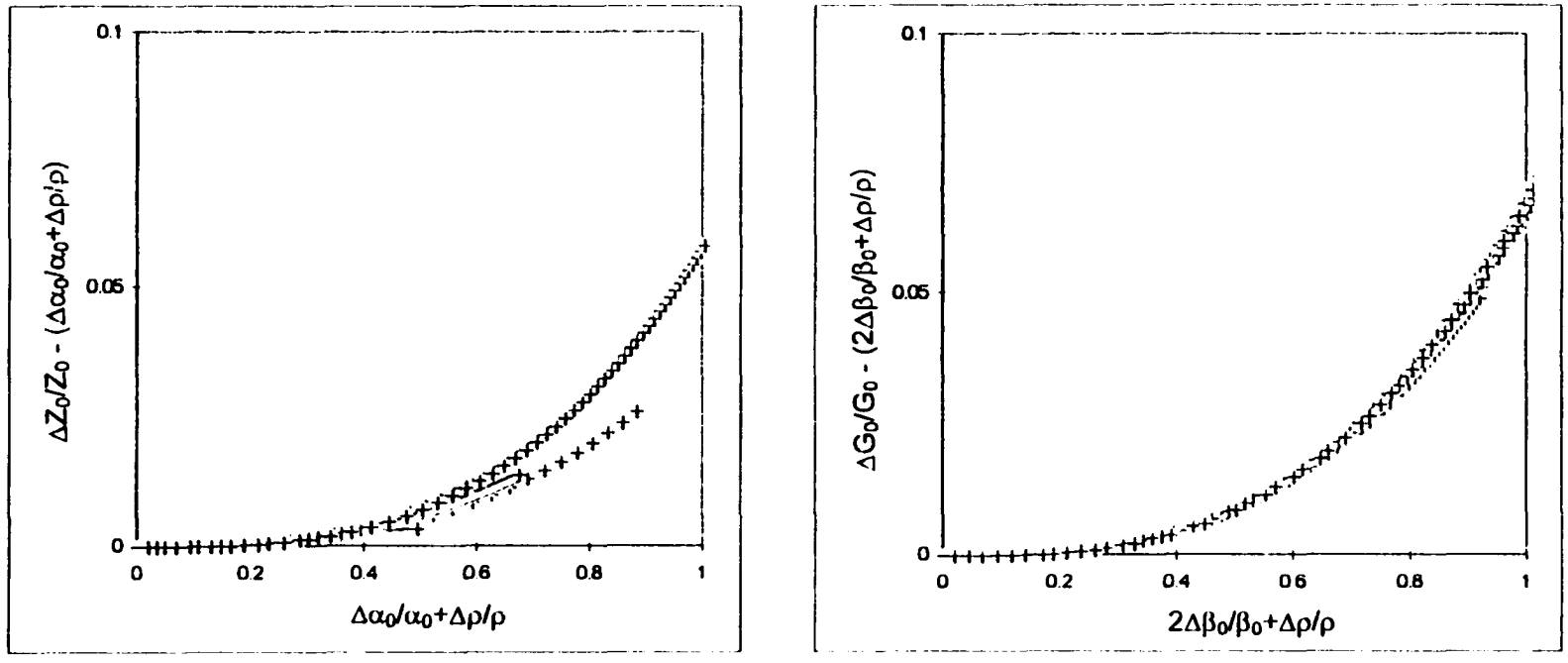

Figure 3.3 Test measurement on error introduced by transfermation of

$$\Delta Z_0/Z_0 \approx \Delta\alpha_0/\alpha_0+\Delta\rho/\rho,\ \ \Delta G_0/G_0 \approx 2\Delta\beta_0/\beta_0+\Delta\rho/\rho$$

Ruger (1995)

$$R_{11}(\theta) = \frac{1}{2}\left(1 - 4\frac{\beta_0^2}{\alpha_0^2}\sin^2\theta\right)\frac{\Delta\rho}{\rho_0} + \frac{1}{2\cos^2\theta}\frac{\Delta\alpha}{\alpha_0} - \frac{4\beta_0^2}{\alpha_0^2}\sin^2\theta\frac{\Delta\beta}{\beta_0}$$
$$+ \frac{\sin^2\theta}{2}\Delta\delta + \frac{1}{2}\Delta\varepsilon\sin^2\theta\tan^2\theta \qquad \text{.....(3.31)}$$

Chen (1995)

$$R_{11}(\theta) = \frac{1}{2}\left(1 - 4\frac{\beta_0^2}{\alpha_0^2}\sin^2\theta\right)\frac{\Delta\rho}{\rho_0} + \frac{1}{2\cos^2\theta}\frac{\Delta\alpha}{\alpha_0} - \frac{4\beta_0^2}{\alpha_0^2}\sin^2\theta\frac{\Delta\beta}{\beta_0}$$
$$+ \frac{\sin^2\theta}{2}\Delta\delta - \Delta\varepsilon\sin^2\theta \qquad \text{.....(3.32)}$$

After collecting terms in the order of $\Delta\alpha_0/\alpha_0$, $\Delta\beta_0/\beta_0$, or $\Delta\rho/\rho$, it is easy to find that Banik's equation, in which the only anisotropic term is $(\Delta\delta/2)\sin\theta$, is the simplest of the approximations, as the other three approximations have additional terms which depend upon ε.

3.3 Comparison studies

Here the approximate and the exact results are compared to find the circumstances under which the various equations are most applicable.

Using Banik's, Thomsen's, Ruger's and Chen's approximations, four FORTRAN90 subroutines (see Appendix C) were written to calculate the approximate PP reflection coefficients across a boundary between two TI media. All of the original

equations are used in the programming. Model studies are performed in both isotropic and anisotropic situations, using a wide range of model parameters.

3.3.1 Model test in isotropic media

From the analytical discussion above, for any incident angle in isotropic models, the four approximations should generally agree with each other. Here, the incident medium with the parameters of (α_{01}, β_{01}, ρ_{01}, etc.) and the reflecting medium with (α_{02}, β_{02}, ρ_{02}, etc.) are assumed. Table 3.3 lists 4 isotropic portions of the models with the same density values for both incident and reflecting media, but with the P-wave and SV-wave velocities alternated so that the models stand for four categories of isotropic situations (Table 3.2):

Table 3.2 Categories of Isotropic Models

	From Incident to Reflecting		Abbreviation
Model 1:	Vp Increase	Vs Increase	PiSi
Model 2:	Vp Increase	Vs Decrease	PiSd
Model 3:	Vp Decrease	Vs Increase	PdSi
Model 4:	Vp Decrease	Vs Decrease	PdSd

Table 3.3 Isotropic model parameters

	α_{01} (m/s)	β_{01} (m/s)	ρ_1 (g/cm^3)	α_{02} (m/s)	β_{02} (m/s)	ρ_2 (g/cm^3)
Model 1	2000	1200	2.15	2500	1400	2.15
Model 2	2000	1400	2.15	2500	1200	2.15
Model 3	2500	1200	2.15	2000	1400	2.15
Model 4	2500	1400	2.15	2000	1200	2.15

Figure 3.4a - d. show the PP reflection coefficients (including Daley's and the other 4 approximations) corresponding to Model 1 - 4 respectively. The results show: 1) The four approximate reflection coefficient curves almost lay on top of each other. This also confirms that the transformation from $\Delta Z_0/Z_0$ and $\Delta G_0/G_0$ to $\Delta\alpha_0/\alpha_0$, $\Delta\beta_0/\beta_0$, and $\Delta\rho/\rho$ are applicable under small contrast situations. 2) For small incidence angles, the four approximations are close to the exact solution. As the incidence angle increases, all approximations begin to stray from the exact one. It should be noticed that the deviation point, beyond which approximations are not valid at all, is different for the 4 categories of models considered.

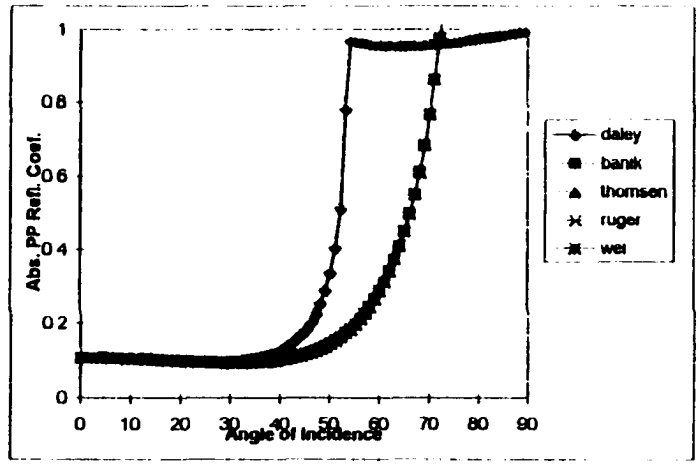

a) Model 1 (PiSi Vp2 > Vp1, Vs2 > Vs1)

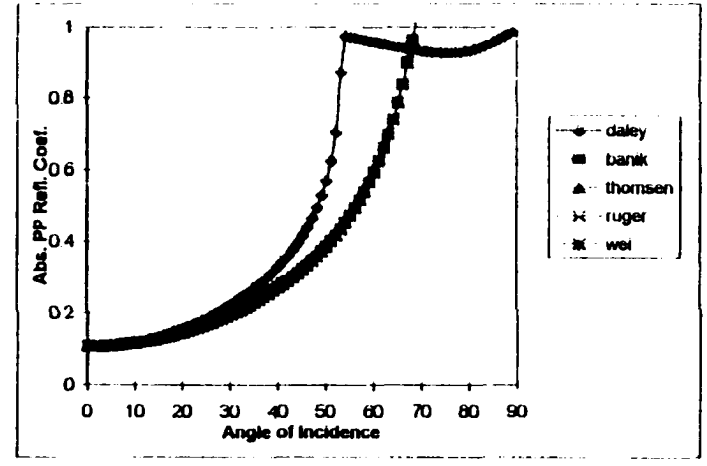

b) Model 2 (PiSd Vp2 > Vp1, Vs2 < Vs1)

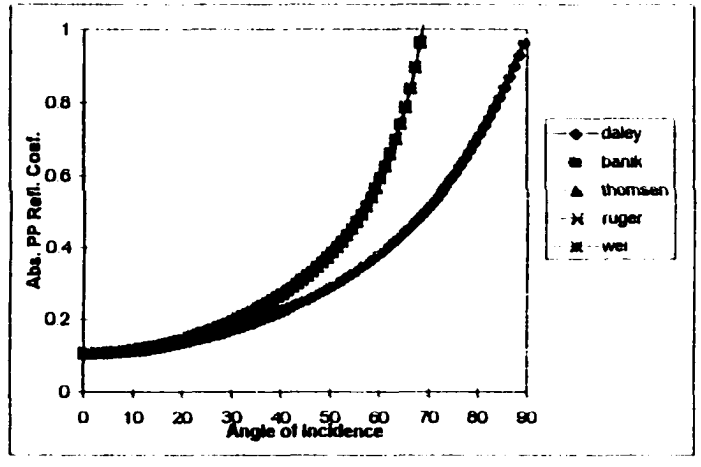

c) Model 3 (PdVi Vp2 < Vp1, Vs2 > Vs1)

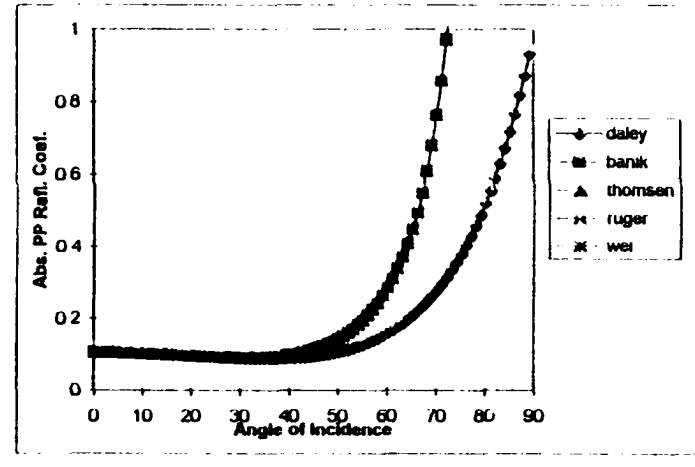

d) Model 4 (PdVd Vp2 < Vp1, Vs2 < Vs1)

Figure 3.4 P-wave reflection coefficients for models in Table 2 under isotropic situations

3.3.2 Model test in anisotropic media

Banik (1987) suggests that δ is roughly the difference between the P-wave and SV-wave anisotropies of the medium:

$$\delta = \varepsilon_p - \varepsilon_s \quad \text{.....(3.32)}$$

Here, ε_p is P-wave anisotropy (the same as Thomsen's (1986)), and ε_s is the SV-wave anisotropy as defined by Banik (1987). Banik's ε_s is the SV-wave anisotopy comparing vertical SV Propagation with SV propagation at an angle of 45 degree.

The 4 isotropic model parameters (Table 3.3) are also used as a basis in this part of the study. The anisotropic parameters are listed on the figures. Figure 3.5 –3.8 show the test result of Models 1 – 4 respectively. In these tests, it should be noticed that:

1) The incident medium is always anisotropic and the reflecting medium is isotropic.

2) In the incident medium, the P-wave anisotropic parameter ε_s is set equal to 0.2.

3) In Figure 3.5a – 3.8a show a strong SV-wave anisotopic situation, where ε_p =0.2, ε_s =0.2, and $\delta = \varepsilon_p - \varepsilon_s$ =0. Figure 3.5b – 3.8b show an elliptical anisotropic situation (ε_p =0.2, ε_s =0.1, and δ = 0.1). Figure 3.5c – 3.8c show an elliptical anisotropic situation ($\varepsilon_p = \delta$ = 0.2, ε_s =0), in which there is no SV-wave anisotropy (Thomsen, 1986).

Figures 3.5 show that Ruger's approximation performs better than the others in the PiSi (i.e. P-wave increase, S-wave increase) case. As we can see from Figures 3.5a – 3.6c, Ruger's curve approaches Daley's exact solution over a larger range of incidence

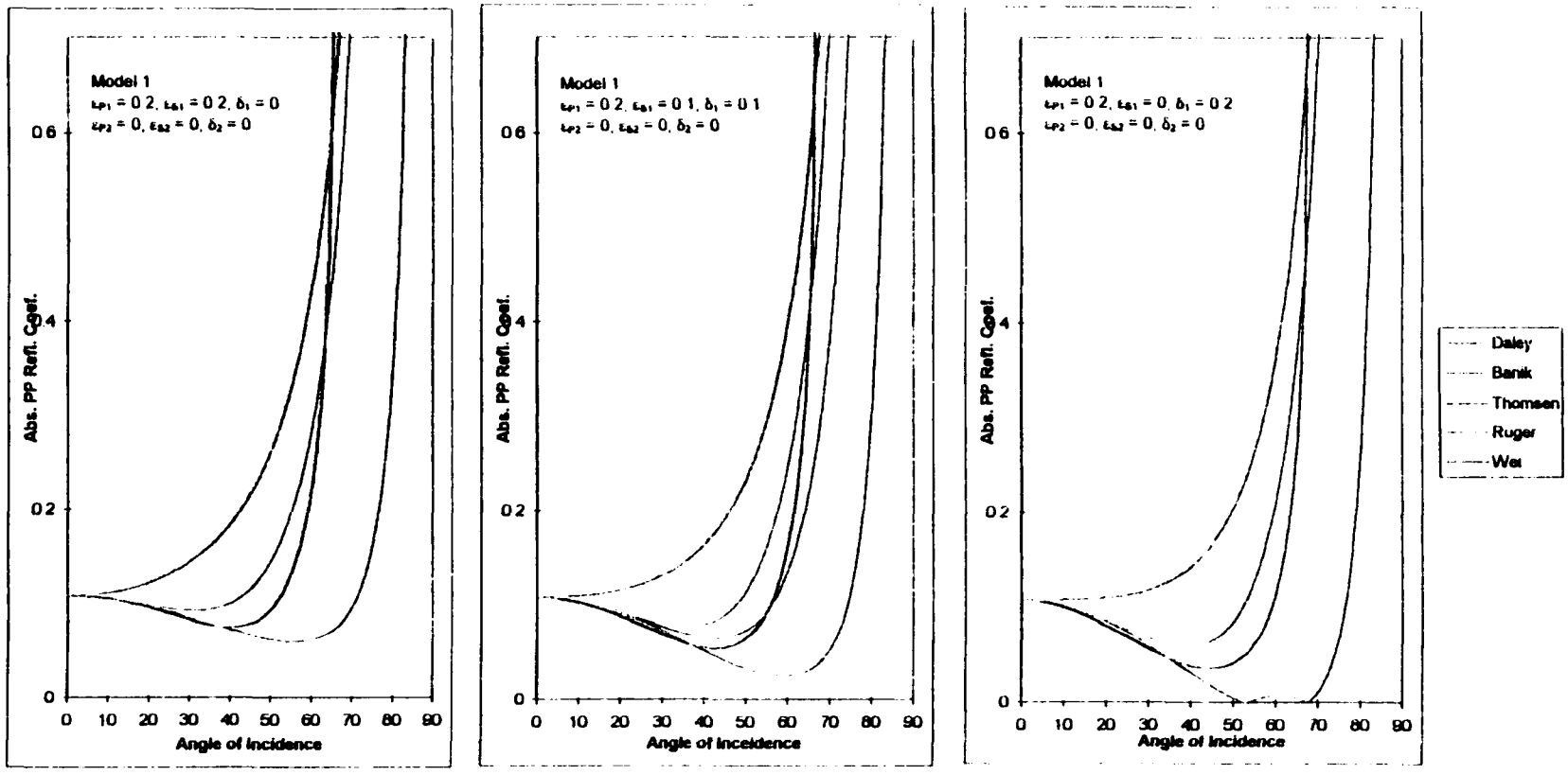

Figure 3.5 P-wave reflection coefficients for Model 1 in Table 2

angles. This was found to be true for a wide range of other models not shown here with other sets of anisotopic parameters.

The same comparisons are made in Figures 3.6 – 3.8. The results show that Banik's approximation performs better for a large angular range in these 3 cases, which correspond to PiSd, PdSi, and PdSd isotropic situations . Thus Banik's equation works for a wider range of basic isotropic starting models.

Notice that Tomsen's approximation varies between Ruger's and Banik's as shown in Figures 3.5-3.8. As noted by Ruger (1997), the only difference between Thomsen's and Ruger's equations is an extra term $(\Delta\delta/2)*\sin^2\theta*\tan^2\theta$ apparently due to an algebraic error by Thomsen. So, whenever $\Delta\delta=0$ across the boundary, Thomsen's approximation is equal to Ruger's. It should also be noticed that when $\Delta\delta=\Delta\varepsilon$ across the boundary then Thomsen's approximation is equal to Banik's. See the Figures 3.5b – 3.8b to compare the results for intermediate values of $\Delta\delta$.

Note that Chen's approximation does not work well in all of these tests.

More tests are needed for all possible parameter sets, however, thus far it seems that Ruger's approximation deals with anisotropy parameters better than the others under the PiSi condition, while Banik" performs better in the other 3 isotropic situations (i.e, PiSd, PdSi, and PdSd) over a wide angular range.

3.4 Conclusions

Daley's solution is the exact result under the condition that all of the elastic constants (a total of ten considering both media) and densities of the TI media are

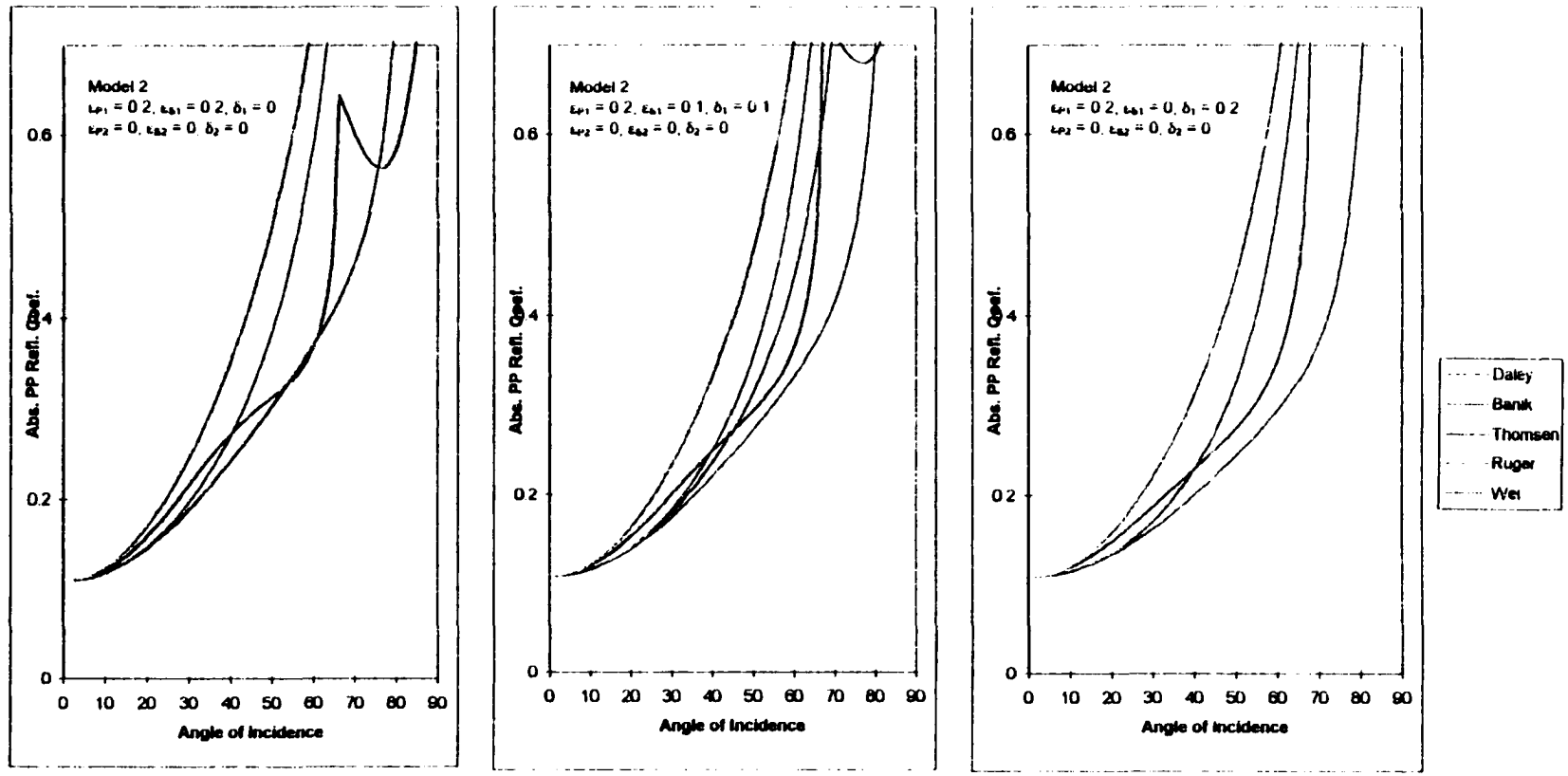

a) b) c)

Figure 3.6 P-wave reflection coefficients for Model 2 in Table 2

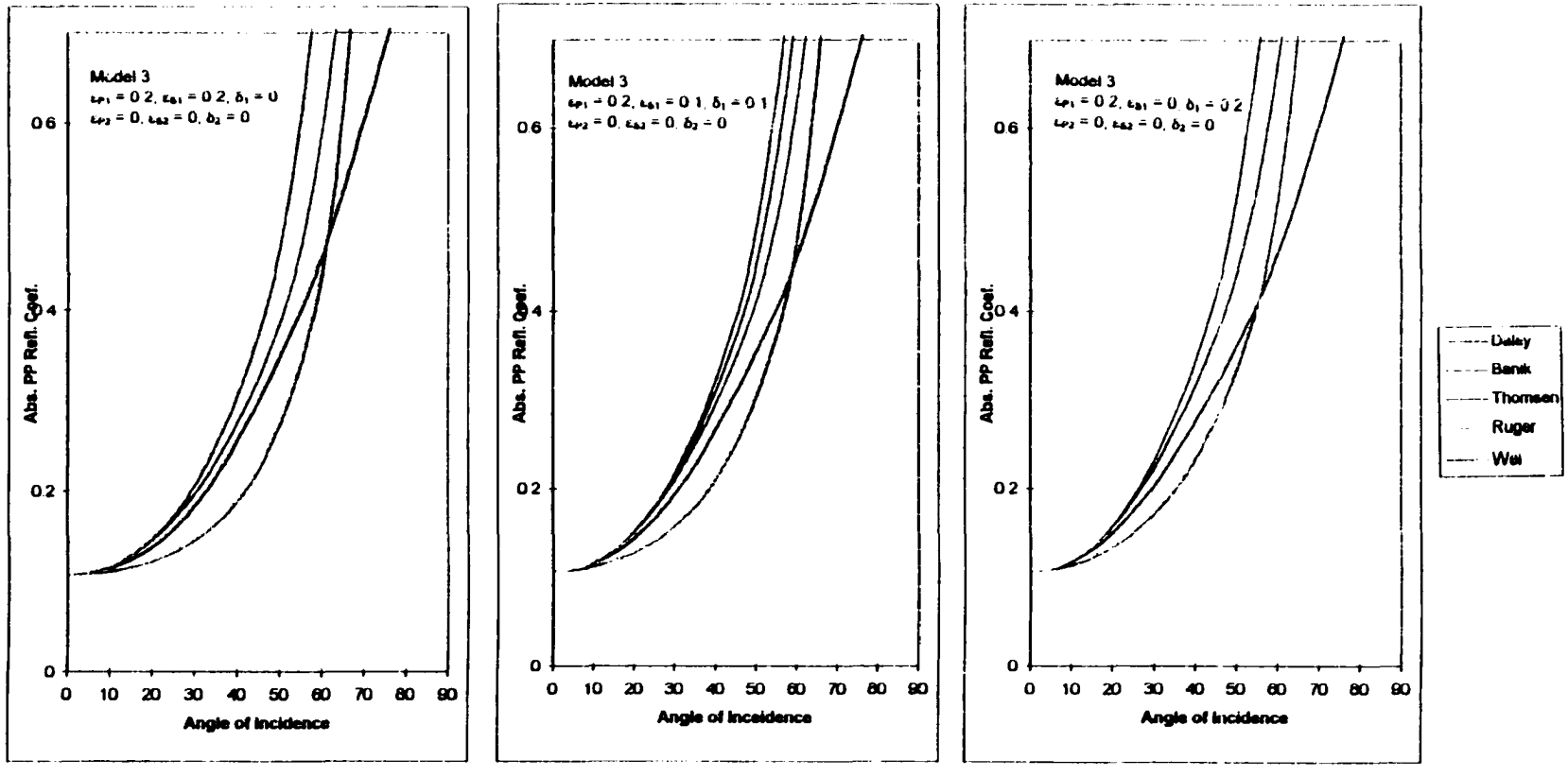

Figure 3.7 P-wave reflection coefficients for Model 3 in Table 2

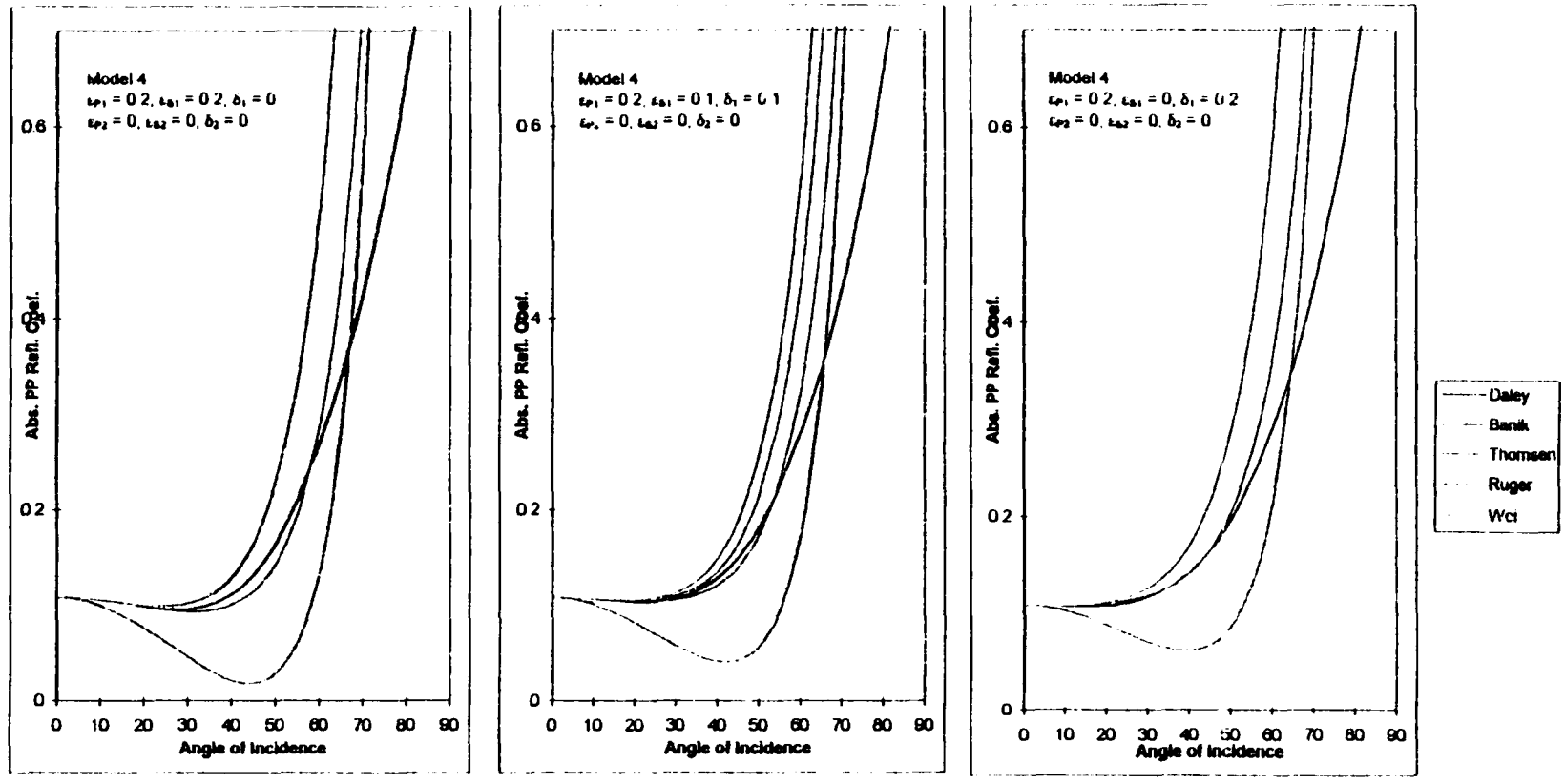

Figure 3.8 P-wave reflection coefficients for Model 4 in Table 2

known. However, a number of typographical errors have been corrected in the solutions published by Daley and Hron (1977 & 1979).

For the isotropic situation, all 4 approximations perform exactly well for small contrasts in elastic parameter and small angles of incidence.

For anisotropic situations, the tests show that different approximations work better for different categories of variations in isotropic base parameters. Under the PiSi condition, Ruger's approximation deals with anisotropy parameters better than the others. However in the other 3 isotropic base modes (i.e., PiSd, PdSi, and PdSd), Banik's yield a better approximation result for wide angular range and Ruger's performs the best at small angle. Thus, although Banik's work was earlier and perhaps simpler than the later publications, his results seem to be superior to the others for many models.

Chapter 4

Three-Parameter AVO Crossplotting in Anisotropic Media

The objective of this chapter is to study the effects of transverse anisotropy on angle dependent reflectivity. This problem is important because large mistakes can be made in the interpretation by neglecting the effects of TI anisotropy.

Amplitude versus offset (AVO) interpretation can be facilitated by crossplotting AVO intercept (A), gradient (B) and curvature (C) terms. However, anisotropy, which exists in the real world, usually complicates AVO analysis. Recognition of the anisotropic behavior on AVO crossplots can help avoid AVO interpretation errors.

As opposed to predictions made using 3-term (A, B, and C) approximations to the exact anisotropic reflection coefficients for transversely isotropic media, it is found that anisotropy has a non-linear effect on an A versus C crossplot while causing slope changes and differing intercepts on A versus B or C crossplots. Empirical corrections that result in more accurate crossplot interpretation are introduced for specific circumstances.

4.1 Introduction

Crossplotting of AVO intercept (A) and gradient (B) (eg. Castagna et al., 1998) can be a useful seismic lithologic analysis tool. Shuey's (1985) approximation to the Zoeppritz reflectivity equations for reflected P-waves can be written as:

$$R_{pp}(\theta) = \underbrace{\frac{1}{2}\left[\frac{\Delta Z}{Z}\right]}_{A_{iso}\ (\text{intercept})} + \underbrace{\frac{1}{2}\left[\frac{\Delta\alpha}{\alpha} - \left(\frac{2\beta}{\alpha}\right)^2 \frac{\Delta G}{G}\right]}_{B_{iso}\ (\text{gradient})} \sin^2\theta + \underbrace{\frac{1}{2}\left[\frac{\Delta\alpha}{\alpha}\right]}_{C_{iso}\ (\text{curvature})} \sin^2\theta \tan^2\theta \qquad \text{.....(4.1)}$$

where R_{pp} is the P-wave reflection coefficient as a function of average incidence angle θ, α is the average vertical P-wave velocity, β is the average vertical SV-wave velocity, ρ is the average density, $Z = \rho\alpha$ is the average vertical P-waveimpedance, $G = \rho\beta^2$ is the average vertical shear modulus. The difference between parameters across the boundary are denoted as: $\Delta\alpha = \alpha_2 - \alpha_1$, $\Delta Z = Z_2 - Z_1$, $\Delta G = G_2 - G_1$.

By crossplotting AVO intercept (A) and gradient (B), Fig 4.1 shows an example of the typical AVO analysis method under isotropic assumption. The deviations form the background petrophysical trends, as would be caused by hydrocarbons, cause deviations from the background A versus B trend (note that the A-B trend of the gas sands does not pass through the origin) (Castagna, 1998). It should be noticed that the curvature (C) is a higher order coefficient that becomes increasingly important as θ increases. It is theoretically possible to subtract C from A to isolate density contrasts. In this way, there is the potential for distinguishing commercial gas accumulations from higher-density low gas-saturation.

Unfortunately, this method has met with mixed success in practice due to the poor signal/noise ratio of the C term (Swan, 1993) and the effects of anisotropy. In this chapter, the complications caused by local anisotropy (transverse isotropy) at the target are investigated. The exact and approximate reflection coefficients are also compared. In order to simplify the analysis, elliptical anisotropy is assumed.

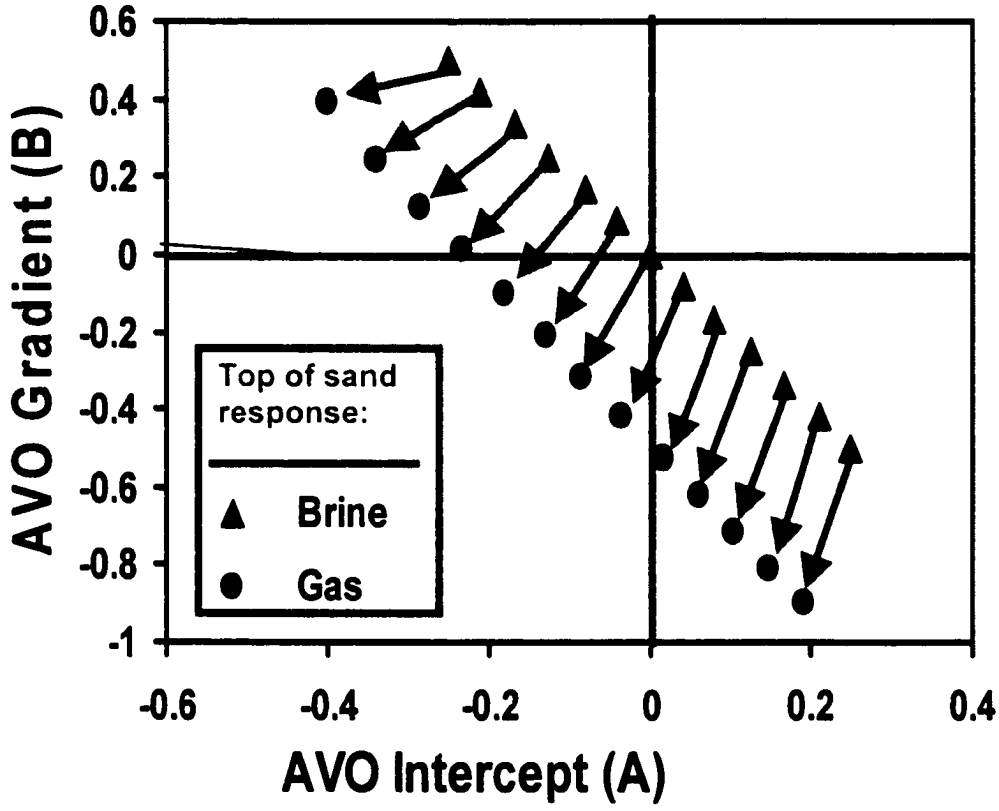

Figure 4.1 A synthetic hydrocarbon's anomaly on AVO A vs B crossplot under isotropic candition (Castagna, 1998)

The main conclusion of this research is that AVO gradient and curvature depend on absolute anisotropy in addition to anisotropy contrasts. Existing isotropic approximations may be particularly inadequate for the curvature term.

4.2 Anisotropic Effects on A vs. B and A vs. C crossplots

Crossplotting of A, B and C parameters can be a useful AVO analysis tool (Smith, 1996). In this section, we define some anisotropic corrections to the B and C terms for isotropic media. These corrections will be used later to quantify the effects of anisotropy on A vs. B and A vs. C crossplots.

Daley and Hron (1977) derived the exact equations for reflection coefficients as a function of angle of incidence, R(θ), in VTI media. Since then, numerous linearized approximations of R(θ) have been derived (Ruger 1997, Banik 1987, Thomsen 1986, etc.). Among these, Ruger's approximation is particularly useful and can be expressed in Shuey's (1985) form:

$$R_{pp}(\theta) = \underbrace{\frac{1}{2}\left[\frac{\Delta Z}{Z}\right]}_{A_{Rug}} + \underbrace{\frac{1}{2}\left[\frac{\Delta\alpha}{\alpha} - \left(\frac{2\beta}{\alpha}\right)^2 \frac{\Delta G}{G} + \Delta\delta\right]}_{B_{Rug}} \sin^2\theta + \underbrace{\frac{1}{2}\left[\frac{\Delta\alpha}{\alpha} + \Delta\varepsilon\right]}_{C_{Rug}} \sin^2\theta \tan^2\theta \quad \text{....(4.2)}$$

(intercept) (gradient) (curvature)

Using the isotropic terms A_{iso}, B_{iso} and C_{iso}, this approximation can be rewritten in the following form:

$$\begin{cases} A_{Rug} = A_{iso} \\ B_{Rug} = B_{iso} + \Delta B_{Rug} \\ C_{Rug} = C_{iso} + \Delta C_{Rug} \end{cases} \quad \text{.....(4.3)}$$

where B_{iso} and C_{iso} are Shuey's isotropic coefficients and ΔB_{Rug} and ΔC_{Rug} are anisotropic corrections. From equation (4.2):

$$\begin{cases} \Delta B_{Rug} = \dfrac{\Delta\delta}{2} \\ \Delta C_{Rug} = \dfrac{\Delta\varepsilon}{2} \end{cases} \quad \text{.....(4.4)}$$

where δ and ε are Thomsen's anisotropy parameters. $\Delta\delta$ and $\Delta\varepsilon$ are the differences in anisotropy parameters across the boundary (value for top medium minus value for bottom medium). Equation (4.5) means that only contrasts in anisotropy parameters effect gradient and curvature.

For the purpose of comparing and judging the anisotropic corrections, "exact" AVO parameters are computed as described below:

For an interface between two TI media, the exact reflection coefficient R_{ext} versus angle values are generated using Daley and Hron's equations. Then, a multiple non-linear regression in the form of:

$$R_{ext}(\theta) = A_{ext} + B_{ext}(\sin^2\theta) + C_{ext}(\sin^2\theta\tan^2\theta) \quad \text{.....(4.5)}$$

is used to curve fit the R_{ext} samples out to an incidence angle of 30°. Figure 4.3 shows an example where the results of the fit yield the "exact" AVO parameters A_{ext}, B_{ext}, and C_{ext}, which are, of course, not exact but a good three-term fit to the exact equation.

The difference between B_{Rug} and B_{ext} (or C_{Rug} and C_{ext}), if there is any, is an indication of difference between Ruger's approximation and the true reflection amplitude. Equation (4.6) is a good representation of the true reflection coefficient behavior, which we expect to be the case, for small parameter contrasts and small angles of incidence.

4.3 Procedure for building a synthetic model

In order to evaluate the effects of anisotropy upon AVO crossplots, a synthetic layered model of the earth was generated using well logs. This synthetic example is meant to be illustrative only. To simplify the analysis, anisotropy was assumed to be elliptical. A crossplot of the γ-ray and SP logs was used to classify the lithologies and quantitatively assign values for anisotropy. High anisotropy (larger value of δ and ε) was assigned to the more shale-prone portions of the log and lower anisotropy to the sand-prone portions of the log. Using this approach, anisotropy values of 0, 0.1, 0.2, 0.3 were assigned to layers in units according to their location on the SP versus γ-ray crossplot. Table 4.1 shows all the possible anistropic boundary contrast types allowed in this synthetic model study. The sonic log was used to obtain P-wave velocities and the shear-wave velocity was predicted using either a constant V_p/V_s ratio or the mudrock trend (Castagna et al., 1985).

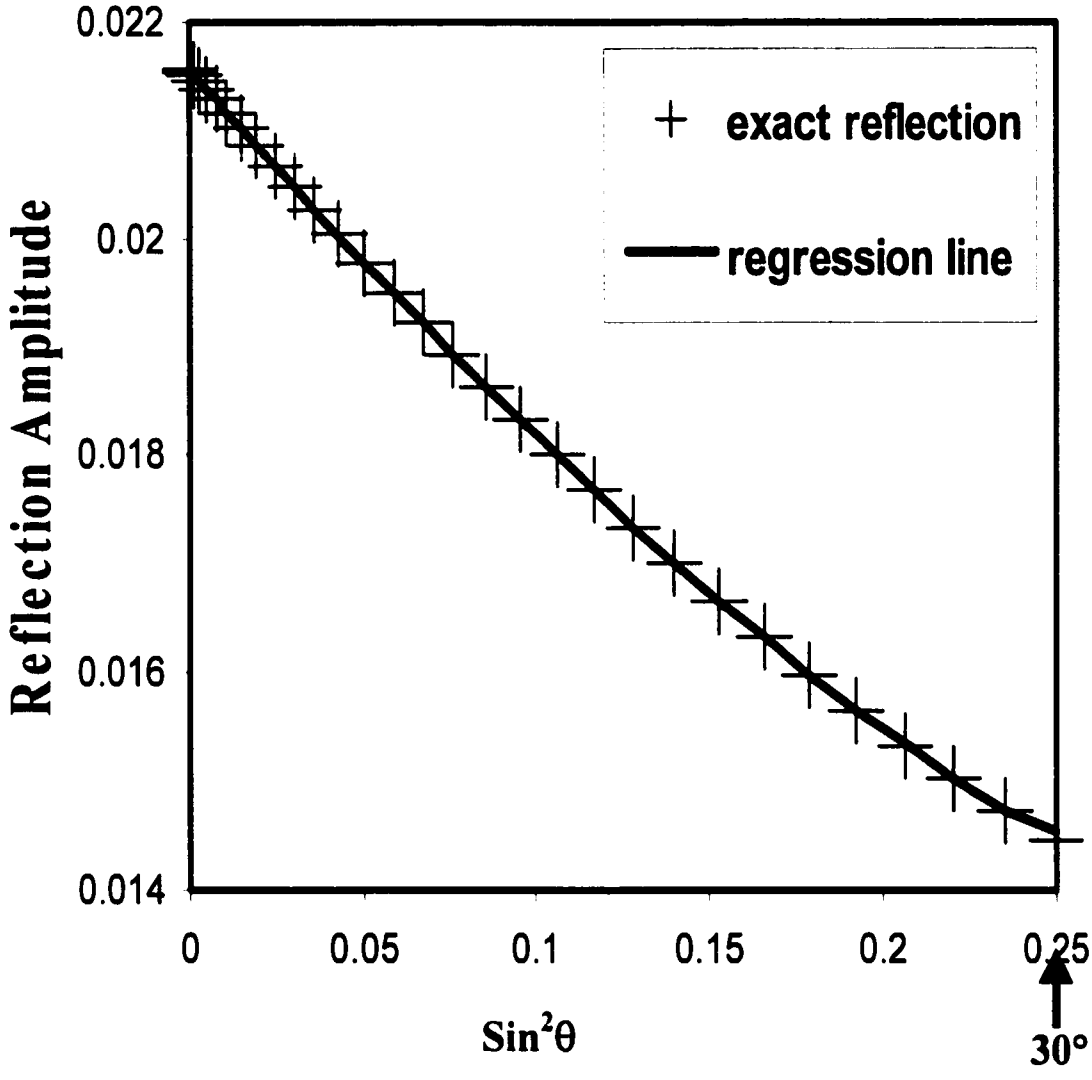

Figure 4.2 An example showing the good fit between the three-term regression line of $R_{ext}(\theta) = A_{ext} + B_{ext}(sin^2\theta) + C_{ext}(sin^2\theta\, tan^2\theta)$ and exact P-wave reflection coefficient curve

Once the layered model of the earth was constructed, the A, B and C terms for each reflector were computed using the "exact" and approximate methods, and the computed values of A, B, and C were crossplotted. The discussion of these results is given in the next section.

4.4 The empirical correction to Ruger's approximation

Even for angles of incidence less than 30°, large errors may result from analytical approximations, obtained by neglecting higher-order terms in the expansion of the exact reflection coefficient equations. Thus, corrections to existing approximations may be desired. We found empirical corrections, ΔB_{emp} and ΔC_{emp}, to Ruger's approximation to be useful for specific circumstances. These are introduced to the B and C terms as follows:

$$\begin{cases} B_{emp} = B_{iso} + \Delta B_{Rug} + \Delta B_{emp} \\ C_{emp} = C_{iso} + \Delta C_{Rug} + \Delta C_{emp} \end{cases} \quad \text{.....(4.6)}$$

where ΔB_{emp} and ΔC_{emp} are empirical anisotropic corrections.

By observing the difference between Ruger's AVO parameters and the "exact" ones, which are dependent on anisotropy variation, the empirical relationship between ΔB_{emp} or ΔC_{emp} with δ and ε were found using trial and error to obtain the forms:

$$\begin{cases} \Delta B_{emp} = A(b_1\delta^{\frac{1}{2}} + b_2\Delta\delta) \\ \Delta C_{emp} = c_0A^2 + c_1A\varepsilon + c_2A^2\varepsilon + c_3(\Delta\varepsilon)^2 \end{cases} \quad \text{.....(4.7)}$$

Table 4.1 Anisotropic Boundary Contrast Types

Difference of Anisotropy	Contrast Types			
-0.3	0.3/0			
-0.2	0.3/0.1	0.2/0		
-0.1	0.3/0.2	0.2/0.1	0.1/0	
0	0.3/0.3	0.2/0.2	0.1/0.1	0/0
0.1		0.2/0.3	0.1/0.2	0/0.1
0.2			0.1/0.3	0/0.2
0.3				0/0.3

where b_1, b_2, c_0, c_1, c_2, and c_3, are regression coefficients that are functions of the compressional-to-shear-wave velocity ratio (V_p/V_s), and δ and ε are the average Thomson parameters across the interface. The empirical corrections depend on the changes in anisotropy as well as the average anisotropy across the reflecting boundary.

4.5 Observations

For the simple case of constant compressional-to-shear-wave velocity ratio shown in Figure 4.3, regression lines are plotted for each group defined by constant $\Delta\delta$. The regression passes through the origin when $\Delta\delta$ is zero, but has an increasing B-intercept as the magnitude of $\Delta\delta$ increases. The lines for different $\Delta\delta$ are not parallel nor

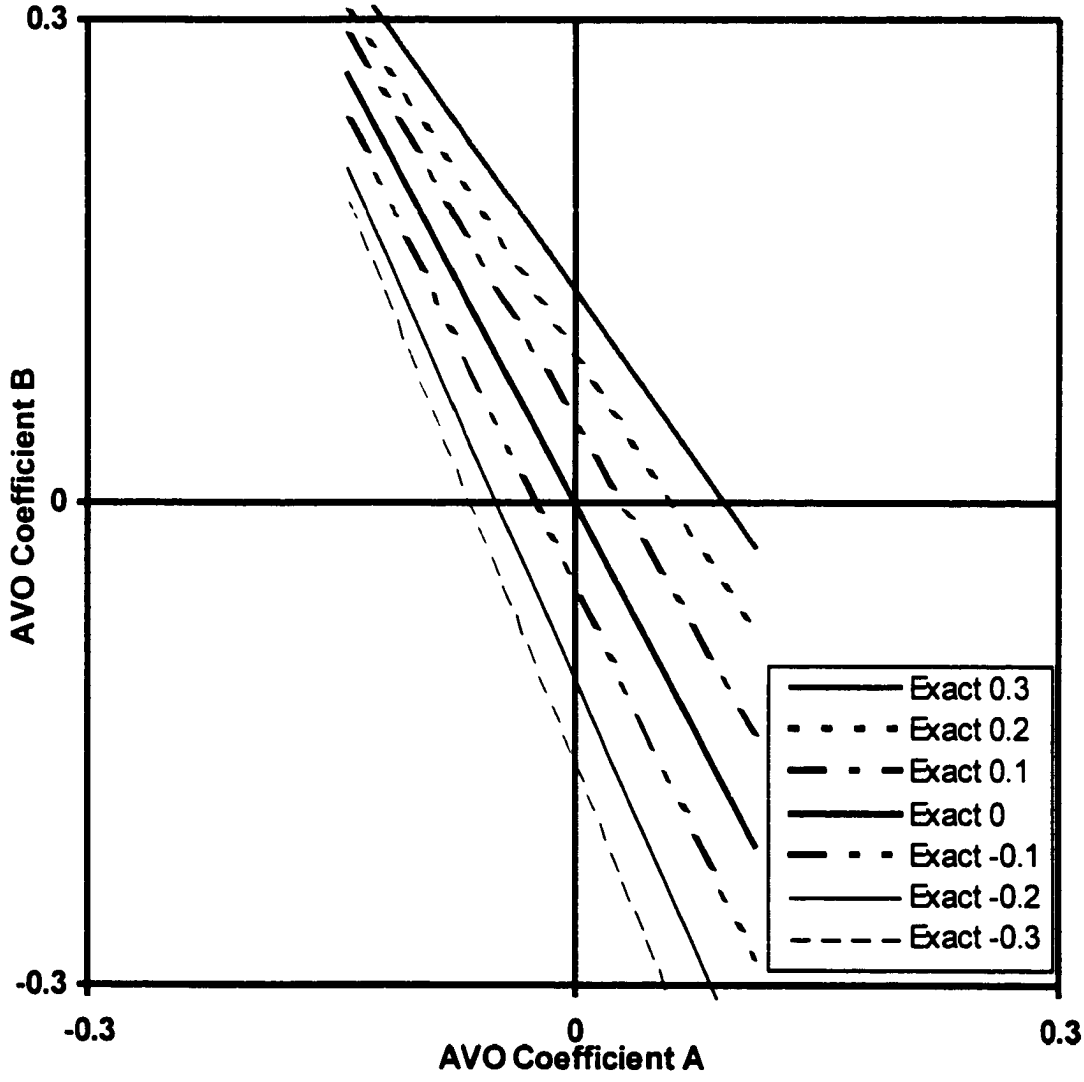

Figure 4.3 AVO coefficient trends obtained from 3-term fit to the exact Daley and Hron (1977) equations for a constant compressional-to-shear velocity (V_p/V_s) ratio of 1.8 and $\Delta\delta$ of 0.3 (gray line), 0.2 (short dashed line), 0.1 (long-short dashed line), 0 (thick solid line), -0.1 (long-short-short dashed line), -0.2 (thin solid line), -0.3 (long dashed line).

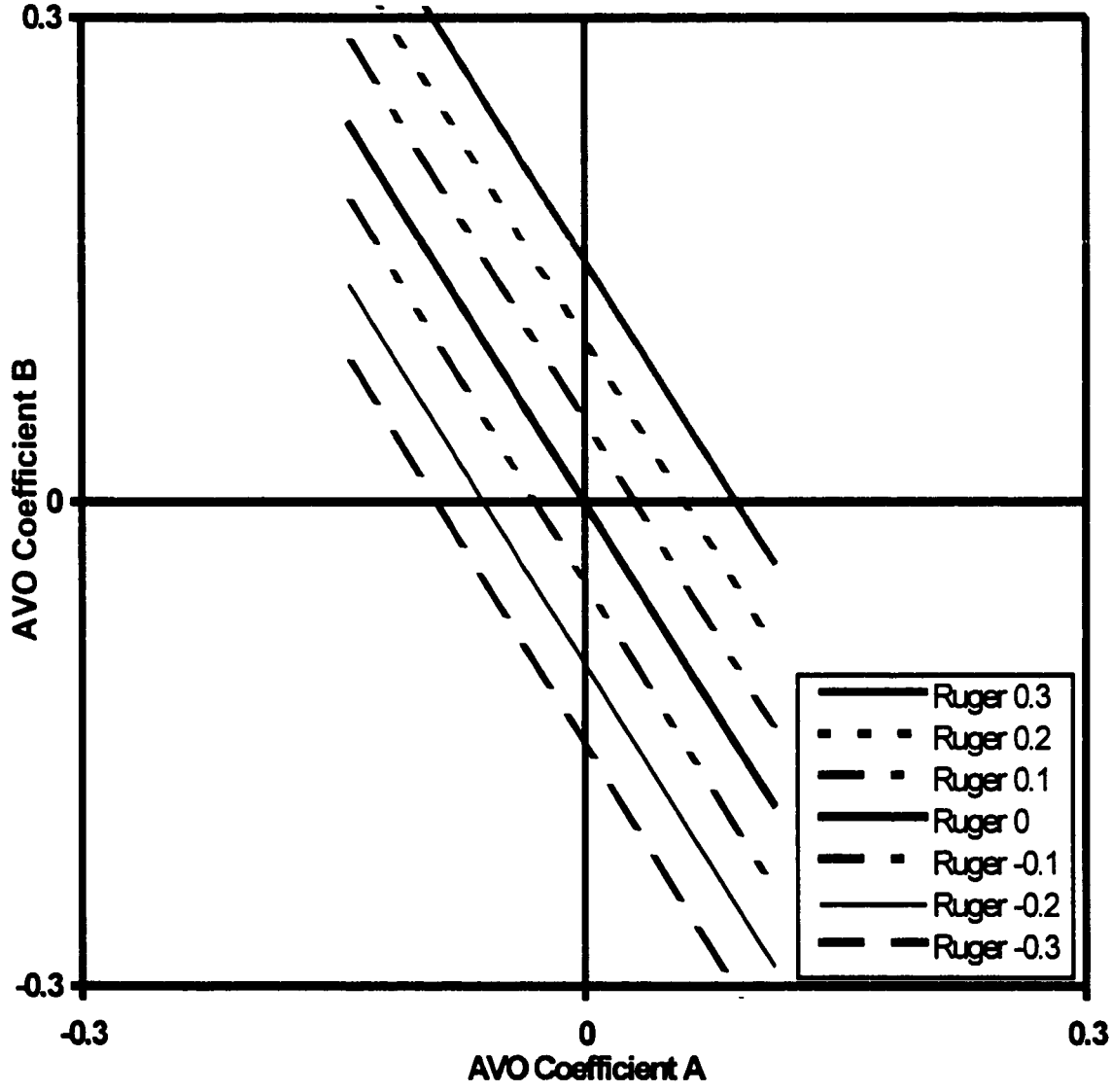

Figure 4.4 AVO coefficient trends obtained from the Ruger (1997) approximation for a constant V_p/V_s ratio of 1.8 and $\Delta\delta$ of 0.3 (gray line), 0.2 (short dashed line), 0.1 (long-short dashed line), 0 (thick solid line), -0.1 (long-short-short dashed line), -0.2 (thin solid line), -0.3 (long dashed line).

symmetrical about the $\Delta\delta = 0$ line. In contrast, Ruger's equation predicts that these lines should be parallel and spaced at equal intervals with a smaller magnitude B-intercept when $\Delta\delta$ is positive, but a larger magnitude B-intercept when $\Delta\delta$ is negative at $A = 0$ (see Figure 4.4). Examination of Ruger's equation in Figure 4.4 indicates that increasing anisotropy affects the B-intercept, ***but not the slope***, on an A versus B crossplot.

For the B term correction, the dependence on the average δ value across the boundary is evident in Figure 4.5, which crossplots all the exact and approximate A-B pairs with $\Delta\delta=0$ and a constant V_p/V_s (=1.8). B_{Rug} keeps the same slope which almost agrees with B_{ext} for isotropic layers. On the other hand, B_{ext} exhibits a slope variation as δ changes. The correction dependence on δ is contained in the empirical factor b_1, while the factor b_2 controls a similar slope correction related to $\Delta\delta$.

With the same synthetic model used to generate Figure 4.5, all the "exact" and approximate A-C pairs are crossploted in Figure 4.6. It clearly shows that a C term correction dependent on the average ε value is necessary. In addition to larger slope changes, the non-linearity of each group of A_{ext} - C_{ext} pairs suggests a higher-order correction associated with A. The c_0 coefficients effects non-linearity also. Notice in Figure 4 that the isotropic/isotropic A_{ext} - C_{ext} group (circles in Figure 4.6) also is non-linear, with the A_{Rug} - C_{Rug} pairs forming a tangent line to the trend at A=0. Non-linear regression shows that a c_0A^2 term can be introduced (equation 4.8) to improve the fit of A_{Rug}- C_{Rug} to the exact isotropic/isotropic trend. This c_0A^2 correction is thus also needed for isotropic approximations to the Zoeppritz equations (eg. Shuey, 1985; Aki and Richards, 1980). We empirically find that c_0 is approximately unity for the cases studied.

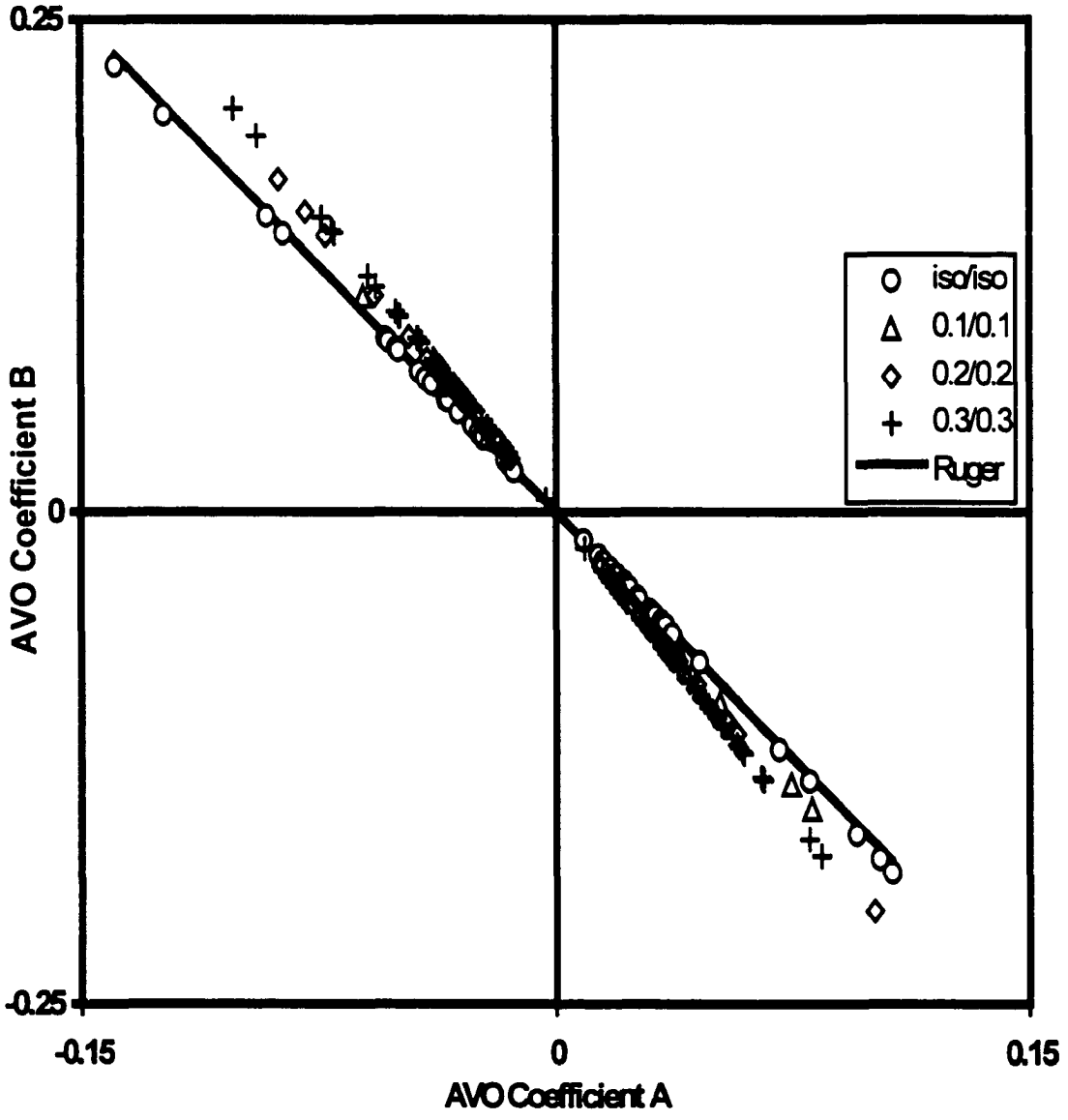

Figure 4.5 A versus B crossplot for a constant velocity ratio of 1.8 with $\Delta\delta = 0$. Solid line is Ruger (1997) prediction. Symbols are AVO coefficients obtained by non-linear regression of the exact Daley and Hron (1977) curves.
Circle: isotropic media. Triangle: $\delta = 0.1$ above and below the interface. Diamond: $\delta = 0.2$ above and below the interface.
Plus Sign: $\delta = 0.3$ above and below the interface

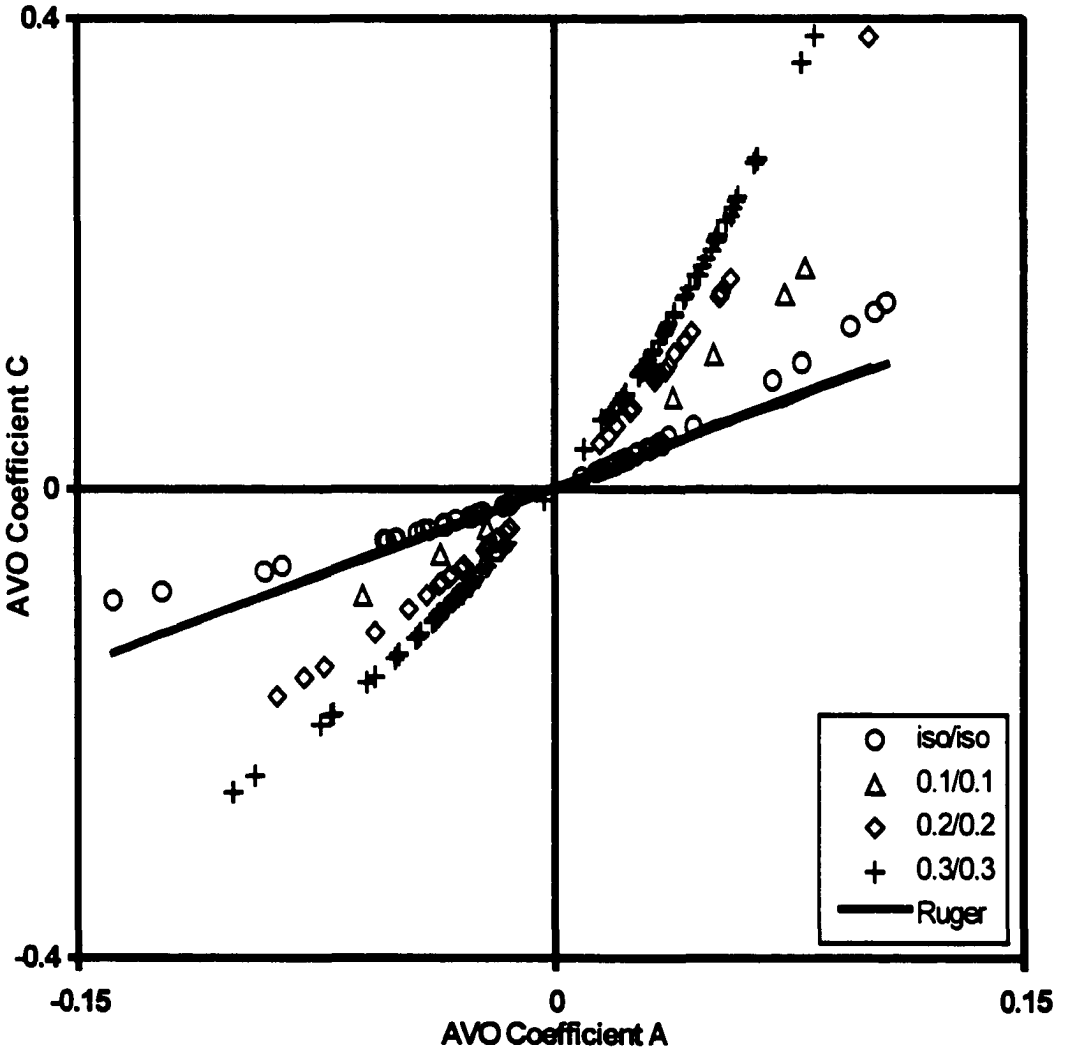

Figure 4.6 A versus C crossplot for a constant V_p/V_s ratio of 1.8 with $\Delta\varepsilon = 0$. Solid line is Ruger (1997) prediction. Symbols are AVO coefficients obtained by non-linear regression of the exact Daley and Hron (1977) curves.
Circle: isotropic media. Triangle: $\varepsilon = 0.1$ above and below the interface. Diamond: $\varepsilon = 0.2$ above and below the interface.
Plus Sign: $\varepsilon = 0.3$ above and below the interface.

With constant V_p/V_s ratio (=1.8), we find by regression that the empirical coefficients are b_1=-0.68, b_2=1.75, c_0=1.00, c_1=8.42, c_2=26.69, and c_3=0.86. Figure 4.7 shows that the empirical A_{emp} vs. B_{emp} fit the "exact" A_{ext} vs. B_{ext} trends well under two kinds of anisotropic conditions. Compared with the performance of Ruger's A_{Rug} vs. C_{Rug} in Figure 4.6, Figure 4.8 shows a distinct improvement in approximating C using the empirical equations (equation 4.8). These coefficients will vary with V_p/V_s ratio. However, for the special case of rocks that follow the mudrock trend and Gardner relation, the empirical coefficients were found to be simple scalars with b_1=-0.74, b_2=1.04, c_0=1.00, c_1=6.67, c_2=10.86 and c_3=0.81. Figure 4.9 shows that the B_{emp} (solid circle) trend fits the B_{ext} (solid line) well. Figure 4.10 is a crossplot of C_{ext} vs. C_{emp} (solid circle) and C_{Rug} (open circle). The empirical predictions fall, for the most part, close to the diagonal (solid line) indicating that the exact C term is well approximated. Only boundaries in which some anisotropy was involved (at least the upper or lower medium was anisotropic) are shown in Figure 4.9 and 4.10. The two figures indicate that, under mudrock and elliptical TI assumptions, the empirical equations (4.8) can provide a good approximation for the PP reflection coefficient.

4.6 Conclusions and Discussion

In this synthetic model study, four important conclusions are found:

1) Anisotropy above and below an interface effects the AVO gradient (B) and curvature (C). On an A versus B crossplot, anisotropy may cause large changes in the B-intercept (which can be mistaken for Poisson's ratio deviations) and may also cause minor changes in slope.

2) On an A versus C crossplot, large differences may occur in both C-intercept (which can be mistaken for density contrasts), slope, and curve shape. According to Shuey's equation, an A versus C crossplot should be linear with a slope of one.

3) Even in the isotropic case, distinct curvature appears in the A versus C crossplot, which is not predicted by Shuey's equation. An A^2 term must be added to the C-term to obtain linearity in the isotropic case. Deviation from this slope can be a direct indication of anisotropy.

4) Empirical approximations provide insight into anisotropic effects on AVO.

Ignoring signal-to-noise problems, our results for a synthetic model suggest that, even for reasonable velocities and anisotropic parameters, Ruger's approximation is probably not sufficient for a quantitative A vs. C crossplot interpretation, even if C could be extracted reliably from the seismic data. Empirical corrections to Ruger's equation were obtained, suggesting that the three-parameter Shuey form may be adequate for fitting anisotropic (elliptical TI) AVO effects, for the case of elliptical TI. Recalibration and/or form modification of these empirical equations for other anisotropy or V_p/V_s conditions is expected to be necessary.

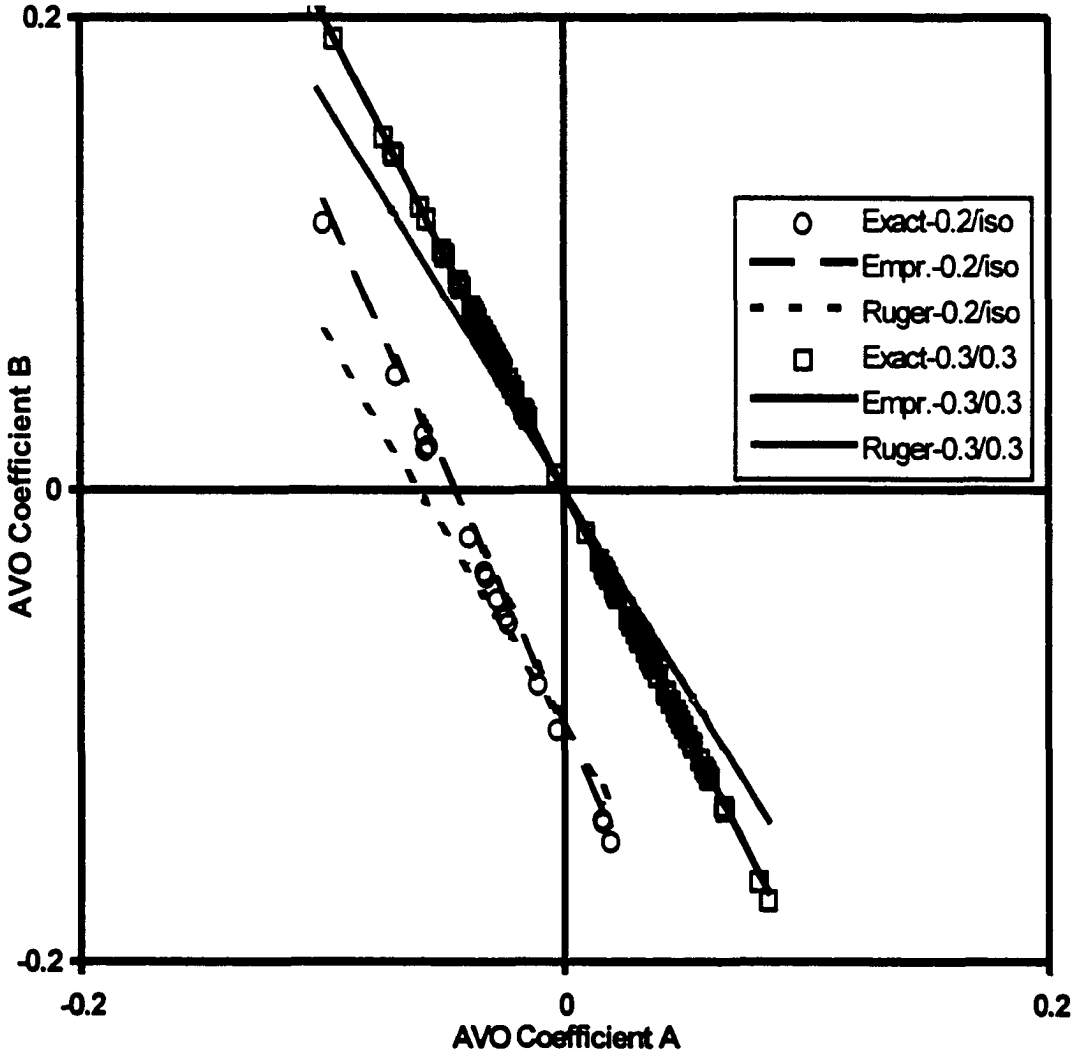

Figure 4.7 A versus B crossplot for a constant V_p/V_s ratio of 1.8 with two cases of different $\Delta\delta$. Symbols are AVO coefficients obtained by non-linear regression of the exact Daley and Hron (1977) curves. Lines represent approximate B calculated from Ruger's approximation or our empirical equation.

Case 1- $\Delta\delta = 0$ and $\delta = 0.3$ above and below the interface: Square: Daley exact. Solid lines: empirical. Grey line: Ruger.

Case 2- $\Delta\delta = 0.2$ and $\delta = 0.2$ above and isotropic medium below the interface: Circle: Daley exact. Long-dashed lines: empirical. Short dashed line: Ruger's.

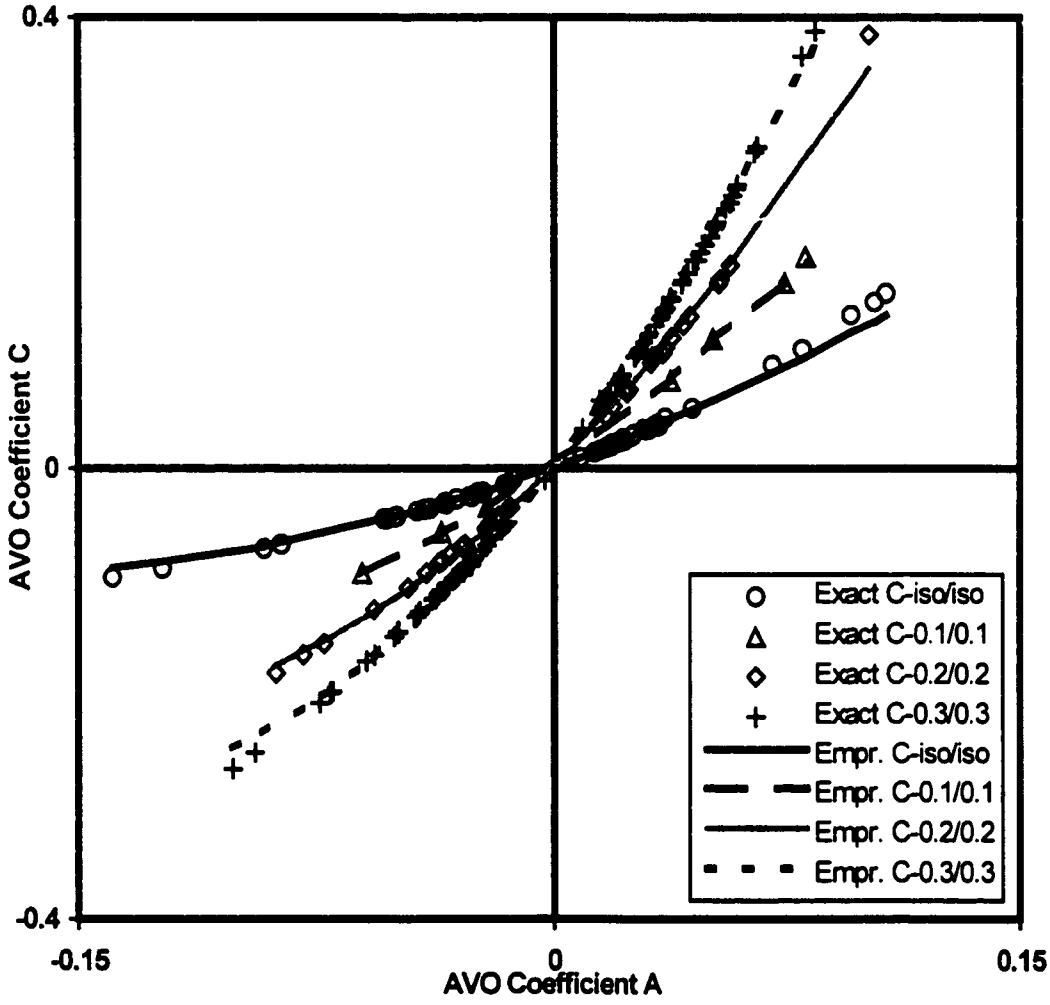

Figure 4.8 A versus C crossplot for a constant V_p/V_s ratio of 1.8 with $\Delta\varepsilon = 0$. Lines represent approximate C calculated from the empirical equation. Solid line: isotropic media. Long-dashed line: $\varepsilon = 0.1$ above and below the interface. Gray line: $\varepsilon = 0.2$ above and below the interface. Short-dashed line: $\varepsilon = 0.3$ above and below the interface. Symbols are AVO coefficients obtained by non-linear regression of the exact Daley and Hron (1977) curves. Circle: isotropic media. Triangle: $\varepsilon = 0.1$ above and below the interface. Diamond: $\varepsilon = 0.2$ above and below the interface. Plus Sign: $\varepsilon = 0.3$ above and below the interface.

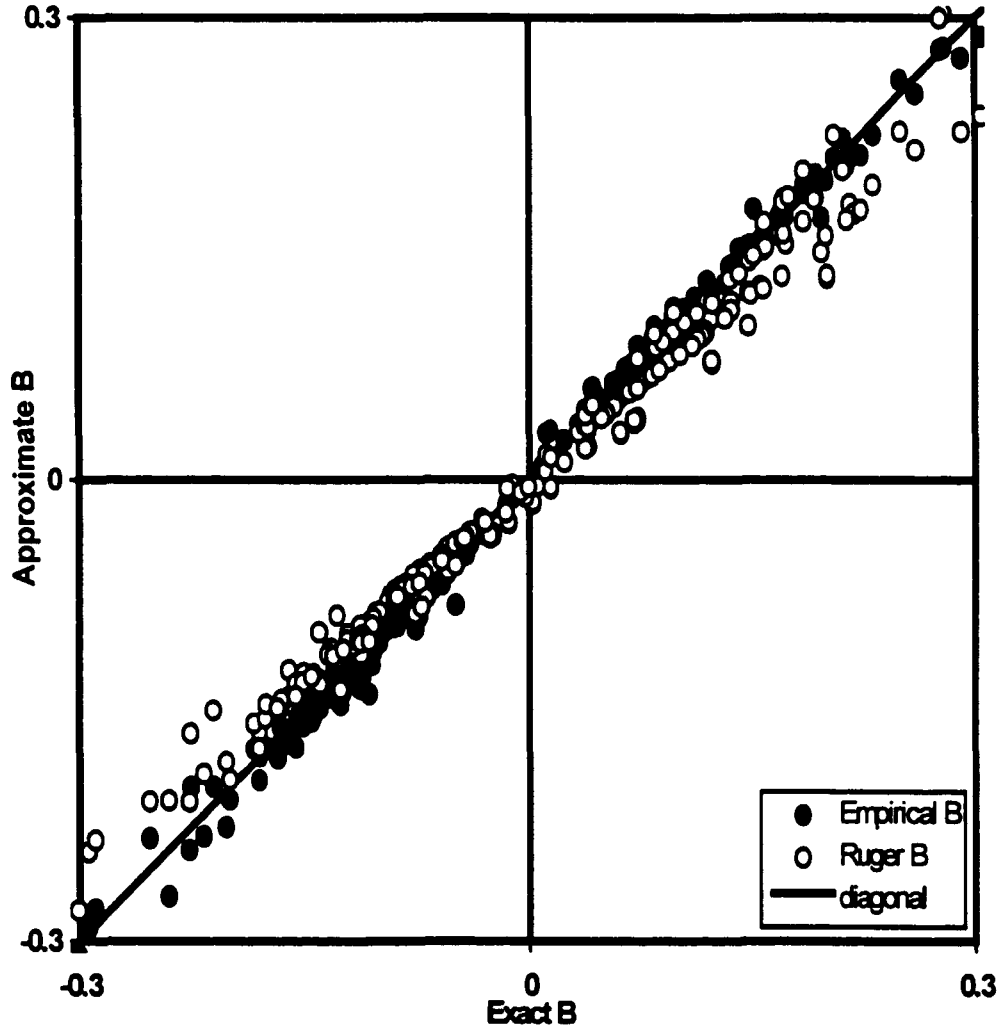

Figure 4.9 Comparison of B extracted from 3-term fit to exact Daley and Hron (1977) curves for mudrocks and approximate B calculated from Ruger (1997) equation (open circles) and empirical equation (solid circles). The diagonal represents perfect agreement between approximate and "exact" B.

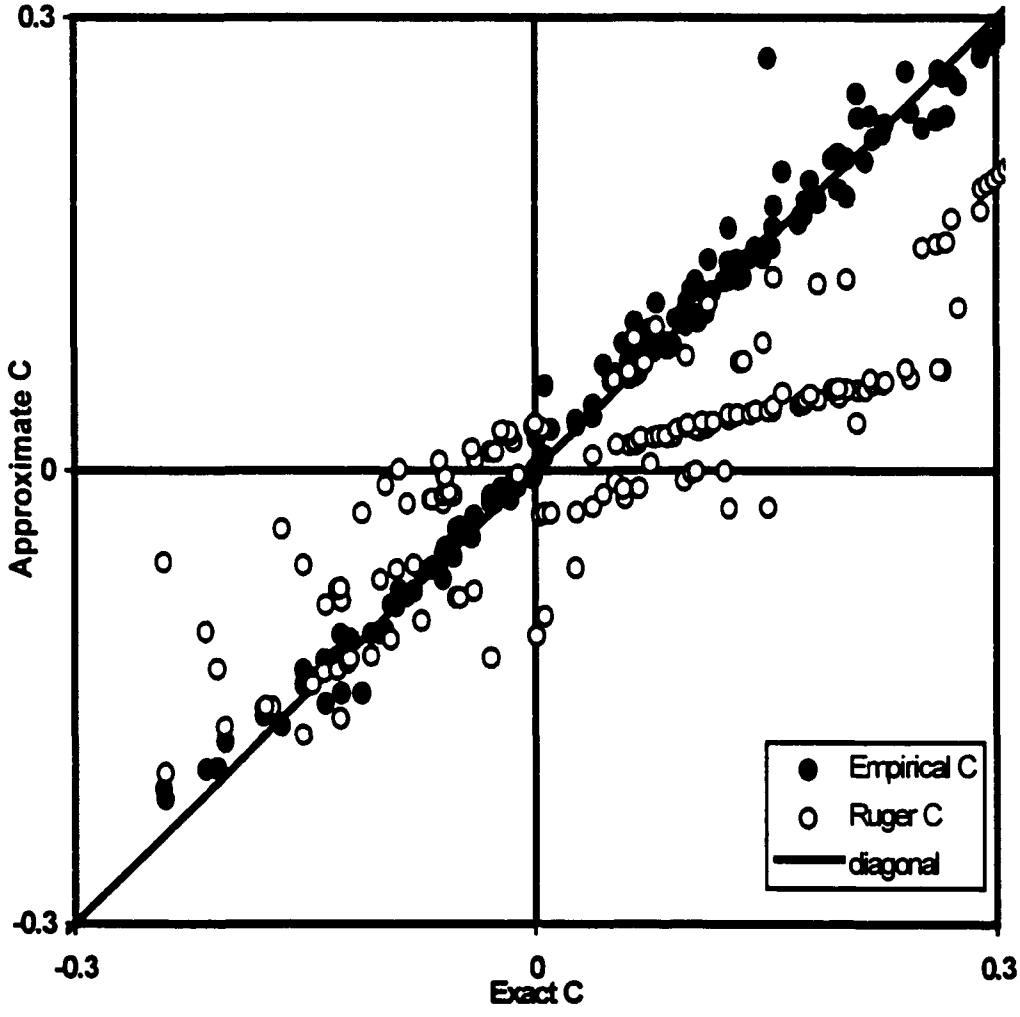

Figure 4.10 Comparison of C extracted from exact Daley and Hron (1977) curves for mudrocks and approximate C calculated from Ruger (1997) equation (open circles) and empirical equation (solid circles). The diagonal represents perfect agreement between approximate and "exact" C.

Chapter5

Anisotropic Effects on Full and Partial Stacks

5.1 Introduction

Anisotropic effects on seismic stacked sections are often ignored during conventional processing. Using anisotropic ray-trace models, this paper shows that many interpretation pitfalls may appear on stacked sections simply due to the existence of anisotropy.

Simple models, which consist of a localized transversely isotropic (TI) block embedded in a layered isotropic medium, are used. The symmetry axis of the TI blocks is assumed to be vertical in all models. Geologically, these models might apply to local changes in layering (apparent aniostropy) or local changes in shale properties (intrinsic anisotopy).

5.2 Method

Ray-tracing is used to generate the anisotropic P-wave seismic synthetic data assuming (Fagin, 1991):

1) Reflection raypaths are in the plane of the seismic section.
2) Reflection arrival times and lateral position are not subject to image ray effects.

The P-wave reflection coefficient during ray-tracing is calculated by Ruger's approximation (equation (3.22)) (Ruger, 1997). Using approximations will result in

incorrect reflection coefficients for large angles of incidence. However, the equation is adequate for demonstration purposes.

The models consist of three-horizontal-layers over a half space (Figure 5.1). A VTI block is embedded in either the first layer (for a near-surface VTI case study), or the second layer (for the deeper VTI case study). Table 5.1 lists the parameters of the models. The anisotropy of the VTI block is described by using anisotropy coefficients ε and δ (Thomsen, 1986). In the VTI block, the vertical velocity is always set equal to the isotropic velocity of the same interval. The ε value is set to be 10% for a weak anisotropy case, and 30% for a strong anisotropy case. Elliptical anisotropy is assumed in all the VTI blocks, so that $\delta = \varepsilon$. Although elliptical anisotropy is not physically realistic, some of the artifacts in processing should be similar to actual observations.

The forward modeling is performed by assembling 48-fold synthetic data across the whole line (offset range: 0 ~ 2350m, offset interval: 50m). The near stack is made of the 24 near traces, and the far stack made of the 24 far traces. Random noise is added to the model data to simulate a realistic stacked section.

5.3 Anisotropic Effects on CDP Gather and Velocity Spectrum

The effect of anisotropy upon CDP gathers is important because it distorts the moveout curve and directly affects the estimated stacking velocity spectrum.

For VTI media, the phase and group velocities change with angle of propagation through the medium. As a result, the near trace stack, the far trace stack, and the full stack can only be fit by the hyperbolic moveout curve over a limited range of offsets. The problem is one of attempting to fit the true non-hyperbolic moveout with an

Model 1

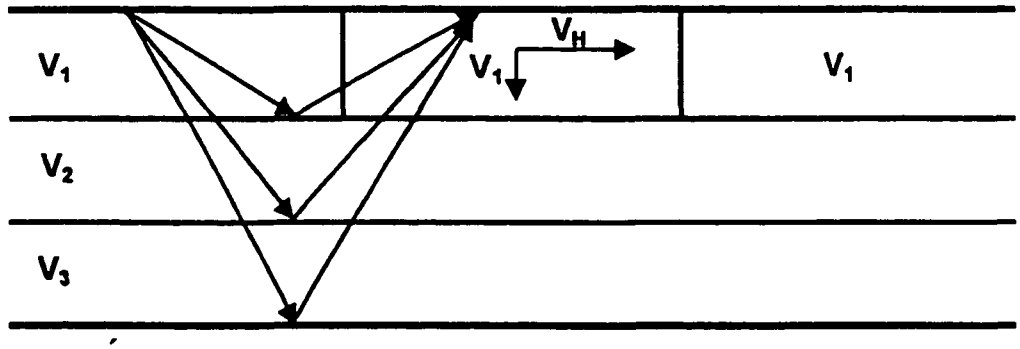

Model 2

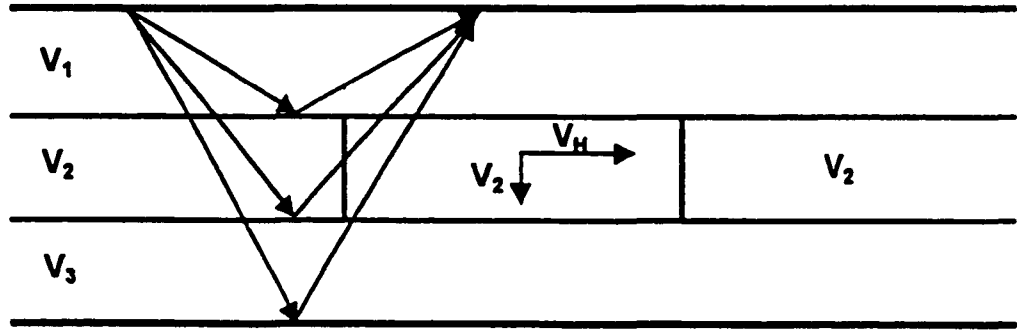

Figure 5.1 Model geometries (parameters defined in Table 1)

Table 5.1 Model Information

		1st layer	2nd layer	3rd layer	VTI block
Model 1	Vp (m/s)	1700	2000	3000	1700
	Vs (m/s)	850	1000	1500	850
	Density (g/cm^3)	1.6	2	2.4	1.6
	epsilon				10% ~ 30%
	delta				10% ~ 30%
	Thickness (m)	800	1000	1200	800
Model 2	Vp (m/s)	1700	2000	3000	2000
	Vs (m/s)	850	1000	1500	1000
	Density (g/cm^3)	1.6	2	2.4	2
	epsilon				10% ~ 30%
	delta				10% ~ 30%
	Thickness (m)	800	1000	1200	1000

assumed hyperbolic formula. This means that noise is introduced to the full or partial stack as a result of ignoring the anisotropy. This section describes how this non-hyperbolic noise affects the CDP gather and ultimately the interpretation.

Figure 5.2 shows 3 CDP gathers plotted on top of each other for a 30% near-surface anisotropy case similar to model 1. CDP gather 1 shows a perfect hyperbolic curve, meaning all the raypaths are within the isotropic region. However, CDP gathers 2 and 3 show that, due to the anisotropy, the curves are non-hyperbolic. This means part, or all of the raypaths of the CDPs pass through the anisotropic region.

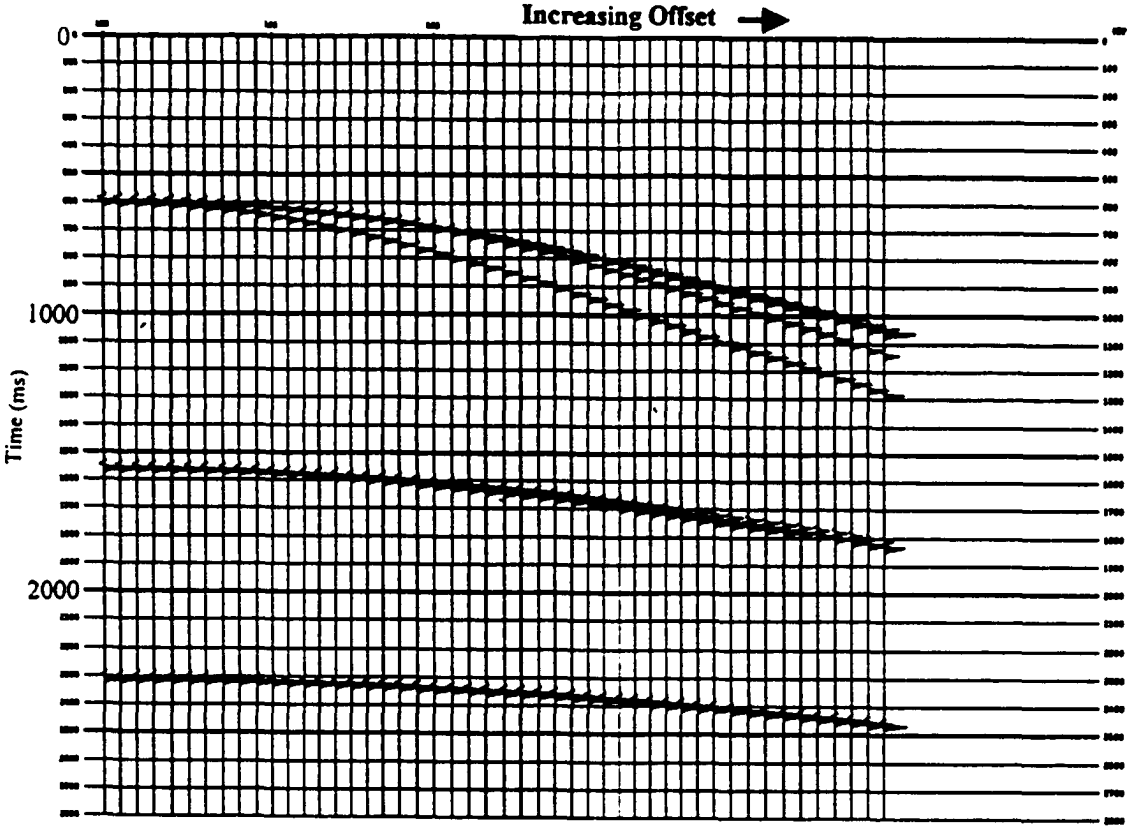

Figure 5.2 Three superimposed CDP gather showing the effects of anisotropy on reflector moveout

(1 = CDP gather in isotropic region; 2 = part of CDP gather in isotropic region while the other in anisotropic region; 3 = CDP gather in anisotropic region)

It is obvious that this near-surface anisotropy has stronger effects on shallow reflections. As a result we can see only small non-hyperbolic moveout remaining on the far end of the second event in Figure 5.2.

Because of the existence of non-hyperbolic effects, picking a proper stacking velocity through conventional processing software without higher order corrections is difficult or impossible. An overestimate of velocity can usually result from the influence of anisotropy. Figures 5.3a and 5.3b show a comparison of velocity picks between purely isotropic and local anisotropic conditions. The very high velocity pick from Fig 5.3b results from the influence of near surface anisotropy.

5.4 Anisotropic Effects on Full and Partial Stacks

Stacking of events with non-hyperbolic moveout can produce apparent structures and responses including faulting, flat spots, folds, amplitude anomalies and AVO artifacts. Figures 5.4a and 5.4b are near-trace and far-trace stacks for 10% weak anisotropy in the TI block in model 1. After careful velocity picking, the anisotropic effect on the near- trace stack (Figure 5.4a) is almost removed. However, a pseudo-structure on the far-stack results from the improperly removed anisotropic effect. Figure 5.5 is a full-stacked section of the boxed portion of Figure 5.4b, in which a mild structure with a flat spot can be observed. This phenomenon is only a result of localized near-surface weak anisotropy. The pseudo flat spot is caused by the near offset traces which are correctly moved out, while the structure is due to far offset traces that have had too much NMO applied.

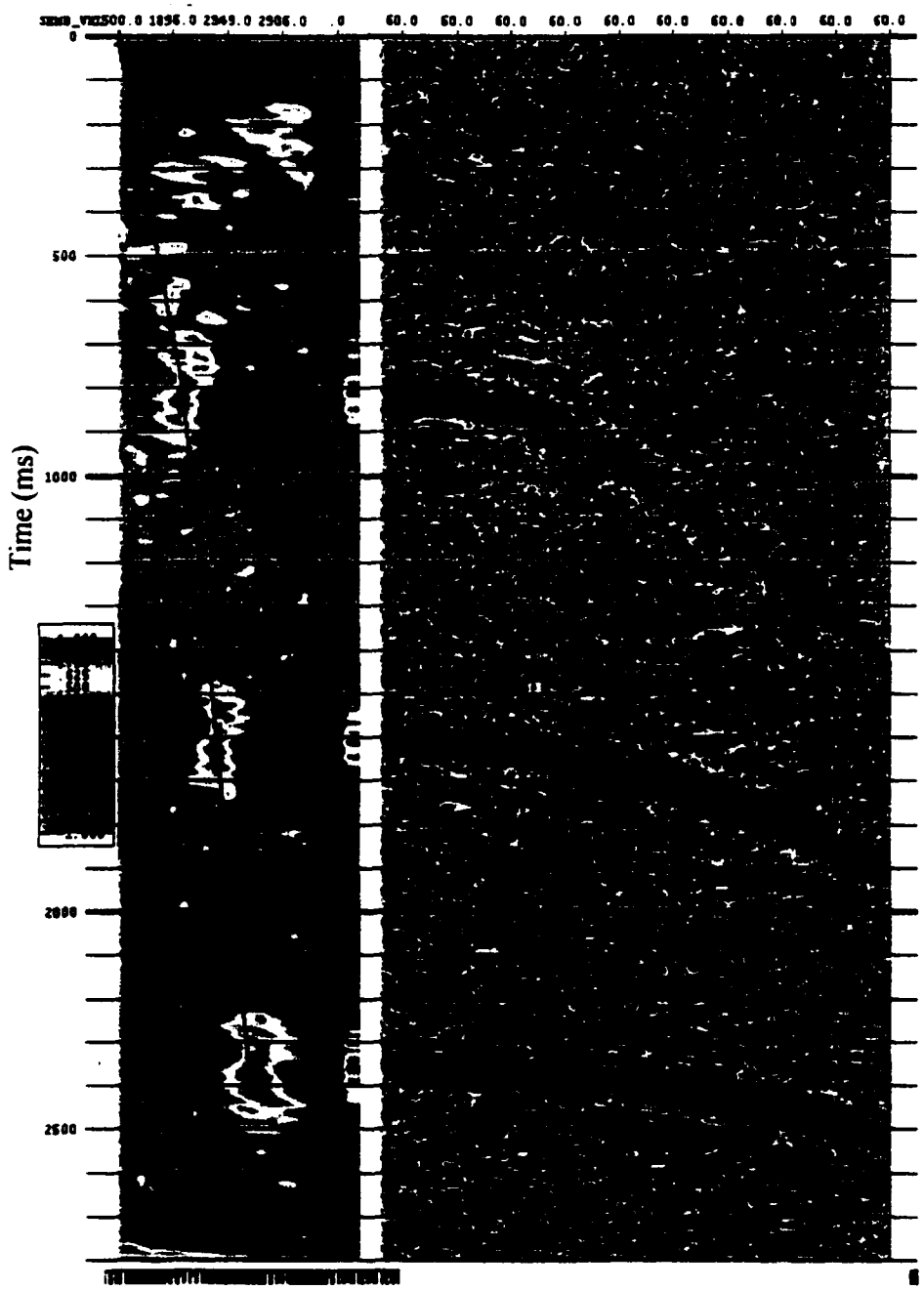

Figure 5.3a Semblance velocity analysis on isotropic CDP gather

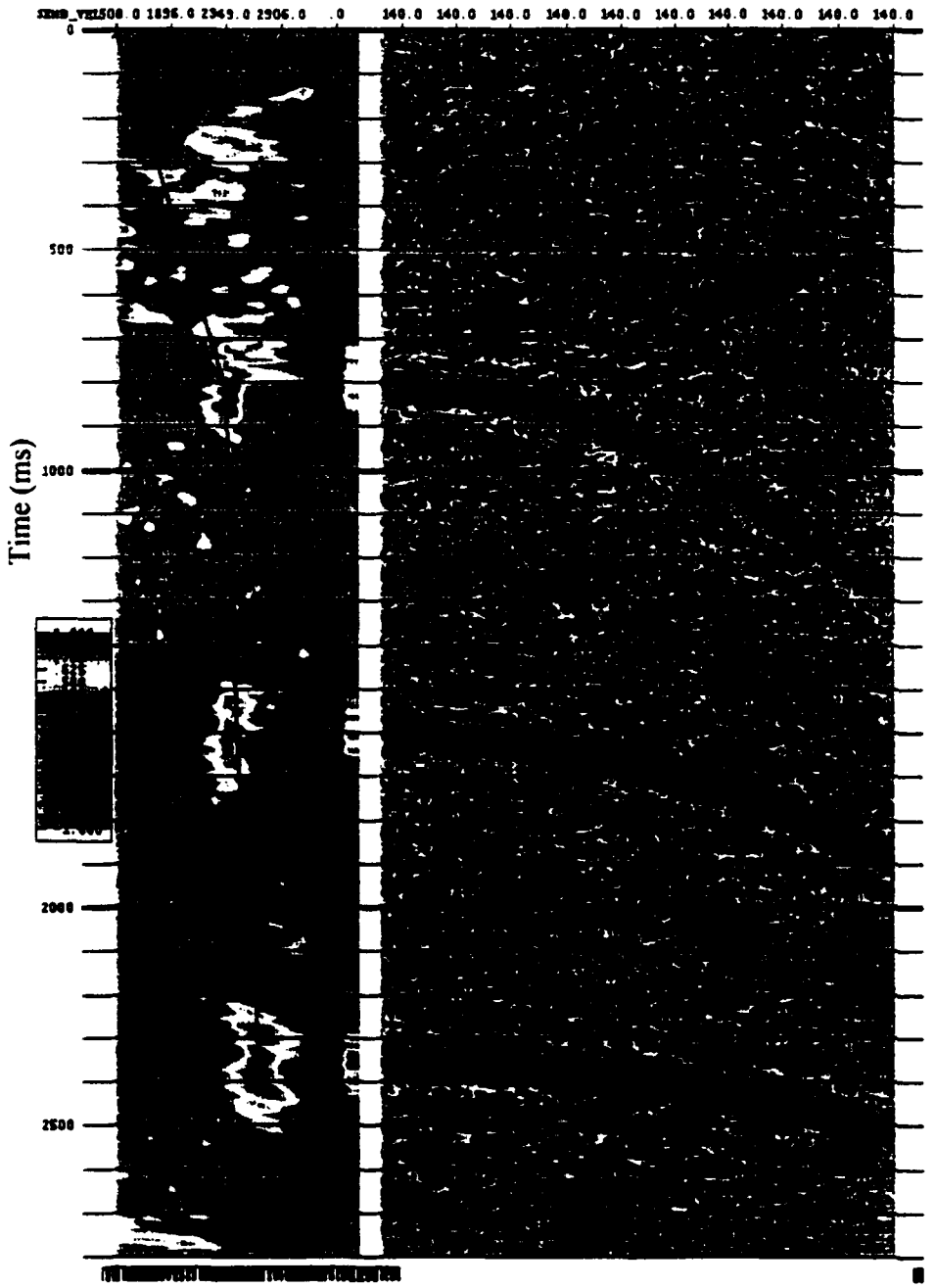

Figure 5.3b Semblance velocity analysis on anisotropic CDP gather

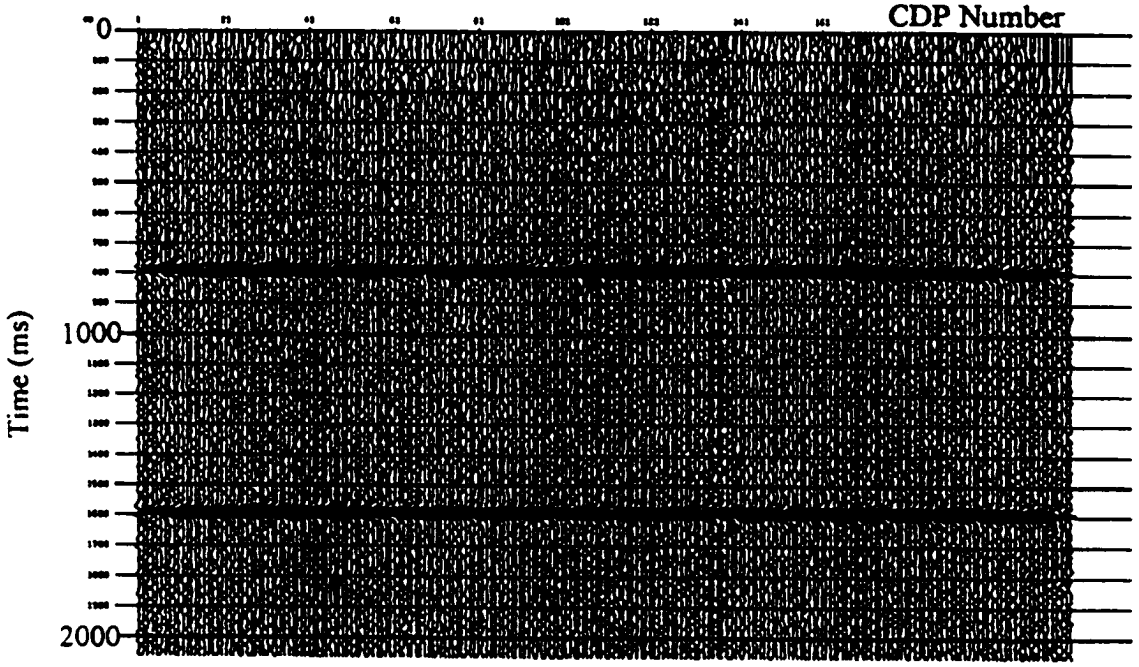

Figure 5.4a Near trace stack (10% anisotropy, Model 1)

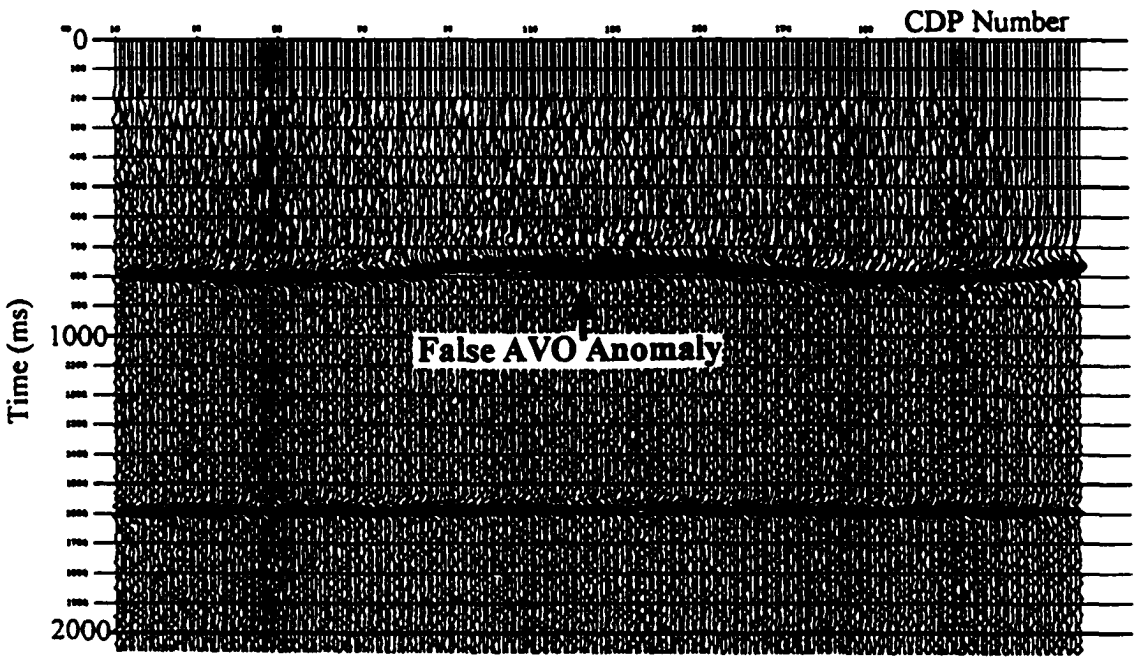

Figure 5.4b Far trace stack (10% anisotropy, Model 1)

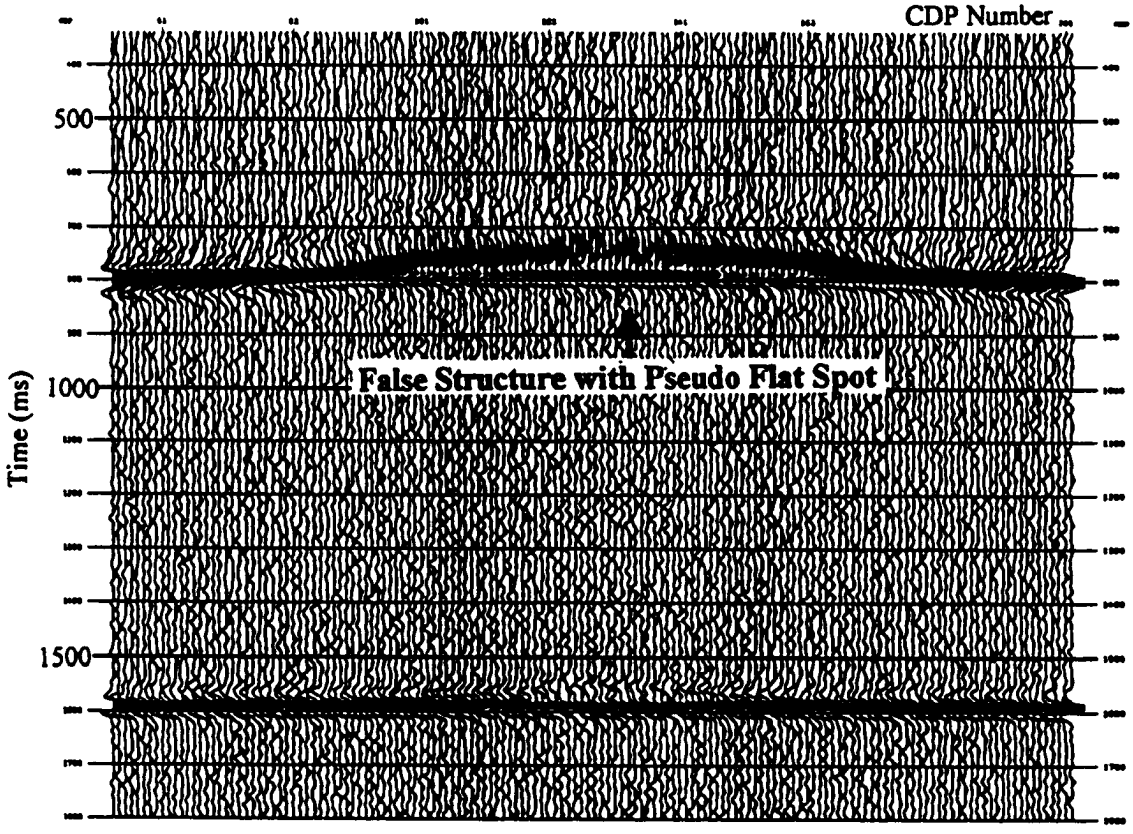

Figure 5.5 Full stack (10% anisotropy, Model 1)

By introducing stronger anisotropy of 30%, the effect on the near-trace stack becomes more serious and cannot be removed totally (Figures 5.6a and 5.6b). On the near-trace stack, an amplitude anomaly is observed irrespective of the chosen velocity. On the far-trace stack, this stronger anisotropy creates not only a structure for the shallow reflections, but also two apparent faults on the deep reflections.

If the near-surface anisotropy is totally ignored and only a constant RMS velocity is applied, some apparent channels may be introduced on the full-stack section as in Figure 5.7.

5.5 Depth Dependence of Anisotropic Effects

In this section, we make comparisons between the effects of a buried VTI block with those of a near-surface block. Figures 5.8a and 5.8b show the near and far trace stack when there is a buried VTI block with weak 10% anisotropic effects (model 2). While there is no effect on the near stack, on the far stack the middle part of the second reflection, corresponding to the bottom VTI block, is slightly pulled up and the amplitude is increased. Compared with Figures 5.4a and 5.4b where the TI block was at the surface with the same degree of anisotropy, the effects of anisotropy are significantly reduced.

Figures 5.9a and 5.9b show the effects of 30% anisotropy (model 2) on the near-trace and far-trace stack. If compared with Figures 5.6a and 5.6b (the near-surface version of this model), the anisotropic effect is reduced on both near and far stacks. However, on the far stacks, twin events show up. This means that the anisotropic effect is still strong enough to cause artifacts. Two apparent faults, although small, appear on

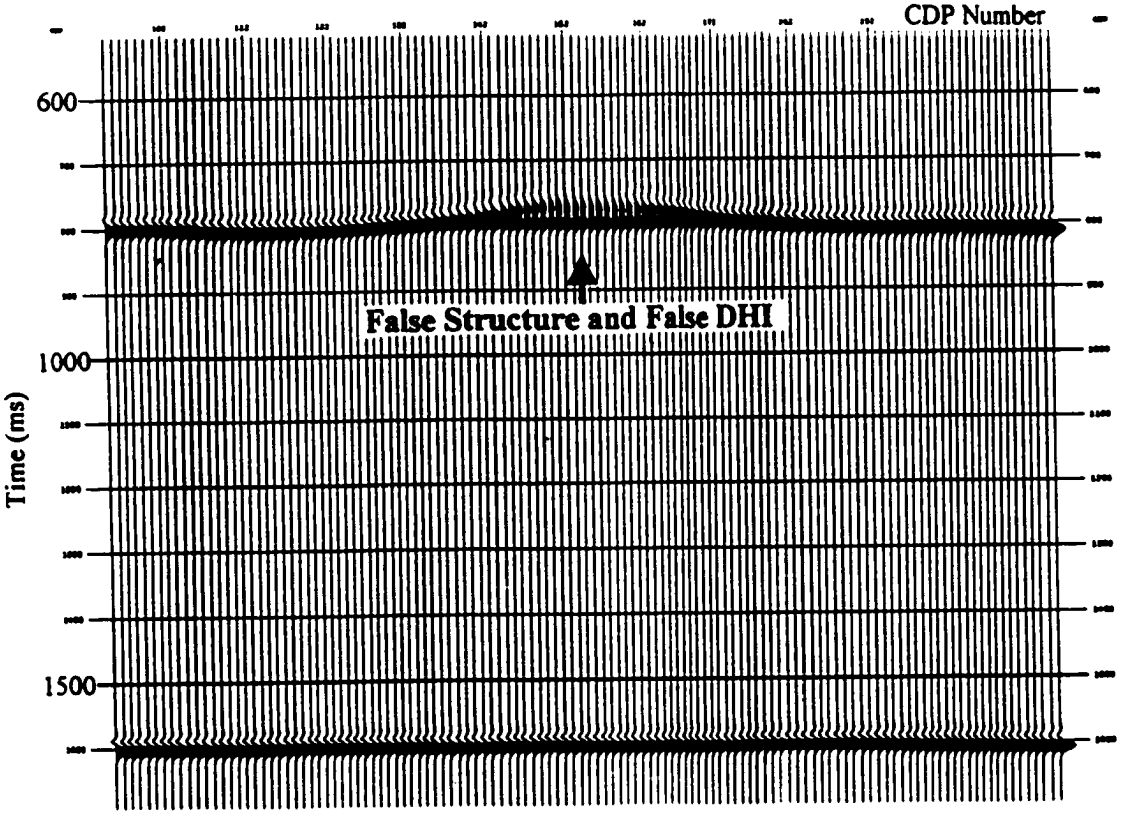

Figure 5 6a Near trace stack (30% anisotropy, Model 1)

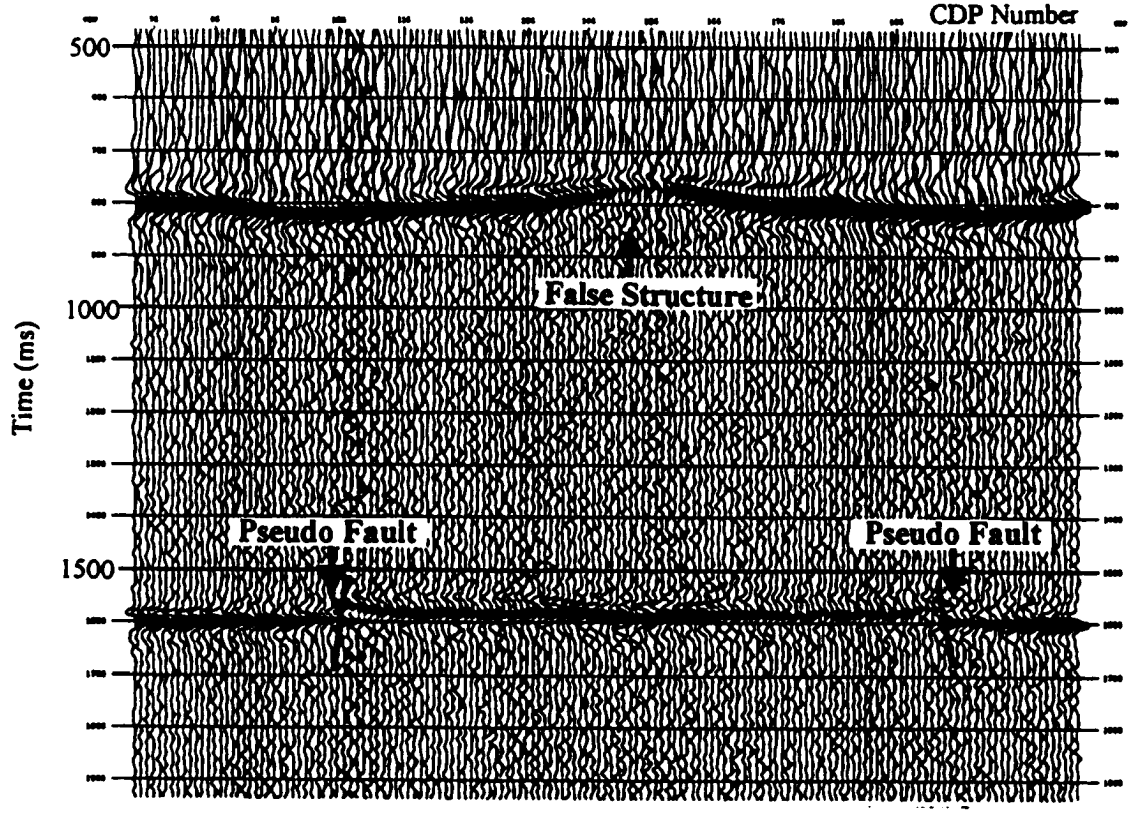

Figure 5 6b Far trace stack (30% anisotropy, Model 1)

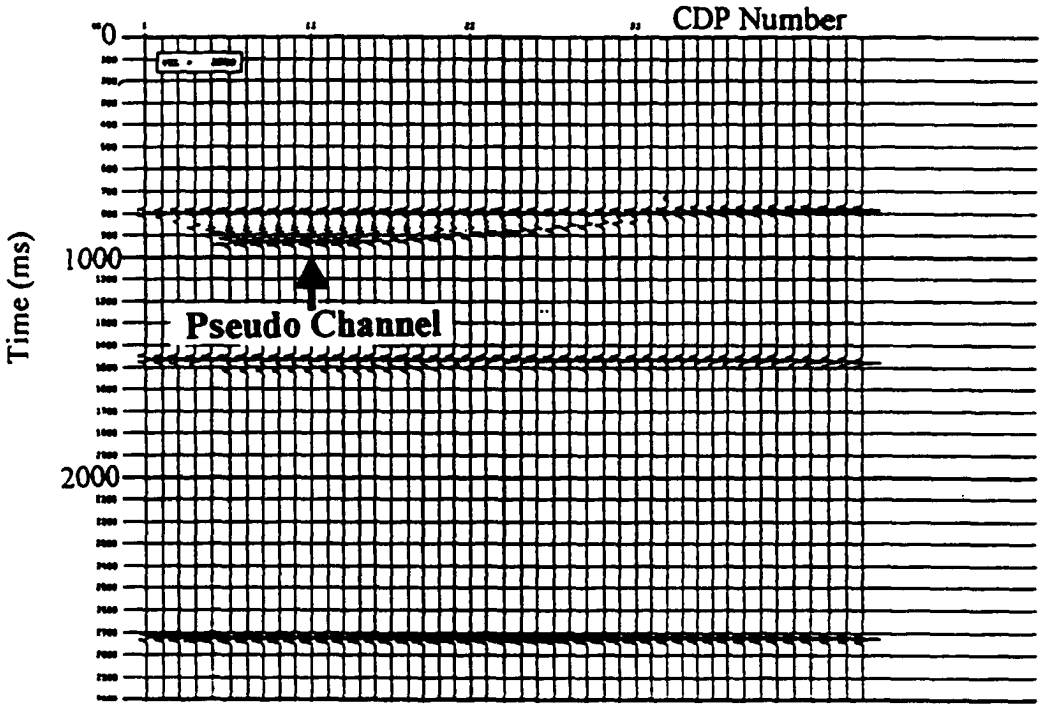

Figure 5.7 Full stack (30% anisotropy, Model 1)

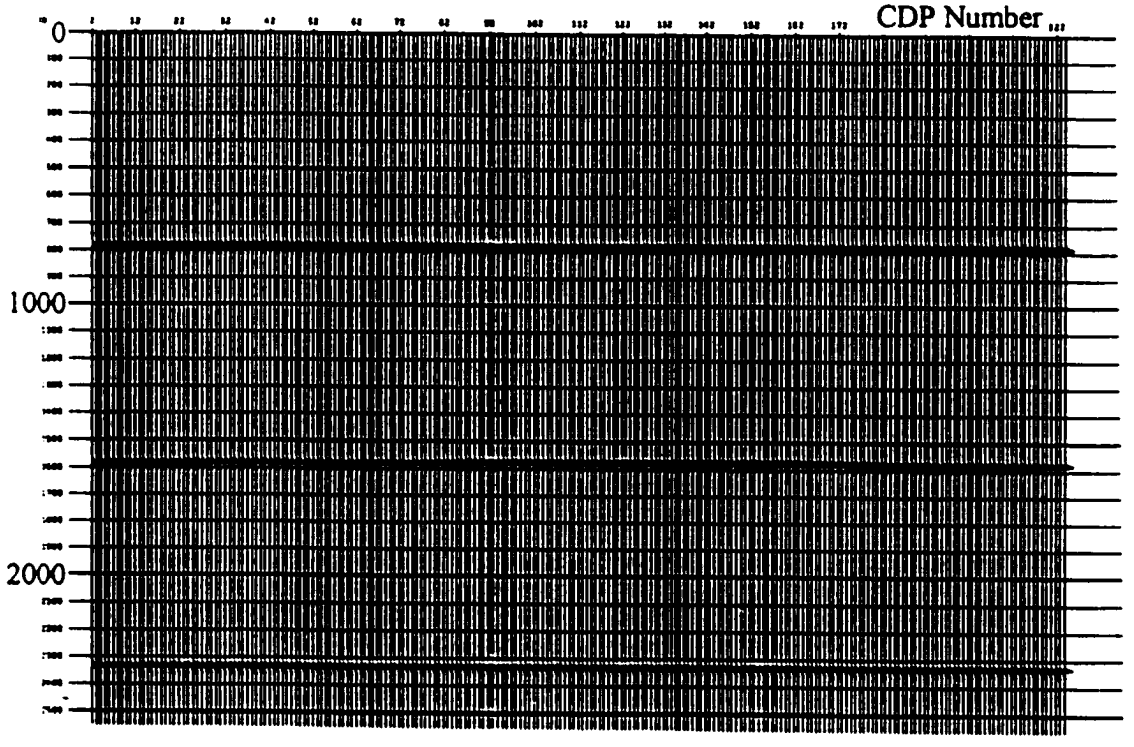

Figure 5.8a. Near trace stack (10% anisotropy, Model 2)

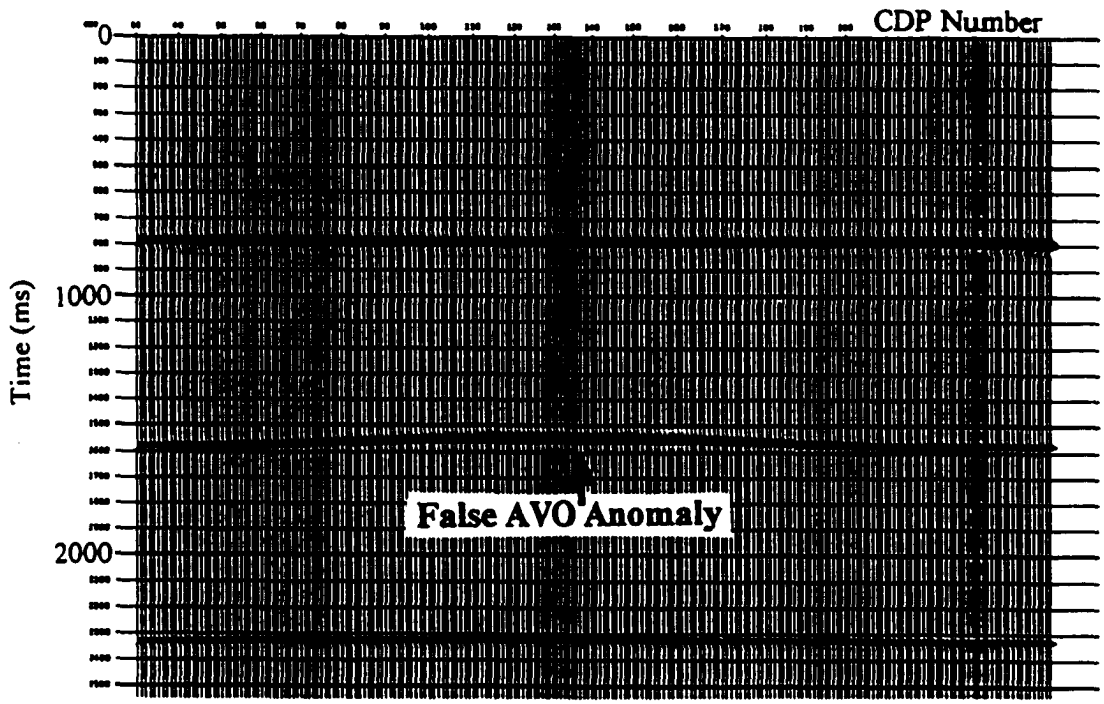

Figure 5.8b Far stack (10% anisotropy, Model 2)

the deeper event. On the full stack section in Figure 5.10a, the middle portion of the second reflection, corresponding to the bottom of the VTI block in model 2, appears to be a strong AVO anomaly (an anomalous AVO decrease can be observed on Figure 5.9a and 5.9b). Figure 5.10b shows the resulting apparent flat spot on the full stack.

In summary, the effect of a localized VTI block diminishes rapidly with depth if the anisotropy is weak (around 10%). However for large but feasible anisotropy, 30% for example, false structures and hydrocarbon indicators may result.

5.6 Conclusions and Discussion

Conventional processing software that assumes hyperbolic moveout may produce false structures and false responses below anisotropic regions due to improper removal of NMO. Thus, anisotropy effects can create pitfalls for interpreters on stacked and partially stacked sections. These pitfalls include pseudo faults, anticlines, channels, amplitude anomalies, and flat spots. The interpreter should be particularly suspicious of structures evident on full or far-offset stacks that do not appear on near-offset stacks.

There are quality control methods (eg. Inspecting NMO corrected gathers) to mute the improperly flattened events. However, when far offset information is important, muting is not a viable solution. Even higher-order moveout corrections may not entirely correct these problems and complete anisotropic processing may be necessary. Short of this, automatic detection of non-hyperbolic moveout may provide a useful diagnostic for identifying such pitfalls.

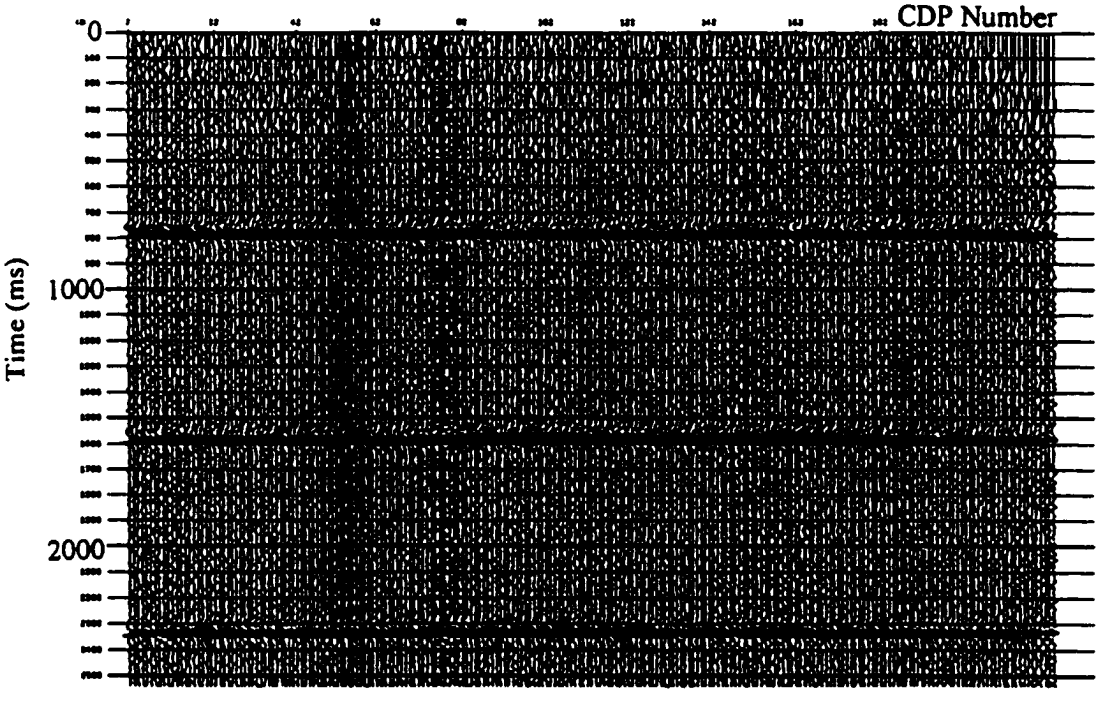

Figure 5.9a Near trace stack (30% anisotropy, Model 2)

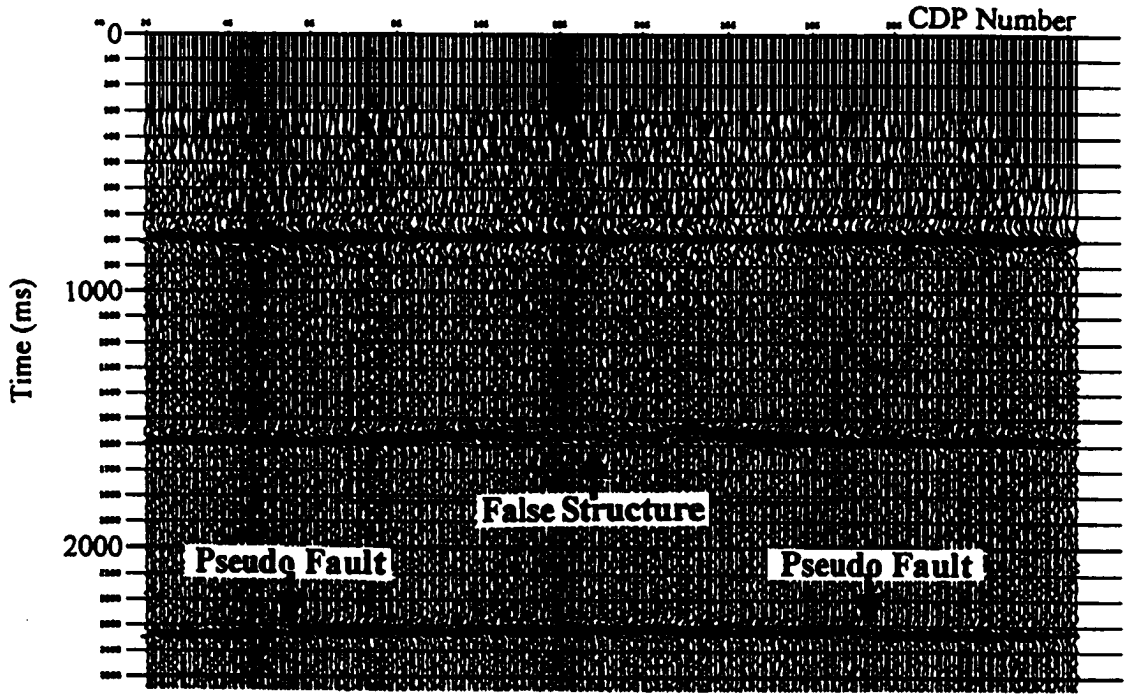

Figure 5.9b Far trace stack (30% anisotropy, Model 2)

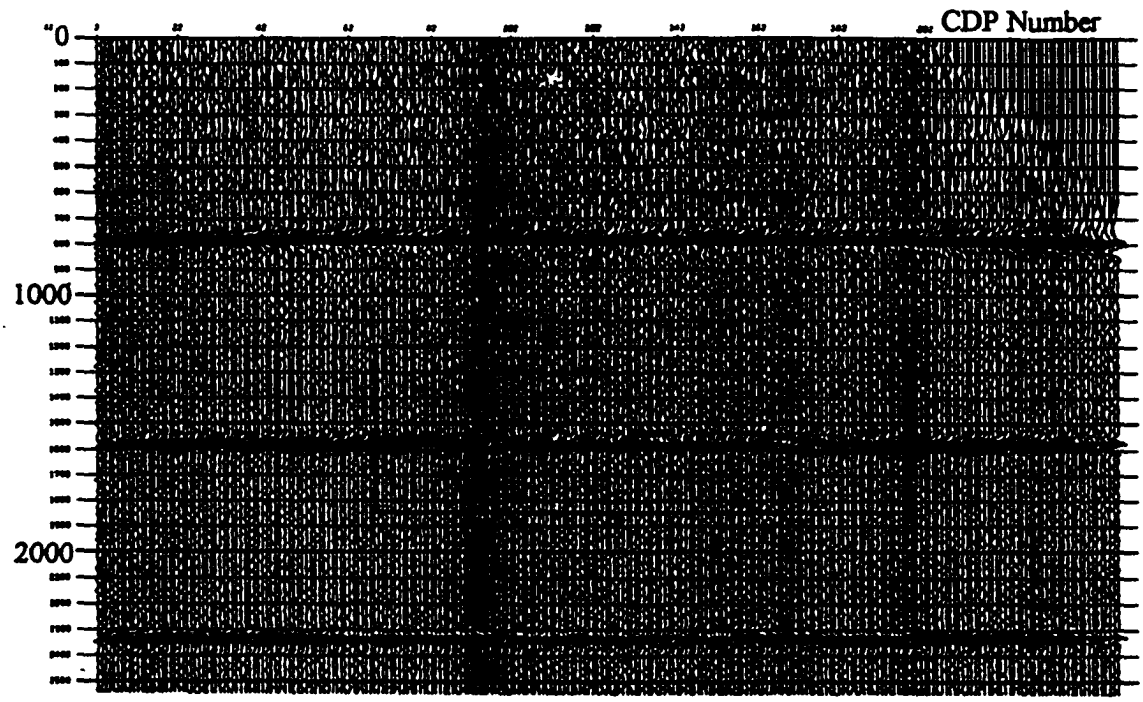

Figure 5.10a. Full stack (30% anisotropy, Model 2)

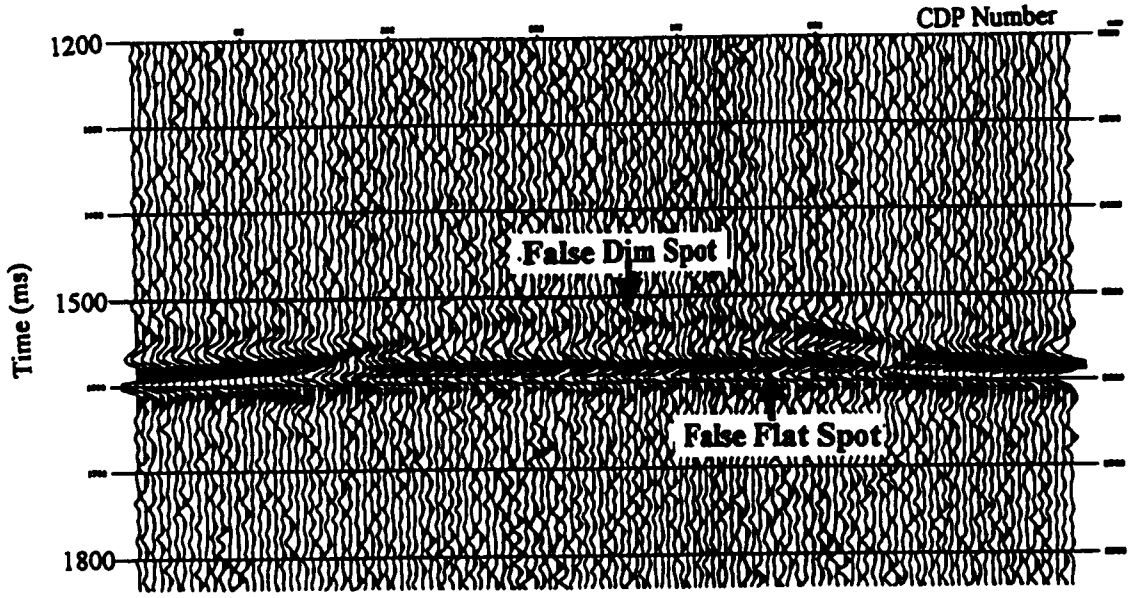

Figure 5.10b Full stack (30% anisotropy, Model 2)

Chapter 6

Reflection and Transmission Coefficients in General Anisotropic Media

Up until this point, the discussion has focused on AVO analysis in VTI media – the simplest type of anisotropy. In current exploration practice, however, it has become necessary to consider more complicated (general anisotropic) models of the Earth's structure in order to obtain synthetic seismograms that are more consistent with actual field data. For example, multiple aligned sets of fracture can cause general anisotropy (Schoenberg, 1995, Hudson, 1980).

In this chapter, a numerical solution of the reflection-transmission problem for general anisotropic media is presented. The chapter begins with an overview of the approach used and then proceeds to give more detail about the individual steps required.

6.1 Theoretical overview for computing reflection and transmission coefficients

The nature of wave propagation in general anisotropic media is significantly different from that in isotropic media. The basic differences can be stated as following (Rokhlin, 1986):

1) For an arbitrarily selected direction in an anisotropic material, the propagation of three different elastic waves is possible – a quasi-P wave and two quasi-SV waves. For special directions called acoustic axes, the velocities of two quasi-S waves coincide.

2) The polarization for each of the waves is uniquely determined by the

direction of wave propagation. Only for propagation along acoustic axes can the quasi-S wave be arbitrarily polarized as in an isotropic material.

3) Each of the waves has different phase and group velocities. The group velocity is greater than or equal to phase velocity and its direction does not coincide with the wave normal.

Figure 6.1 shows a plane wave incident upon a boundary between two general anisotropic media (with incident phase angle θ and azimuthal angle ϕ). The components of particle displacement can be expressed as:

$$u_k = AP_k e^{-ik(n\cdot r - Vt)} \qquad \text{.....(6.1)}$$

where u_k is a component of the displacement vector, A is the amplitude of the wave, P_k is the component of polarization vector, $\mathbf{K} = K\mathbf{n} = (\omega/V)n$ is the wave number, $\mathbf{V} = V\mathbf{n}$ is the phase velocity, $\mathbf{n}$ is the unit vector perpendicular to the wave front, and $\mathbf{r}$ is the position vector.

A 5-step algorithm is described below for numerically calculating the exact reflection and transmission coefficients for a boundary between two anisotropic media with no restrictions upon the symmetries of the two media.

6.2 Step 1 - Calculate the phase velocity of the incident wave

Given the wave normal for the incident wave $\mathbf{n}$, the Christoffel equation (3.5) for general anisotropic case can be expressed in the form below:

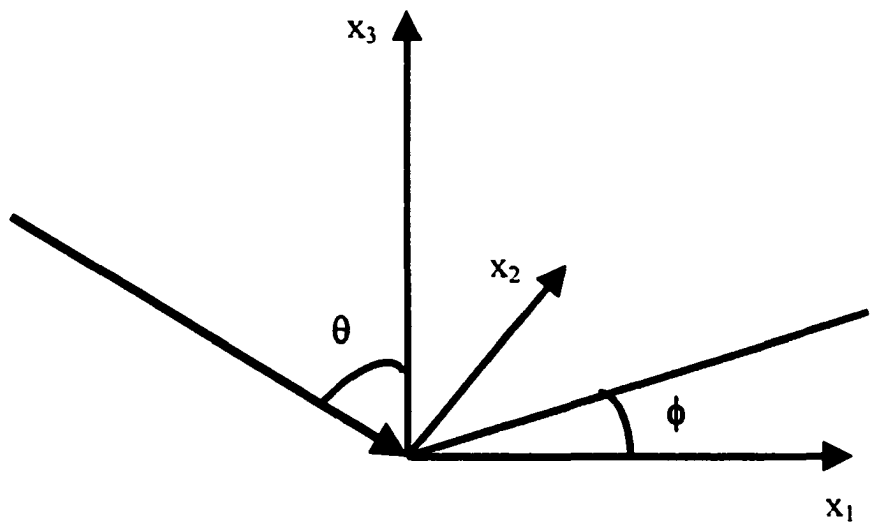

Figure 6.1 The angle between the slowness vector of the incident wave and vertical axis X_3 is defined as incident phase angle θ. The azimuthal angle ϕ is defined with respect to the X_1 axis.

$$\det\left(a_{ijkl} n_j n_l - V^2 \delta_{ik}\right) = 0 \qquad (i, j, k, l = 1,2,3) \qquad \text{.....(6.2)}$$

where V is the phase velocity of the incidence wave, and $a_{ijkl} = c_{ijkl}/\rho$. Thus, for a given wave direction (phase angle) expressed by **n**, the phase velocity can be obtained numerically by solving the equation (6.2). The steps for determining the phase velocity are described below.

1) Set $(B_{ik}) = (a_{ijkl}n_jn_l)$, (i, j, k, l = 1, 2, 3 and sum over repeated indices), then

$$B_{ik} = \sum_{j=1}^{3}\sum_{l=1}^{3} a_{ijkl} n_j n_l \qquad (i,k = 1,2,3) \qquad \text{.....(6.3)}$$

2) Expand equation (6.2) into the form of:

$$C_0 + C_1 V^2 + C_2 (V^2)^2 + C_3 (V^2)^3 = 0 \qquad \text{.....(6.4)}$$

where

$$\begin{cases} C_0 = B_{11}B_{22}B_{33} + B_{12}B_{23}B_{31} + B_{13}B_{21}B_{32} - B_{31}B_{13}B_{22} - B_{23}B_{32}B_{11} - B_{21}B_{12}B_{33} \\ C_1 = B_{31}B_{13} + B_{23}B_{32} + B_{21}B_{12} - B_{11}B_{33} - B_{33}B_{22} - B_{22}B_{11} \\ C_2 = B_{11} + B_{22} + B_{33} \\ C_3 = 1 \end{cases} \qquad \text{.....(6.5)}$$

3) Solve for the phase velocity V of the incidence by solving cubic polynomial (6.4) for V^2. Take the square root of this solution to obtain the phase velocity. The phase velocity (V) and the wave normal **n** are used in the next step to construct the slowness of the incident wave.

6.3 Step 2 - Calculate the 3 reflected and 3 transmitted slowness

This step is used to find the direction and phase velocity for all reflected and transmitted waves.

The method for calculating the reflected and transmitted slowness is based upon the concept of slowness surface. The slowness in a direction is defined as the inverse of the phase velocity in that direction. The slowness surface is defined as the loci of the

endpoints of the slowness vectors. The slowness concept is useful because Snell's law predicts that the component of the slowness parallel to the reflection boundary is the same for all transmitted and reflected waves. However, the application of the slowness surface to solution of the reflection problem in general anisotropic media is significantly different from the problem in isotropic media (Edmund, 1971). In the isotropic case, the slowness surface consists of two concentric spherical sheets, the inner one representing the P wave and the outer sphere the two coincident SV waves. For the anisotropic case, we find three general shaped surfaces, one for each of the wavemodes.

Figure 6.2 shows a plane wave incident onto a plane boundary (with unit normal **n**) between two anistrotrpic media. Let $\mathbf{m}^0$ represent the slowness vector of the incident wave and $\mathbf{m}^i$ represent the reflected and transmitted slowness vectors. The superscript i usually runs from 1 through 6, but may be more or less in certain cases, to account for all waves present. The origin of the coordinate system is assumed to lie on the boundary, then the equation of the boundary plane becomes $\mathbf{r}\cdot\mathbf{n} = 0$ ($\mathbf{r} = x_i\mathbf{i} + x_j\mathbf{j} + x_k\mathbf{k}$ is the wave position vector).

Using the same ideas discussed in Chapter 3, continuity of displacement and traction across the boundary can be expressed as:

$$\begin{cases} u_i^{(1)} - u_i^{(2)} = 0, & at \quad x_i n_i = 0 \\ \sigma_{ij}^{(1)} v_j - \sigma_{ij}^{(2)} v_j = 0, & at \quad x_i n_i = 0 \end{cases} \qquad \text{.....(6.6)}$$

where $u_i^{(1)}$, $u_i^{(2)}$, $\sigma_i^{(1)}$, and $\sigma_i^{(2)}$ are the total displacements and stresses due to the combination of all waves in regions (1) and (2), respectively.

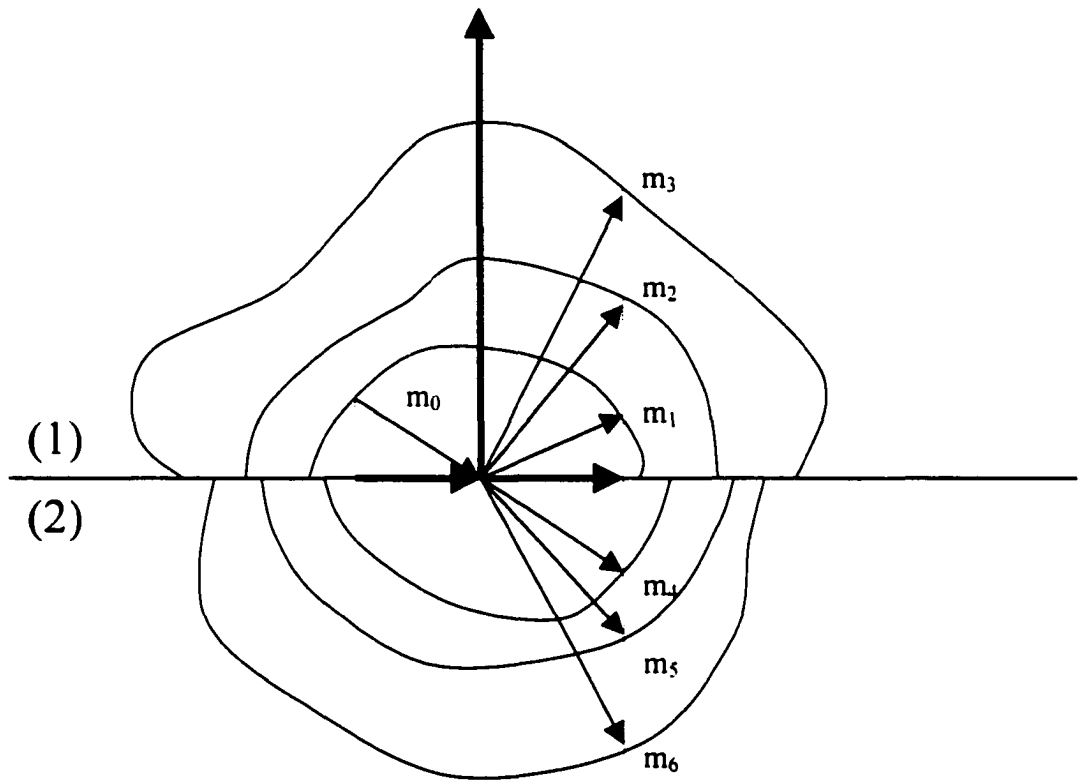

Figure 6.2 An example of the possible waves reflected (m_1, m_2,m_3) and transmitted (m_4, m_5, m_6) by an incident quasi-P wave mode m_0. Notice that all the slowness vectors have the same horizontal component **b**.

One of the important assumptions for these boundary conditions is that the frequency and phase of the reflected and transmitted waves must be equal to that of the incident wave. This assumption yields:

$$m_j^0 x_j = m_j^1 x_j = \cdots = m_j^n x_j, \qquad for\ all \qquad x_i n_i = 0 \qquad \text{.....(6.7)}$$

where the m_j are the slowness components. x_j are components of position vector.

The equation (6.7) can be rewritten into the form below:

$$(m_j^0 - m_j^i)x_j = 0, \qquad for\ all \qquad x_i n_i = 0 \qquad \text{.....(6.8)}$$

where i stands for all possible types of reflected and transmitted waves (in general 1,2,... 6).

The physical meaning of equation (6.8) is that the difference between any two slowness vectors of the incident wave and the permissible reflected and transmitted waves must be parallel to the normal **n**. In other words, the component of the slowness parallel to the boundary plane is the same for all incident reflected and transmitted waves (Snell's law). Thus, as indicated in figure 6.1, the two slowness components parallel to the boundary, m_1 and m_2 satisfy the following equations:

$$\begin{cases} m_1^0 = m_1^1 = m_1^2 = \cdots = m_1^6 \\ m_2^0 = m_2^1 = m_2^2 = \cdots = m_2^6 \end{cases} \qquad \text{.....(6.9)}$$

The third component m_3^i (i = 1, 2, ..., 6) of the slowness vectors that are perpendicular to the boundary plane are the only unknowns. These unknown components can be found solving the sixth-order equation (another form of Christoffel equation) in m_3:

$$A = \det\left(a_{ijkl} m_j m_l - \delta_{ik}\right) = 0 \qquad \text{.....(6.10)}$$

Equation (6.10) represents a 3 by 3 matrix which has to be expanded in order to set up the sixth order polynomial. The approach developed here is:

1) Determine the matrix element

Each element of the matrix in equation (6.10) is a second order polynomial in m_3 (the unknown slowness component). The second order polynomial of the ikth element of (6.10) can be written in the notation below:

$$C_{ik} m_3^2 + D_{ik} m_3 + E_{ik} = a_{ijkl} m_j m_l - \delta_{ik} \qquad (i,k = 1,2,3) \qquad \text{.....(6.11)}$$

where

$$\begin{cases} C_{ik} = a_{i3k3} \\ D_{ik} = (a_{i1k3} + a_{i3k1}) m_1 + (a_{i2k3} + a_{i3k2}) m_2 \\ E_{ik} = (a_{i1k2} + a_{i2k1}) m_1 m_2 + a_{i1k1} m_1^2 + a_{i2k2} m_2^2 + \delta_{ik} \qquad (i,k = 1,2,3) \end{cases} \qquad \text{.....(6.12)}$$

2) Expand the equation (6.10)

Using the above notations, the equation (6.10) can be written as:

$$A = \begin{vmatrix} C_{11} m_3^2 + D_{11} m_3 + E_{11} & C_{12} m_3^2 + D_{12} m_3 + E_{12} & C_{13} m_3^2 + D_{13} m_3 + E_{13} \\ C_{21} m_3^2 + D_{21} m_3 + E_{21} & C_{22} m_3^2 + D_{22} m_3 + E_{22} & C_{23} m_3^2 + D_{23} m_3 + E_{23} \\ C_{31} m_3^2 + D_{31} m_3 + E_{31} & C_{32} m_3^2 + D_{32} m_3 + E_{32} & C_{33} m_3^2 + D_{33} m_3 + E_{33} \end{vmatrix} = 0 \qquad \text{....(6.13)}$$

The expansion of equation (6.13) is algebraically very complicated. To simplify the process for programming purposes, a simplified procedure to divide the expansion into six algebraically similar parts is used. Equation (6.13) can be expended using:

$$A = A^{(1)} + A^{(2)} + A^{(3)} + A^{(4)} + A^{(5)} + A^{(6)} = 0 \qquad \text{.....(6.14)}$$

where

$$\begin{cases} A^{(1)} = (C_{11}m_3^2 + D_{11}m_3 + E_{11})(C_{22}m_3^2 + D_{22}m_3 + E_{22})(C_{33}m_{33}^2 + D_{33}m_3 + E_{33}) \\ A^{(2)} = (C_{12}m_3^2 + D_{12}m_3 + E_{12})(C_{23}m_3^2 + D_{23}m_3 + E_{23})(C_{31}m_3^2 + D_{31}m_3 + E_{31}) \\ A^{(3)} = (C_{31}m_3^2 + D_{31}m_3 + E_{31})(C_{21}m_3^2 + D_{21}m_3 + E_{21})(C_{32}m_3^2 + D_{32}m_3 + E_{32}) \\ A^{(4)} = (-C_{11}m_3^2 - D_{11}m_3 - E_{11})(C_{32}m_3^2 + D_{32}m_3 + E_{32})(C_{23}m_3^2 + D_{23}m_3 + E_{23}) \\ A^{(5)} = (C_{31}m_3^2 + D_{31}m_3 + E_{31})(-C_{22}m_3^2 - D_{22}m_3 - E_{22})(C_{13}m_3^2 + D_{13}m_3 + E_{13}) \\ A^{(6)} = (C_{21}m_3^2 + D_{21}m_3 + E_{21})(C_{12}m_3^2 + D_{12}m_3 + E_{12})(-C_{33}m_3^2 - D_{33}m_3 - E_{33}) \end{cases}$$

.....(6.15)

Each of the above expressions can be written in a general sixth polynomial form as:

$$A^{(i)} = (F_{11}m_3^2 + F_{12}m_3 + F_{13})(F_{21}m_3^2 + F_{22}m_3 + F_{23})(F_{31}m_3^2 + F_{32}m_3 + F_{33})$$

$$= G_0^{(i)} + G_1^{(i)}m_3 + G_2^{(i)}m_3^2 + G_3^{(i)}m_3^3 + G_4^{(i)}m_3^4 + G_5^{(i)}m_3^5 + G_6^{(i)}m_3^6 \qquad \text{.....(6.16)}$$

Where the F_{ij} represent the polynomial coefficients used in equation (6.15) and the G_i are given below:

$$
\begin{cases}
G_0^{(i)} = F_{13}F_{23}F_{33} \\
G_1^{(i)} = F_{13}F_{23}F_{32} + F_{13}F_{22}F_{33} + F_{12}F_{23}F_{33} \\
G_2^{(i)} = F_{13}F_{23}F_{31} + F_{13}F_{22}F_{32} + F_{12}F_{23}F_{32} + F_{11}F_{23}F_{33} + F_{13}F_{21}F_{33} + F_{12}F_{22}F_{33} \\
G_3^{(i)} = F_{13}F_{22}F_{31} + F_{12}F_{23}F_{31} + F_{11}F_{23}F_{32} + F_{13}F_{21}F_{32} + F_{12}F_{22}F_{32} + F_{11}F_{22}F_{33} + F_{12}F_{21}F_{33} \\
G_4^{(i)} = F_{11}F_{23}F_{31} + F_{13}F_{21}F_{31} + F_{12}F_{22}F_{31} + F_{11}F_{22}F_{32} + F_{12}F_{21}F_{32} + F_{11}F_{21}F_{33} \\
G_5^{(i)} = F_{11}F_{22}F_{31} + F_{12}F_{21}F_{31} + F_{11}F_{21}F_{32} \\
G_6^{(i)} = F_{11}F_{21}F_{31}
\end{cases}
\quad \text{.....(6.17)}
$$

Finally, collecting the parameters of different powers of m_3 leads to the following 6th order equation:

$$
A = \sum_{i=1}^{6} G_0^{(i)} + \sum_{i=1}^{6} G_1^{(i)} m_3 + \sum_{i=1}^{6} G_2^{(i)} m_3^2 + \sum_{i=1}^{6} G_3^{(i)} m_3^3 + \sum_{i=1}^{6} G_4^{(i)} m_3^4 + \sum_{i=1}^{6} G_5^{(i)} m_3^5 + \sum_{i=1}^{6} G_6^{(i)} m_3^6 = 0 \quad \text{.....(6.18)}
$$

3) Solve the unknown m_3 (vertical component of slowness) from the sixth order polynomial (6.18). There will be six solutions. However, only the physical solutions (usually three out of the six for one medium), that satisfy the conservation of energy flux away from the boundary, are used.

The above procedure must be carried out twice, once for the incident medium and the one for transmission medium. Assuming an incident wave propagating downward upon an interface, the three reflected slowness vectors should point into the

upper medium (with positive signs), while the three transmitted slowness vectors point into the lower medium (with negative signs). At the critical angle the appropriate ray must be parallel to the interface (Edmund, 1970).

Once the slowness for each wave is determined, the direction and phase velocity of the wave can be determined. The next step described below concerns the polarization vector for each of the reflected and transmitted waves.

6.4 Step 3 - Calculate polarization for each wave

In each direction of wave propagation (defined by the slowness vector) $\mathbf{n} = \mathbf{m}/|\mathbf{m}|$, three polarization vectors should be found (one quasi-P and two quasi-S) corresponding to the three slowness vectors of different wave modes. So, if one reflected or transmitted slowness vector $\mathbf{m}$ has been determined, the polarization of the wave mode can be calculated by determining eigenvectors for the Christoffel equation:

$$\left(a_{ijkl} m_j m_l - \delta_{ik}\right) P_k = 0 \qquad \text{.....(6.19)}$$

where the m_j are the components of the slowness vector, $a_{ijkl} = c_{ijkl}/\rho$ (c_{ijkl}: elastic constant; ρ: density), and P_k is the k^{th} component of the polarization vector corresponding to the input slowness.

The procedure for calculating the polarization vector is described below:

1) Set up the eigenvalue matrix

Set $(H_{ik}) = (a_{ijkl} m_j m_l - \delta_{ik})$, $(i, j, k, l = 1, 2, 3)$, then

$$H_{ik} = \sum_{j=1}^{3}\sum_{l=1}^{3} a_{ijkl} m_j m_l - \delta_{ik} \qquad (i, j = 1,2,3) \qquad \text{.....(6.20)}$$

2) Compute the polarization component value

Equation (6.19) usually has two non-zero eigenvalues. This means that it has two non-linear equations that can be used for calculating polarization components. A part of the computation problem is to choose which two equations to use. The third equation comes from the definition of the normalized polarization: $\Sigma P_k^2 = 1$. Suppose the *i*th and *j*th ($i, j \subset [1, 2, 3]; i \neq j$) equations of (6.19) are non-linear, then the final equations chosen for computing a polarization vector are:

$$\begin{cases} H_{i1}P_1 + H_{i2}P_2 + H_{i3}P_3 = 0 \\ H_{j1}P_1 + H_{j2}P_2 + H_{j3}P_3 = 0 \\ P_1^2 + P_2^2 + P_3^2 = 1 \end{cases} \qquad \text{.....(6.21)}$$

The absolute value of the polarization components can be solved explicitly using:

$$\begin{cases} P_1 = \dfrac{1}{\sqrt{1 + A_1^2 + A_2^2}} \\ P_2 = \dfrac{A_2}{\sqrt{1 + A_1^2 + A_2^2}} \\ P_3 = \dfrac{A_1}{\sqrt{1 + A_1^2 + A_2^2}} \end{cases} \qquad \text{.....(6.22)}$$

where

$$\begin{cases} A_1 = \dfrac{H_{j1}H_{i2} - H_{i1}H_{j2}}{H_{i3}H_{j2} - H_{j3}H_{i2}} \\ A_2 = \dfrac{H_{j1}H_{i3} - H_{i1}H_{j3}}{H_{i3}H_{j2} - H_{j3}H_{i2}} \end{cases}$$

The solution to (6.21) requires the use of pivoting (reference) to avoid numerical problems.

The solution (6.22) can be applied to directly compute the polarization vectors providing all wave phase velocities are different in the wave propagation direction. However, in some cases when the two S wave velocities coincide, the equation (6.19) has only one non-zero eigenvalue and the solution (6.21) can not be used for calculation of the polarization vector. Wave directions with this property are called acoustic axes, and the polarization vector of the quasi-S wave may not be uniquely determined. Thus, it may have any direction in the plane perpendicular to the displacement direction of the quasi-P wave.

In this situation, the desired displacement of the quasi-S wave has to satisfy only one condition: it must lie in the plane whose normal coincides with the displacement of the quasi-P wave. A procedure is given below to find one proper set of polarization vectors for the two quasi-S waves based on the principle: The three polarization vectors (one quasi-P and two quasi-S) must be orthogonal to each other:

a) Find the quasi-P wave polarization $\mathbf{P}^{(p)}$ along the direction of quasi-S slowness **m** by solving the equation (6.19).

b) Set one quasi-S wave polarization $P^{(s1)}$ orthogonal to $P^{(p)}$ (parallel to the XY plane):

$$\begin{cases} P_1^{(s1)} = \dfrac{-P_2^{(p)}}{\sqrt{(P_1^{(p)})^2 + (P_2^{(p)})^2}} \\ P_2^{(s1)} = \dfrac{P_1^{(p)}}{\sqrt{(P_1^{(p)})^2 + (P_2^{(p)})^2}} \\ P_3^{(s1)} = 0 \end{cases} \quad \text{.....(6.23)}$$

c) Find the other quasi-S wave polarization $P^{(s2)}$ by letting it orthogonal to both $P^{(p)}$ and $P^{(s1)}$ (perpendicular to the XY plane):

$$\begin{cases} P_1^{(s2)} = \dfrac{P_2^{(s1)} P_3^{(p)}}{\sqrt{(P_2^{(s1)} P_3^{(p)})^2 + (P_1^{(s1)} P_3^{(p)})^2 + (P_1^{(s1)} P_2^{(p)} - P_2^{(s1)} P_1^{(p)})^2}} \\ P_2^{(s2)} = \dfrac{-P_1^{(s1)} P_3^{(p)}}{\sqrt{(P_2^{(s1)} P_3^{(p)})^2 + (P_1^{(s1)} P_3^{(p)})^2 + (P_1^{(s1)} P_2^{(p)} - P_2^{(s1)} P_1^{(p)})^2}} \\ P_3^{(s2)} = \dfrac{P_1^{(s1)} P_2^{(p)} - P_2^{(s1)} P_1^{(p)}}{\sqrt{(P_2^{(s1)} P_3^{(p)})^2 + (P_1^{(s1)} P_3^{(p)})^2 + (P_1^{(s1)} P_2^{(p)} - P_2^{(s1)} P_1^{(p)})^2}} \end{cases} \quad \text{.....(6.24)}$$

6.5 Step 4 - Select the right sign for the polarization components

The numerical solution of the direction cosine P_k does not give an indication that it points in the right direction. The correct signs must be selected for defining the polarization direction using the following rules:

1) For the reflected and transmitted quasi-P wave, the positive polarization direction is selected such that the dot product of **P** (polarization vector) and **m** (slowness vector) is positive:

$$\mathbf{P}\cdot\mathbf{m} > 0 \qquad \text{.....(6.25)}$$

2) For the reflected and transmitted quasi-S wave, the vector **N** that is normal to the incident plane has to be found first. Then, the positive polarization direction is defined such that the dot product of ***P*** and **N** is positive.

$$\begin{cases} \mathbf{N} = \mathbf{m}\times\mathbf{n} \\ \mathbf{P}\cdot\mathbf{N} > 0 \end{cases} \qquad \text{.....(6.26)}$$

where **n** is the unit vector normal to boundary plane (Z = 0).

In summary, for reflected and transmitted waves, we have to in general compute the polarization of all three wave types in the directions of the reflected and transmitted waves in order to handle problems with acoustic axes where the quasi-S polarity can be anywhere within a plane.

6.6 Step 5 - Calculate reflection and transmission coefficients

Assuming an incidence wave with unit amplitude, the boundary conditions (6.7) can now be written in the form of six linear algebraic equations (Rokhlin, 1985):

$$\begin{cases} P_i^0 + \sum_{\nu=1}^{6} R^\nu P_i^\nu = 0 \\ C_{j3kl}^0 m_k^0 P_i^0 + \sum_{\nu=1}^{6} R^\nu C_{j3kl}^\nu m_k^\nu P_i^\nu = 0 \qquad (i = 1,2,3) \end{cases} \qquad \text{.....(6.27)}$$

where the P_i are the polarization components, and the m_i are the slowness components. R^{ν} stands for a reflection or a transmission coefficient depending on the integer value of ν between 1 - 6. These coefficients have the following meaning: $\nu = 0$ - incidence wave; $\nu = 1$ - reflected quasi-P wave; $\nu = 2$ - reflected quasi-S wave 1; $\nu = 3$ - reflected quasi-S wave 2; $\nu = 4$ - transmitted quasi-P wave; $\nu = 5$ - transmitted quasi-S wave 1; $\nu = 6$ - reflected quasi-S wave 2. The C^{ν}_{j3kl} are the elastic constants of incident medium (if $\nu = 0, 1, 2, 3$), or reflecting medium (if $\nu = 4, 5, 6$).

For convenience, the equations in (6.25) can be written in terms of a set of linear equations for the unknown reflection and transmission coefficients in the form:

$$(I_{m0} + I_{mn} R_n) = 0 \qquad (m, n = 1,2,....6) \qquad \text{.....(6.28)}$$

where

$$\begin{cases} I_{mn} = P_{nm} & (m = 1,2,3;\ \ n = 0,1,2,3) \\ I_{mn} = -P_{nm} & (m = 1,2,3;\ \ n = 4,5,6) \\ I_{mn} = \sum_{i=1}^{3}\sum_{k=1}^{3} C^{i}_{(m-3)3ki} m_{nk} P_{ni} & (m = 4,5,6;\ \ n = 0,1,2,3) \\ I_{mn} = -\sum_{i=1}^{3}\sum_{k=1}^{3} C^{r}_{(m-3)3ki} m_{nk} P_{ni} & (m = 4,5,6;\ \ n = 4,5,6) \end{cases} \qquad \text{.....(6.29)}$$

The six reflection and transmission coefficients can be obtained by solving the six linear equations (6.28).

The last quantity that is calculated for each wave is the energy flux vector. The energy flux **E** is a vector having the direction of energy flow at a point with a magnitude equal to the amount of energy flowing per unit area perpendicular to **E**. The energy flux **E** and be expressed as:

$$E_i = \sigma_{ij}\dot{u}_j \qquad \text{.....(6.30)}$$

The component normal to the reflection boundary is used to verify that conservation of energy is obeyed (used as a confidence check for the reflection coefficients).

A FORTRAN90 subroutine (See Appendix IV) was written to calculate the exact reflection coefficients for reflected quasi-P wave and quasi-S waves when the incident angle (with the wave mode) is specified upon a boundary between two anisotropic media. Figure 6.3 presents the flowchart of this calculation procedure.

6.7 Summary

In this chapter, the basic equations are derived which can be used for determination of reflection and transmission coefficients in the general anisotropic case. Consideration of wave propagation in the acoustic-axis directions (direction for which velocities of both transverse waves are equal to one another) is included in the general algorithm. The discussions also involve some of the numerical problem that can occur during computation. Specifically the determination of polarization is more difficult because of numerical problems and polarity conventions.

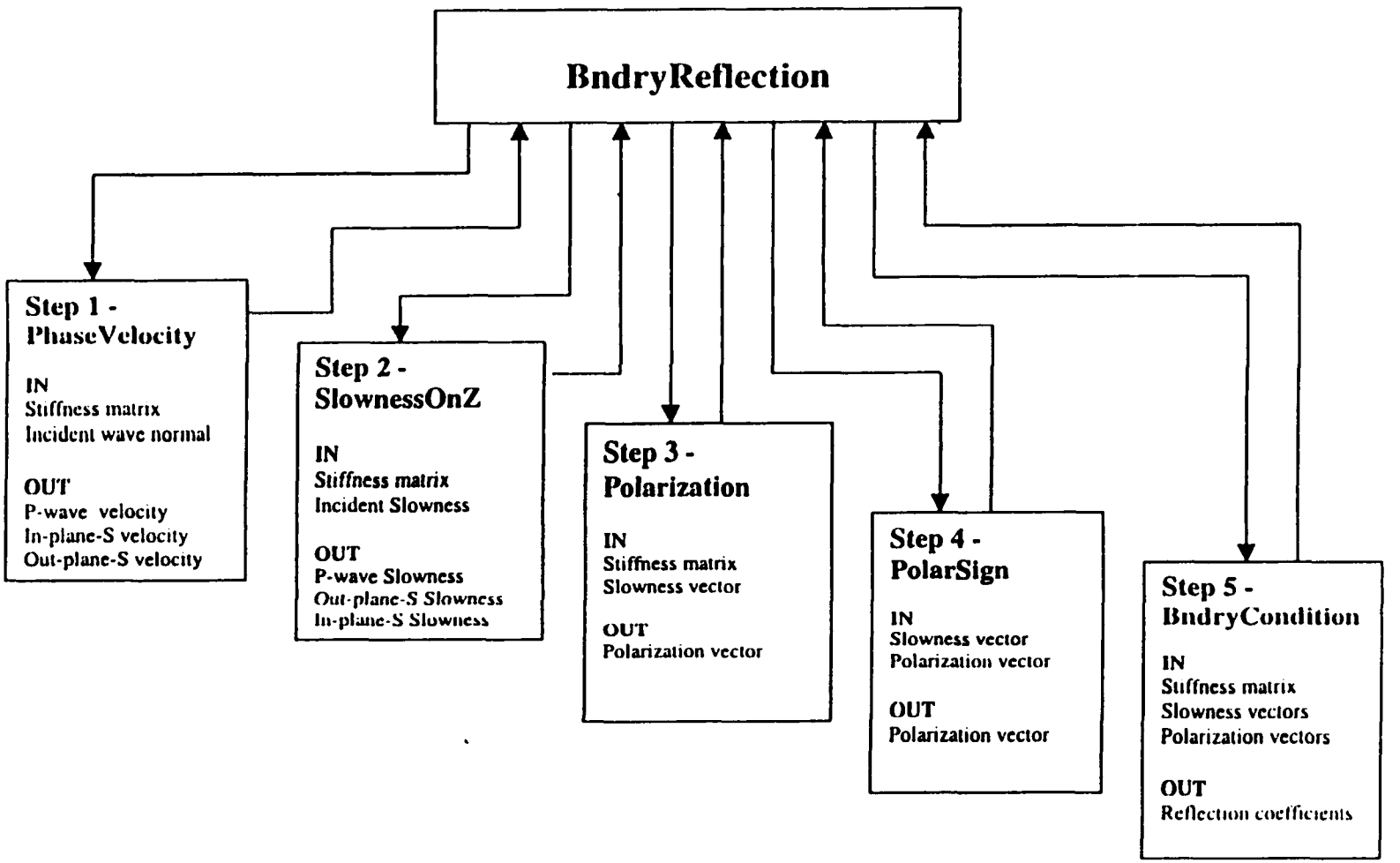

Figure 6.3 Program flowchart for calculation of reflection coefficients in general anisotropic media

Chapter 7

Synthetic AVO Study of Fractured Reservoir Models With Multiple Fracture Sets

7.1 Introduction

One of the problems facing modern seismic exploration is the use P-wave AVO analysis for characterizing fractured reservoirs. Cores and well logs offer methods of describing fractures but these approaches often suffer from scale effects. The seismic method offers the best approach to characterizing the reservoir at approximately the same scale as that required for predicting reservoir properties. In this chapter the AVO effects from a fractured reservoir are studied with a view toward identifying those approaches best suited for identifying the properties of fractured reservoirs.

In the first part of this chapter, the popular concept of fracture density is introduced along with the model for the fracture compliance for a single set of fractures. The assumption will be used that the excess compliance due to different crack sets can be added. The advantage of this approach is that, when the assumptions used apply, this approach can be accomplished without the need for a detailed analysis of core and scaling up to the reservoir scale.

The second part of the chapter examines the azimuthal AVO variations of two fractured models using the exact reflection coefficient method described Chapter 6. Model 1 is designed containing a single fracture set, and Model 2 with two fracture sets. The interesting result here is that the single fracture set model presents a stronger

azimuthal AVO variation. Here certain problems are identified with the interpretation. Suggestions are made in the conclusions regarding approaches that can be used when multiple fracture sets exist.

7.2 Relating fracture density to the elastic compliance

One useful approach in the geophysical literature for describing crack models is via the use of crack or fracture "sets" (e.g., Schoenberg and Sayers, 1995). Each set is a number of parallel cracks that all have the same normal. The results of each crack set (compliance or permeability) is then simply added (neglecting any interaction) as if the results were additive. This approach will be the preferred method in exploration and development when the detailed information on individual fracture statistics is not available.

Typically the anisotropy introduced by a crack set is proportional to a quantity described by geophysicists as "the crack density". A brief derivation of the important equations is given below.

The excess compliance of a fractured rock due to fractures can be computed using averages of strains and stresses over a selected volume (Horri and Nemat-Nasser, 1983). Oda et al. (1984) used this approach to derive an expression for the compliance of a fractured rock. The basic idea is to assume that the average or effective strain measured on the surface of a volume is due to the average strain over the matrix material that contains the fractures and the average strain over the volume of the fractures.

$$\bar{\varepsilon}_{ij} = \bar{\varepsilon}_{ij}^{M} + \bar{\varepsilon}_{ij}^{C} \qquad \text{.....(7.1)}$$

Equation (7.1) can be rewritten in the form (Horri and Nemat_Nasser, 1983)

$$\bar{\varepsilon}_{ij} = S_{ijkl}^{M}\bar{\sigma}_{kl} + S_{ijkl}^{C}\bar{\sigma}_{kl} = S_{ijkl}^{M}\bar{\sigma}_{kl} + \frac{1}{V_{Total}}\int_{V(Cracks)} \frac{1}{2}\left(\frac{\delta_i}{x_j} + \frac{\delta_j}{x_i}\right) dV^{C} \qquad \text{.....(7.2)}$$

where S_{ijkl} with the superscipt M represents the compliance tensor without fractures (the background or matrix) and S_{ijkl} with superscript C is the excess compliance due to the presence of the fractures. These compliances are the inverse of the elastic stiffness constants typically used in geophysical exploration literature. The δ's in the above expression are the components of the displacement discontinuities across the cracks and the x_i's can be written in the following form:

$$X_j = \frac{A}{n_j} \qquad \text{.....(7.3)}$$

where A is the aperture of the fracture and n_j is the j^{th} component (j = 1, 2, 3) of the normal to the fracture. Writing the integral in equation (7.2) as a summation, equation (7.2) and (7.3) yield the following relationship for the average excess strain due to N penny-shaped cracks with diameter (D) and aperture A

$$\bar{\varepsilon}_{ij}^{C} = \frac{1}{V_{Total}}\sum_{k=1}^{N} \frac{1}{2}\left(\frac{\delta_i}{A_k}n_j^k + \frac{\delta_j}{A_k}n_i^k\right)\left(\frac{\pi D_k^2}{4}\right)A_k \qquad \text{.....(7.4)}$$

The excess strain associated with each crack is multiplied times the volume of the crack in a weighted sum. Simplifying the above expression leads to the following equation for the excess strain due to the presence of fractures.

$$\bar{\varepsilon}_{ij}^{c} = \frac{1}{V_{Total}} \sum_{k=1}^{N} \frac{1}{2}\left(\delta_i n_j^k + \delta_j n_i^k\right)\left(\frac{\pi D_k^2}{4}\right) \qquad \text{.....(7.5)}$$

Now the assumptions used at this point are:

1) There is a simple linear relationship between the traction applied to the surface of the crack and the displacement discontinuity across the crack.

2) The stress acting upon the crack is the same average stress applied to the volume being studied (neglecting the crack interaction).

For example, Oda et al. (1974) assumed a relation of the following form

$$\delta_i = K_0 D \sigma_{ij} n_j \qquad \text{.....(7.6)}$$

across the crack surfaces where the constant of proportionality between the displacement and the traction is assumed to be proportional to the diameter (D) of the penny-shaped cracks. The constant of proportionality (K_o) can be pressure dependent. Substitution of (7.6) into (7.5) leads to the following expressions for the average strain over the cracks

$$\bar{\varepsilon}_{ij} = \frac{K_0}{2D}\left[F_{jk}\bar{\sigma}_{ik} + F_{ik}\bar{\sigma}_{ij}\right] \qquad \text{.....(7.7)}$$

where

$$F_{jk} = \frac{\pi}{4}\frac{1}{V_{Total}} \sum_{k=1}^{N} D_m^3 n_k^m n_j^m \qquad \text{.....(7.8)}$$

is Oda's fabric tensor. By adding two copies of the expressions within equation (7.7) and changing the summation indices, equation (7.7) can be written in the form

$$\bar{\varepsilon}_{ij} = \frac{K_0}{4}\left[F_{jk}\delta_{il} + F_{jl}\delta_{ik} + F_{ik}\delta_{jl} + F_{il}\delta_{kj}\right]\bar{\sigma}_{kl} \qquad \text{.....(7.9)}$$

Thus the contribution of the fractures to the compliance of the matrix rock, i.e., the excess compliance due to the cracks, is given by

$$\bar{S}^{c}_{ijkl} = \frac{K_0}{4}\left[F_{jk}\delta_{il} + F_{jl}\delta_{ik} + F_{ik}\delta_{jl} + F_{il}\delta_{kj}\right] \qquad \text{.....(7.10)}$$

where the fabric tensor F_{jk} is given in equation (7.8). For a single set of parallel (scalar) cracks (penny-shaped with diameter D), the excess compliance can be written in the form (modified from Schoenberg and Sayers, 1995 and Oda, 1983)

$$\bar{S}^{c}_{ijkl} = \frac{K_0 e}{4}\left[\delta_{il}n_k n_j + \delta_{ik}n_l n_j + \delta_{jl}n_k n_i + \delta_{jk}n_l n_i\right] \qquad \text{.....(7.11)}$$

where e is the crack density, i.e., the number of cracks per unit volume multiplied times the diameter (D) cubed. The constant K_0 is assumed to be dependent upon the elastic properties of the rock that is fractured. The product $Z_0=K_0e$ will be referred to here as the specific compliance of the crack set.

Equation 7.11 describes "scalar" cracks where the tangential and normal stresses have the same constant of proportionality. A more general relationship accounting for the shear (Zt) and normal (Zn) components of traction and displacement has been

described by Schoenberg and Sayers (1995). The calculations in this thesis uses values of Zn and Zt described in the papers by Hudson (1980, 1981).

Based on equation (7.11), a FORTRAN90 subroutine (See Appendix 5) was completed to compute the compliance matrix caused by each set of fracture. This program is also capable of assembling arbitrary models of fractures and convert the total compliance into the elastic stiffness.

7.3 Synthetic fractured reservoir models and method

Two models of fractured reservoirs are set up for synthetic azimuthal AVO studies in this thesis. The matrix material of the reservoirs is assumed to be a limestone with 10% porosity, and the overlying seal layer is assumed to be a shale. Both incident and transmitted layers are assumed isotropic before fracture sets are added to the models. Table 7.1 lists the petrophysical parameters used as the background of the models. All of these parameters are set within the range of the laboratory and empirical relationships between V_p, V_s and ρ described by Castagna, et. al.. (1993).

Table 7.1 Model Matrix Information

	Reservoir Matrix	Overlying Shale
Vp (m/s)	5877	3700
Vs (m/s)	3039	1982
Density (g/cm^3)	2.44	2.41
Porosity	10%	

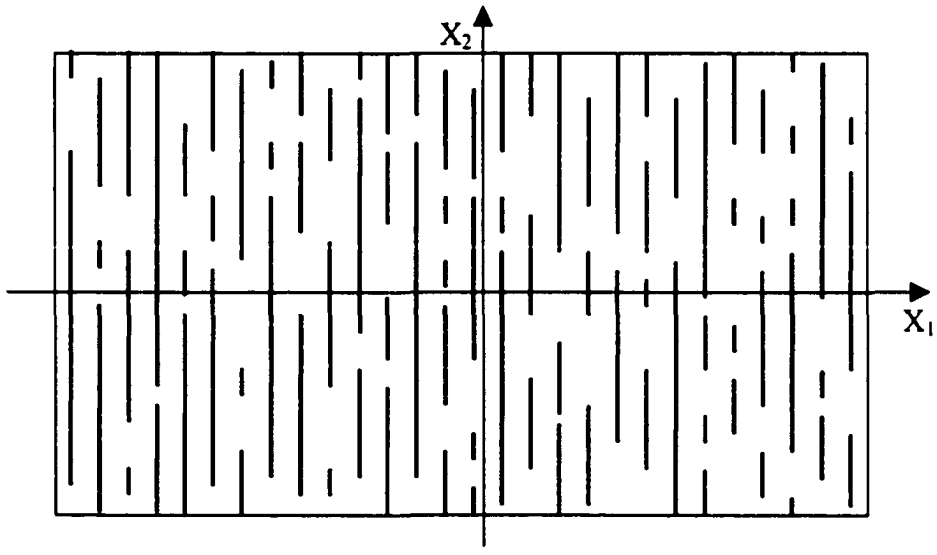

Figure 7.1a X_1X_2-plane sketch of fracture's orientation in model 1

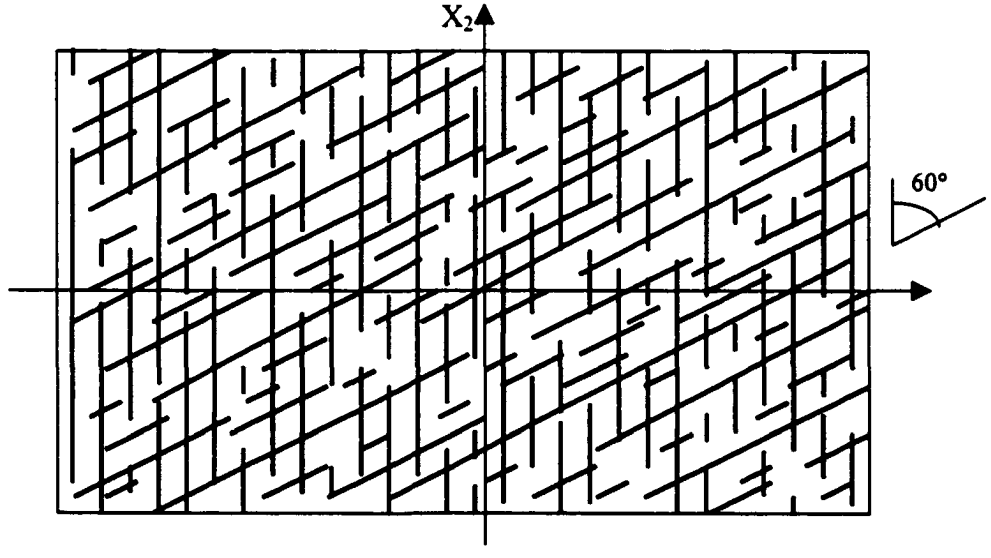

Figure 7.1b X_1X_2-plane sketch of fracture's orientation in model 2

All fracture sets in the models discussed are assumed to be vertical and perpendicular to the reflection boundaries (X_1–X_2 plane). Model 1 is assumed to have one set of fractures at an azimuth of 0° (normal pointing parallel to the X_1 axis). Model 2 has two sets of fractures at azimuths of 0° and 60°. Figure 7.1a and 7.1b show the X_1X_2-plane sketches of models 1 and 2. The crack density of the fracture set in model 1 is set equal to 0.1. For the purpose of a comparison study, the total crack density in model 2 is also set as 0.1%, with the crack density of each fracture set equal to 0.05%. Table 7.2 shows all the fracture information described above.

The exact solution of the reflection coefficient between general anisotropic media is used for the study presented here. The advantage of this approach is that any errors from using approximate (conventional) AVO modeling can be avoided.

An incident P-wave is assumed for each model. The three expected reflections are a quasi-P (PP) wave, a quasi-in-plane-S (PSI) and a quasi-out-of-plane-S (PSO) wave. The incidence phase angle range for the study is varied between 0° to 45°. The azimuthal variation of amplitudes with angle of incidence is observed at four different azimuth angles - 0°, -30°, -60°and -90°, respectively.

According to Hudson (1980, 1981), one vertical set of the fractures can introduce transverse isotropy with a horizontal symmetry axis (HTI), while multiple sets of fractures can cause arbitrary anisotropy.

7.4 Azimuthal interpretation of AVO from reservoir top

Figures 7.2 and 7.3 show the exact azimuthal PP reflection amplitudes from models 1 (single fracture set) and 2 (two fracture sets), respectively. First of all,

Table 7.2 Model Fracture Information

		Crack Density	Azimuthal Angle	Dip Angle
Model 1	fracture set #1	0.1	0	90
Model 2	fracture set #1	0.05	0	90
	fracture set #2	0.05	60	90

comparing these two figures, there are only slight differences on the normal-incidence PP reflection coefficients, showing that the total crack density may be the primary factor related to fractures that influences the zero-offset PP reflections.

Secondly, the azimuthal variations of the PP reflection can be only clearly observed within each curve family when the incidence angles exceed 25°. Note that model 1 shows more azimuthal AVO than model 2. Note also that, in Figure 7.3, the azimuth -90° curve is identical to the azimuth -30° curve. It is found that, in these two situations, that the incidence plane happens to be along the orientation direction of one of the fracture sets. The P-wave sees the same fractured property because the two fracture sets have the same crack density.

Figure 7.4 and 7.5 show the out-plane shear reflections amplitudes from models 1 and 2, respectively. The interesting points for these two figures are:

1) Compared with Figure 7.2 and 7.3, the azimuthal variation of the converted

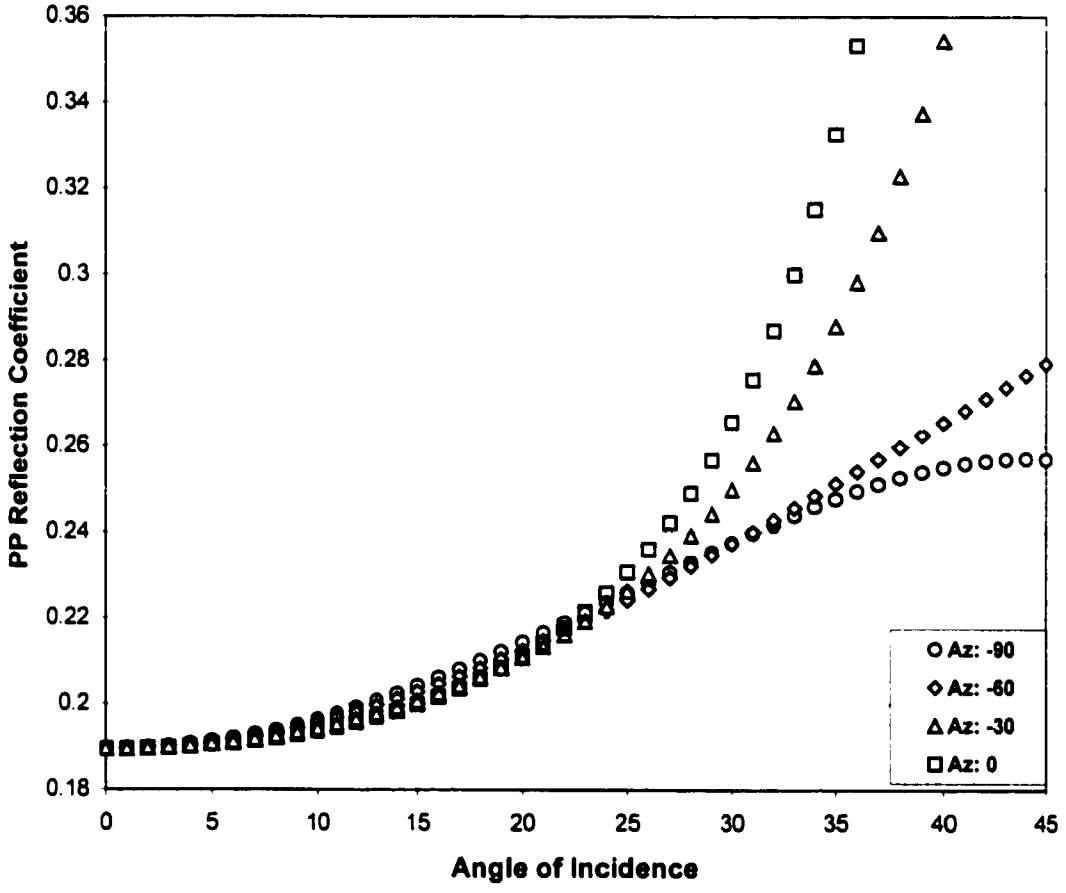

Figure 7.2 Azimuthal P-wave reflection coefficients for Model 1

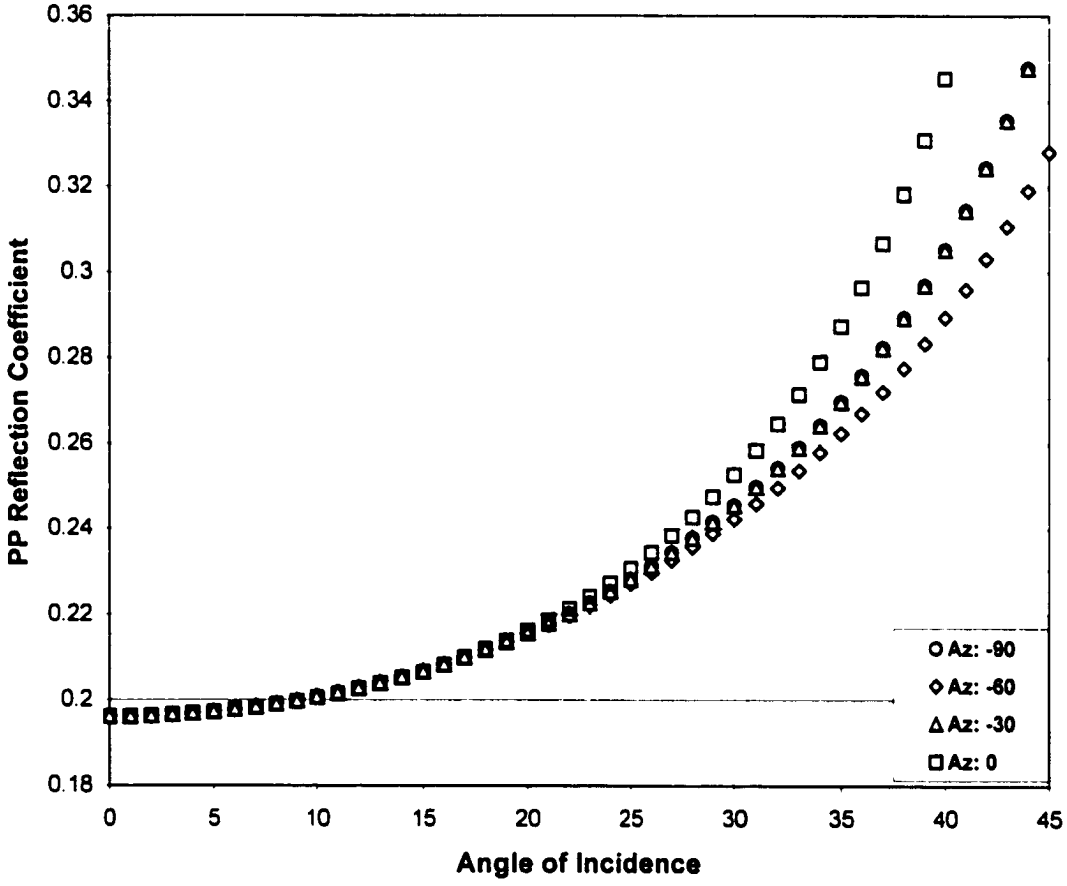

Figure 7.3 Azimuthal P-wave reflection coefficients for Model 2

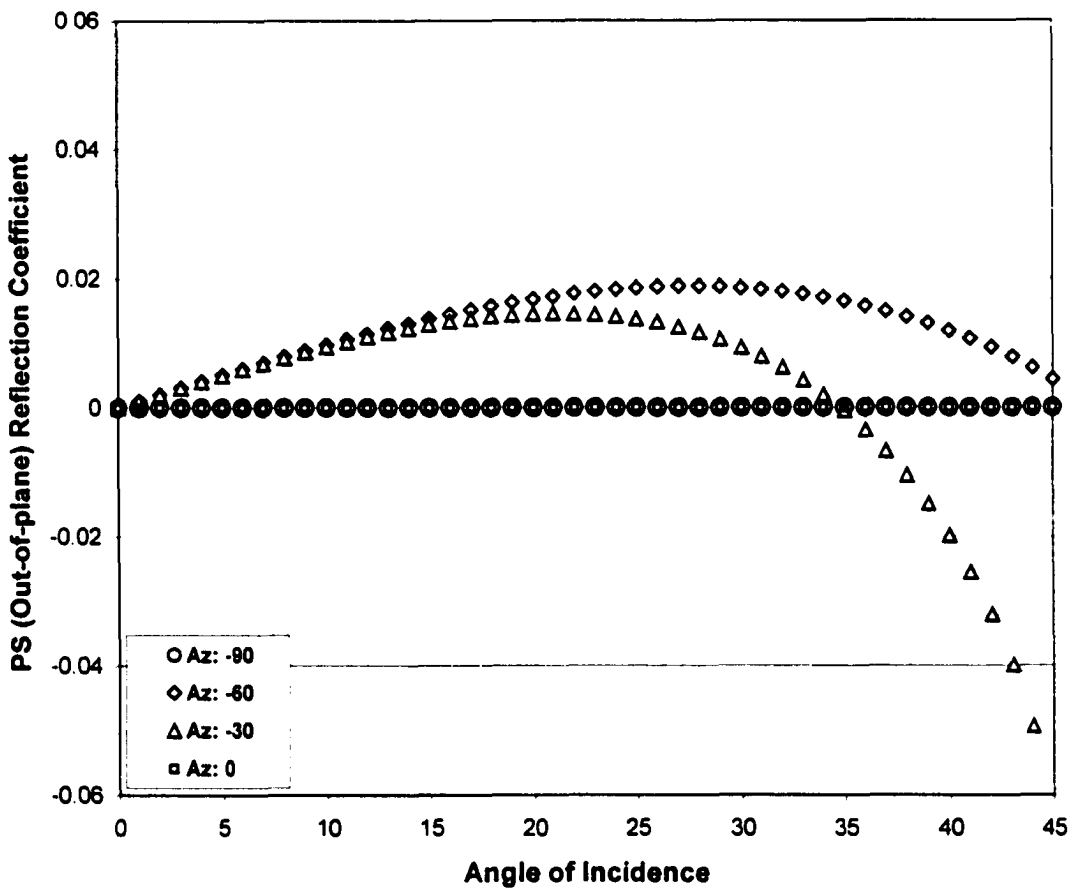

Figure 7.4 Azimuthal out-of-plane S-wave reflection coefficients for Model 1

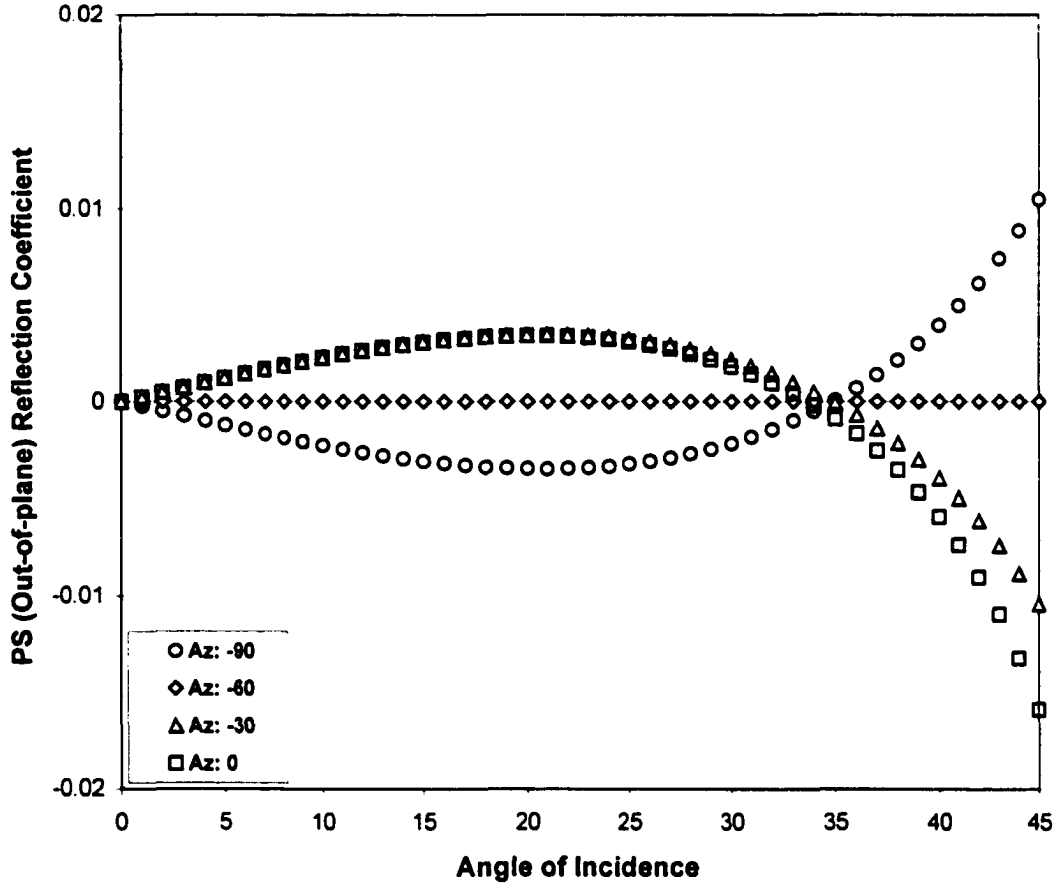

Figure 7.5 Azimuthal out-of-plane S-wave reflection coefficients for Model 2

PS reflections is much more sensitive to fractures than PP reflections. Even at small incidence angles, Figure 7.4 and 7.5 show a distinct azimuthal AVO response for both Models 1 and 2.

2) The normal incidence reflections are always zero for all quasi-S waves because all the fracture sets are vertical. There is no converted shear wave when the P-wave is normally incident upon the reflection surface for the model assumed.

3) In Figure 7.4 for model 1, notice that the azimuth -90° and 0° AVO curves are zero. With only one set of vertical fractures at azimuth -90°, the reservoir model can be treated as an HTI medium (Hudson ,1980, 1981) with two symmetry planes. One of the symmetry planes is the isotropic plane at azimuth -90° and the other one is an effective VTI plane at azimuth 0° direction (Tsvankin, 1995, 1996). This modeling work shows that the shear wave reflection can be used to find the orientation of the fracture set under the condition that only one fracture set exists.

4) In Figure 7.5 for model 2, a zero-reflection curve is also observed. This reflection curve happens at the azimuth -60°, which equally splits the two fracture systems. It is also noticed that the two reflection curves of the azimuths -90° and -30° show up as mirror images of each reflected about the azimuth -60° curve.
These observations indicate that the azimuth -60° plane acts as a symmetry plane, but it is not parallel, or perpendicular, to any fracture sets. In this model, the azimuth -60° plane can be misinterpreted as an 'apparent effective' orientation of one fracture set.

Figures 7.6 and 7.7 show the quasi in-plane shear reflections for models 1 and 2, respectively. Once again, as in the out-of-plane S-wave case, the in-plane S-wave reflection curves show strong azimuthal variations for fracture models under small

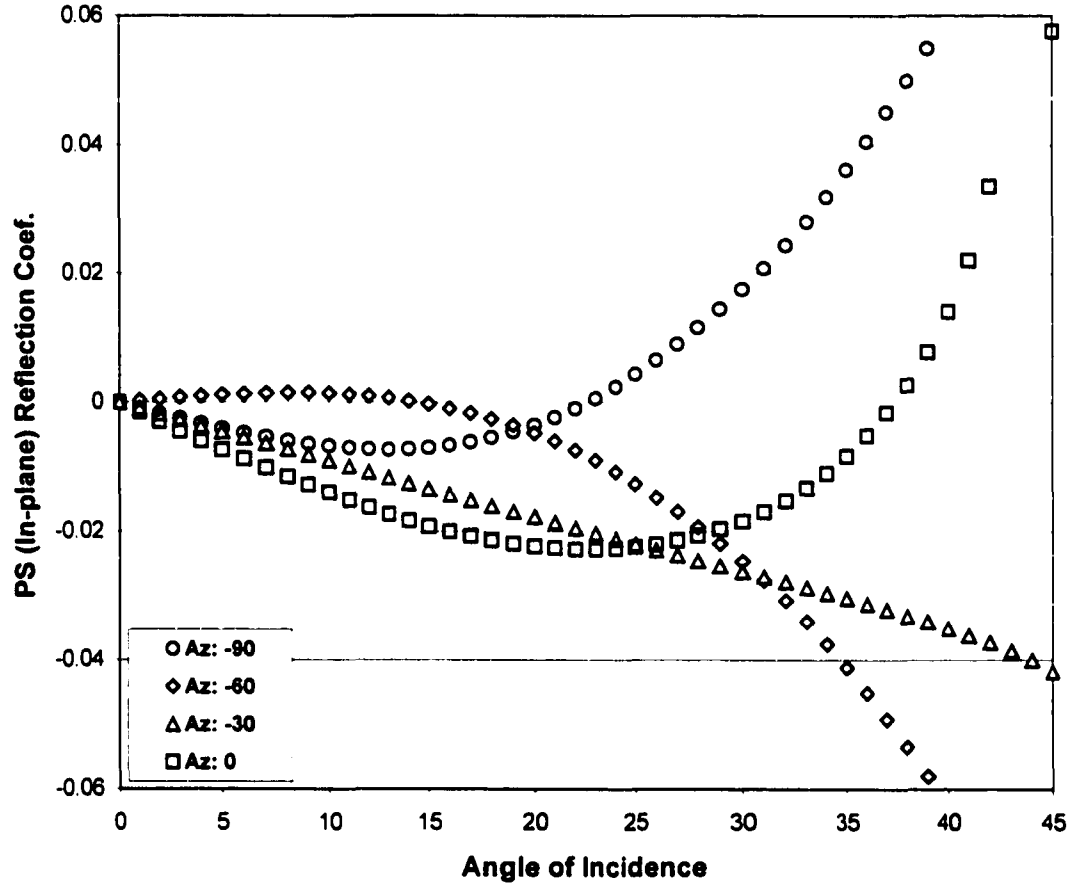

Figure 7.6 Azimuthal in-plane S-wave reflection coefficients for Model 1

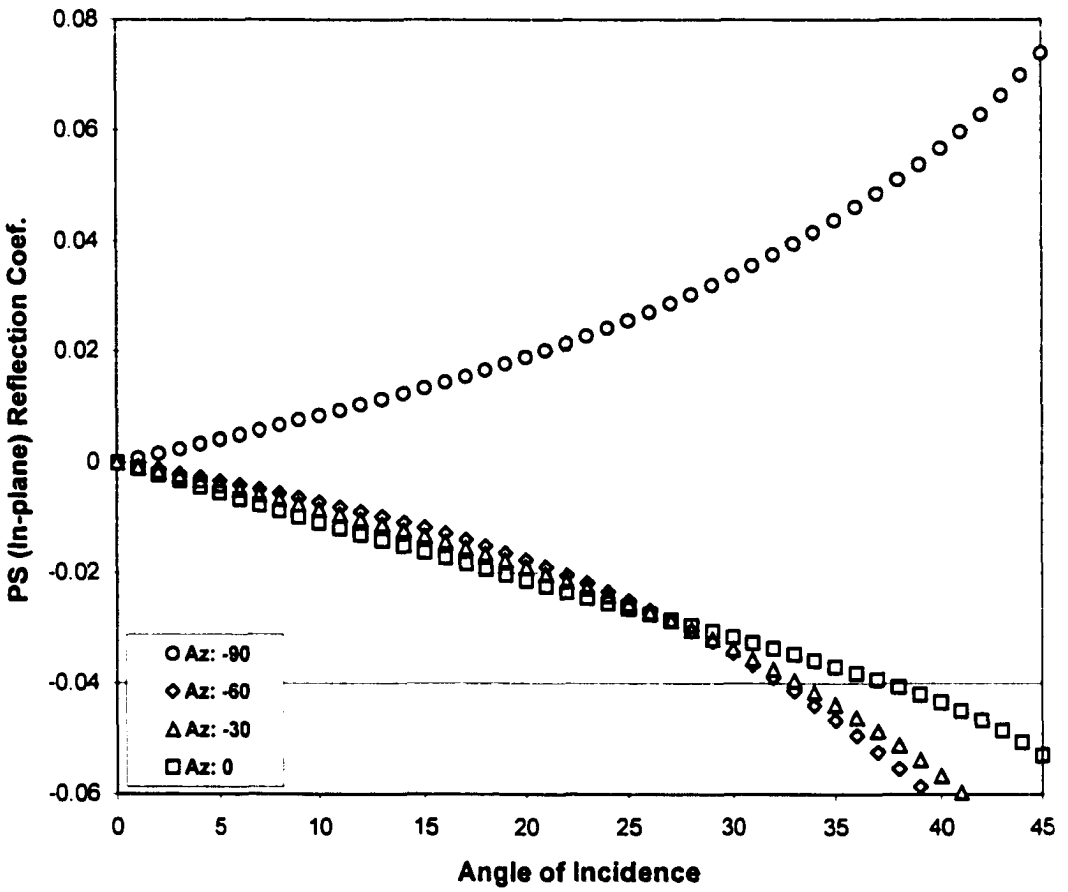

Figure 7.7 Azimuthal in-plane S-wave reflection coefficients for Model 2

incidence angle conditions. Even more importantly, the azimuthal AVO variations are larger than those of out-of-plane S-wave curves (compare to Figure 7.4 and 7.5). Another observation is that the azimuthal AVO from the single fracture set model (Model 1) is larger than those of the two-fracture set model (Model 2).

7.5 Conclusions

The azimuthal variation of the converted PS reflections is more sensitive to fractures than PP reflections. The evidence is that, under small incidence angle conditions, the S-wave reflection curves show distinct azimuthal AVO variations. However, the azimuthal variations of the PP reflection due to fractures can be only clearly observed when incidence angle is large (greater than 25° for the models in this synthetic study).

It is found that, with the same total crack density, a model containing a single fracture set presents the largest variation on azimuthal AVO. Multiple fracture sets tend to weaken the azimuthal anisotropic effects.

With large offset data, the large azimuthal variation in P-wave reflections may indicate the existence of fractures zone. The larger the relative amplitude variations with azimuth, the greater the possibility for a single fracture set.

The out-of-plane S-wave azimuthal AVO can be used to identify symmetry planes that may indicate an orientation direction of one fracture set. However, the symmetry plane, under particular situations, may not directly be related to any orientation directions of the fracture sets. Theoretically, in a fractured area, if there is no PS reflection at normal incident angle, the fracture sets should be vertical to the

reflection boundary. AVO modeling using the exact reflection coefficient modeling developed in this thesis is a useful tool for studying methods for detecting fracture properties. Based upon this study, S-waves have the greatest potential for studying fracture properties.

Chapter 8

Case Study: Determine Petrophysics Parameters Using Exact AVO trend

The variation of seismic reflection amplitude with offset is dependent on intrinsic rock parameters such as compressional-wave velocity (Vp), shear-wave velocity (Vs), density, and anisotropy, etc. (Castagna and Buckes, 1993). In this chapter, a case study of anisotropic modeling of real AVO behavior is performed to investigate tradeoffs between anisotropic and conventional AVO parameters.

8.1 Data

The AVO analysis is performed on a deep-water Gulf of Mexico seismic dataset. The event of interest is indicated by an arrow in the stacked section (Figure 8.1) where a clear amplitude anomaly is observable. This anomaly is selected as the research target for this thesis. It happens at a shallow depth (two-way travel-time ≈ 1625ms) where AVO techniques are expected to be robust if the mute occurs at sufficiently far offset. The lithologic column of the shallow portion consists exclusively of sands and shales.

Figure 8.2 shows the CDP gathers across the anomaly. Between the times 1600-1700 ms, amplitude increases with offset for all five CDP gathers. The maximum offset of this gather is 817 m. Table 8.1 lists semblance velocity analysis results from the nearest velocity analysis. Figure 8.3 illustrates the picked semblance velocity of thick layers increasing with time.

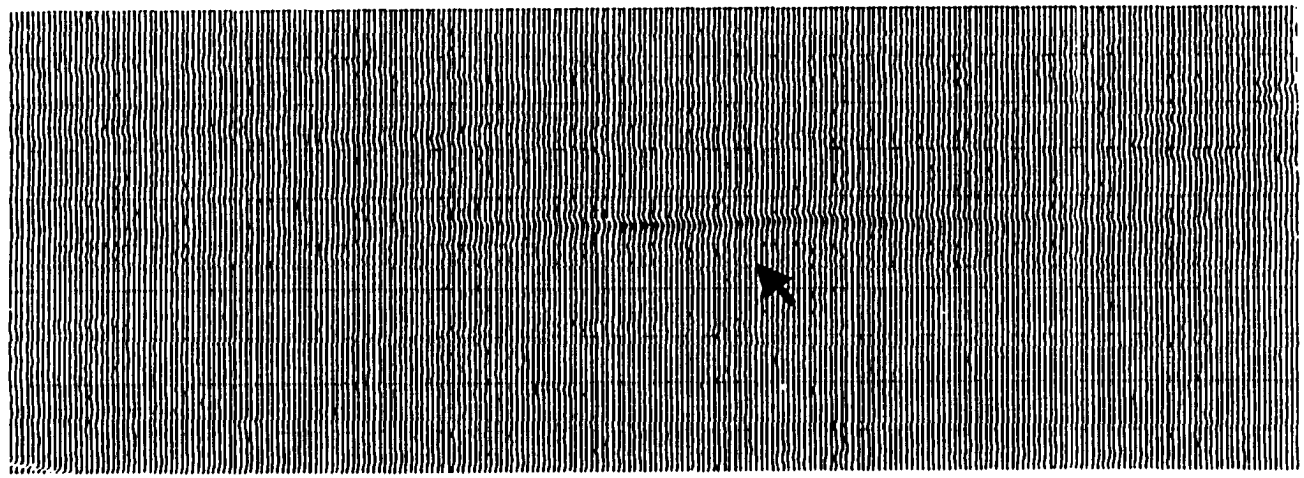

Figure 8.1 An amplitude anomaly on stacked section

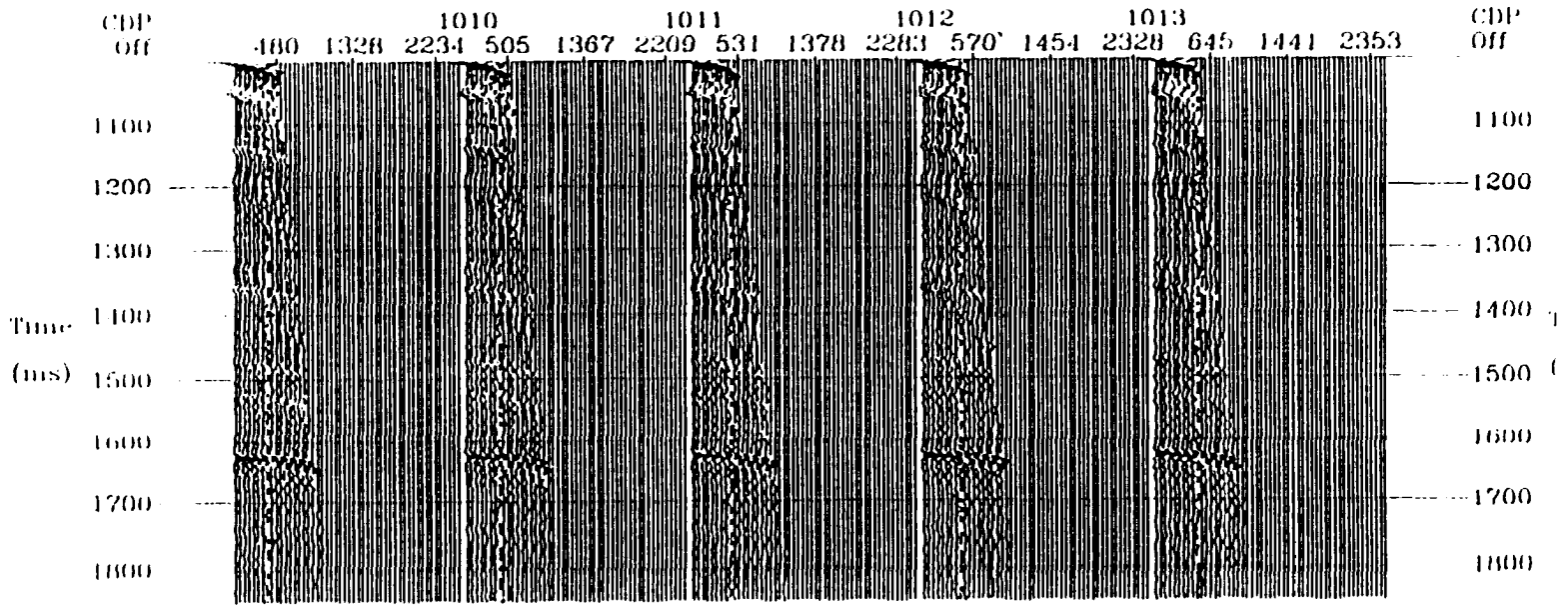

Figure 8.2 CDP gathers across the anomaly in Figure 8.1

Table 8.1 Semblance Velocity Table at CDP No. 1000

Two Way Time (ms)	Semblance Velocity (m/s)
424	1480.6
922.7	1532.1
1293.7	1562.5
1653.2	1614
2035.9	1716.9
2372.2	1834.6
2708.4	1937.5
3021.5	2084.6

8.2 Strategy

For extracting petrophysical parameters using measured AVO, the strategy below is developed:

8.2.1 Extract AVO trend from data

One of the important AVO techniques is to investigate the relative variation of trace amplitudes within a CDP gathers. This requires that the all trace amplitudes have to be preserved and recovered. In figure 8.2, the CDP gathers are already a result of careful data processing, with high signal-to-noise ratio and recovered relative seismic amplitudes. An amplitude-vs-offset measurement is made on the central CDP shown in Figure 8.2, which shows a distinct amplitude increase with offset (Figure 8.4a).

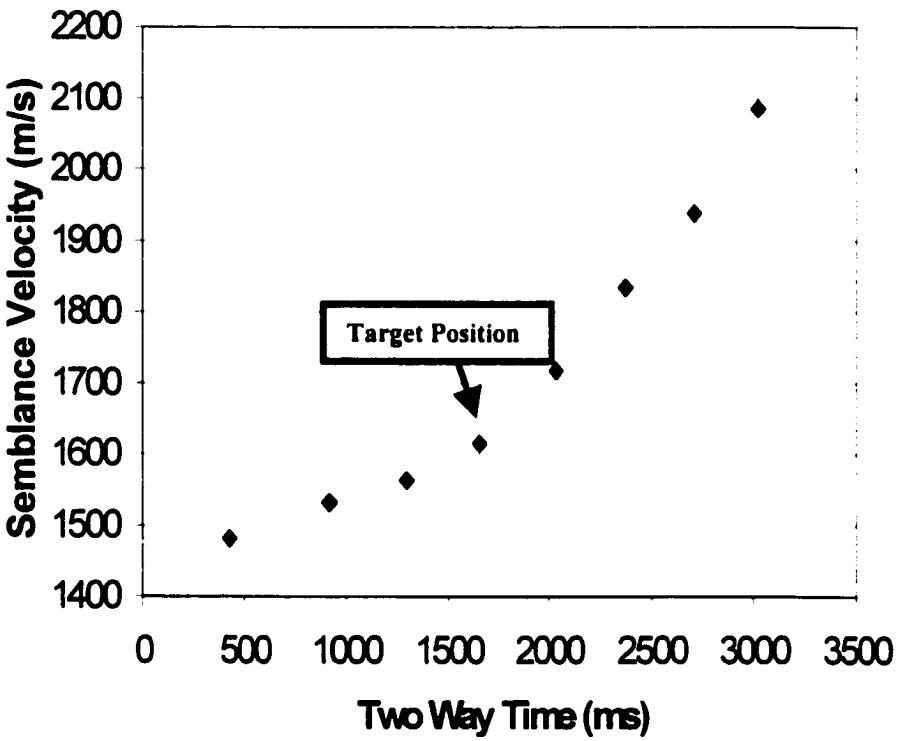

Figure 8.3 Semblance velocity analysis result at CDP No. 1000

The incidence angle corresponding to each offset must be found before computing the synthetic reflection coefficients. As the first step, comparison is made between the time depth on CDP gathers (Figure 8.2) and layering from semblance velocity values in Table 8.1. This work reveals that the target reflector lays on the fourth reflective velocity boundary. Using the semblance velocity table (Table 8.1), the interval velocities of each layer can be obtained from Dix equation (Dix, 1955):

$$V_{int} = \sqrt{\frac{V_{rms,N}^2 t_N(0) - V_{rms,N-1}^2 t_{N-1}(0)}{t_N(0) - t_{N-1}(0)}} \qquad \text{.....(8.1)}$$

where V_{int} is the interval velocity between N^{th} and $N\text{-}1^{th}$ reflection boundary. $V_{rms,N}$ and $V_{rms,N-1}$ are the RMS velocities for the N^{th} and $N\text{-}1^{th}$ reflection boundary respectively, and $t_N(0)$ and $t_{N-1}(0)$ are the corresponding two-way-times to the reflectors.

The assumptions at this point are that:

1) The lithology of these four thick layers are basically isotropic and homogenous.

2) All the four reflective boundaries are horizontal.

Conventional angle-of-incidence calculation are not sufficient for these data as the receivers are ocean bottom labels and the water depth is great. Thus, given an offset length, an isotropic ray-tracing procedure is applied iteratively to find the corresponding incidence angle upon the target boundary. The amplitude-vs-offset (AVO) measurement (Figure 8.4a) is then converted into amplitude-vs-angle (AVA) measurement (Table 8.2). Figure 8.4b presents the extracted AVA data, which shows the amplitude increase with incidence of angle.

Table 8.2 PP Reflction Amplitude Measurement at CDP No. 1011

Offset (m)	Angle of Incidence	PP reflection
0	0	2.05468
36	0.868467	2.0577188
73	1.761122	2.0632474
131	3.160712	2.079468
196	4.741999	2.1086063
231	5.587397	2.1290944
295	7.146384	2.1752441
331	8.017215	2.2061386
395	9.591071	2.2698359
430	10.451585	2.3094206
495	12.053468	2.3918455
531	12.940638	2.442481
595	14.535267	2.5412731
631	15.437664	2.601779
695	17.038331	2.7181184
717	17.601439	2.760704
796	19.613913	2.9245629
817	20.155236	2.9709992

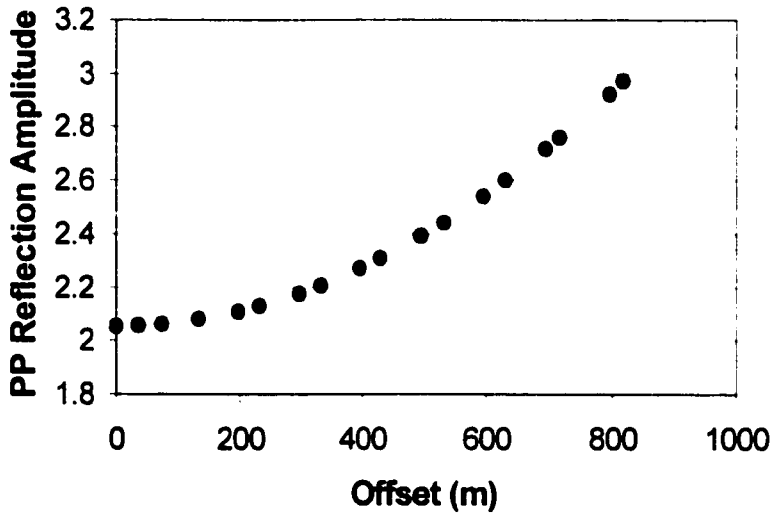

Figure 8.4a PP Reflection Amplitude vs Offset

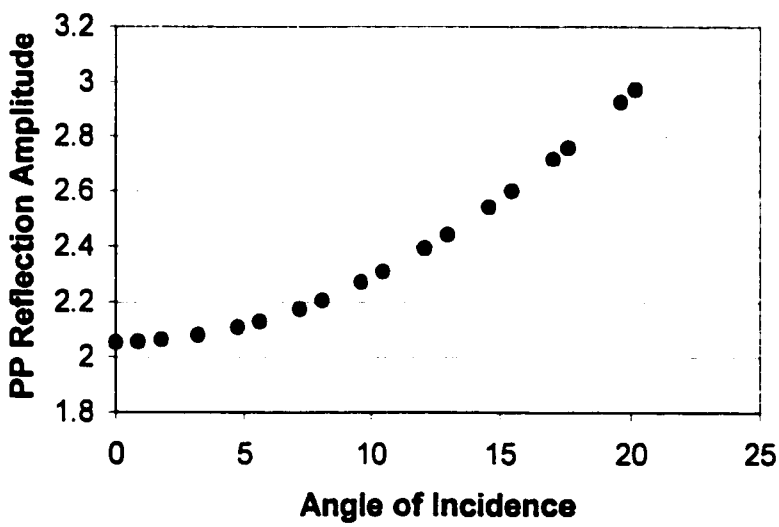

Figure 8.4b PP Reflection Amplitude vs Angle of Incidence

8.2.2 Set up the synthetic models

Different synthetic reflection models are set up for comparison studies under the following assumptions:

The magnitude of reflection is determined by petrophysical parameters across the target boundary. These parameters, such as V_p, V_s, density, and anisotropy, etc., may not agree with the thick-layer's petrophysical

properties extracted from the seismic data.

1) The target reflector is a consequence of a sand reservoir overlaid by a thin layer of shale.

2) The reservoir is isotropic, but its P-wave and S-wave velocities may vary due to porosity change, fluid content and properties change, etc.

3) The shale is expected to exhibit high intrinsic anisotropy. This assumption result from the preferred orientation of micas and clay minerals in shales, fine laminations, and low aspect ratio pores.

According to the assumption, the Shale's P-wave velocity is set to be the same as the fourth layer interval velocity. The S-wave velocity and density are obtained from Castagna's equations (after Castagna, et. al., 1993):

$$V_s\ (m/s) = 0.77V_p - 867.4 \quad \text{.....(8.2)}$$

and (Gardner, 1974):

$$\rho\ (kg/m^3) = 1.741V_p^{1/4} \quad \text{.....(8.3)}$$

8.2.3 Petrophysics parameter extraction

The theoretical AVA response is computed by using the exact general anisotropic procedure (as described as Chapter 6) for each set of petrophysics parameters. All model comparison studies are accomplished on the basis of normalization with the normal-incident-reflection amplitudes of the extracted data.

The normalized extracted AVA curve is compared to the theoretical curve family, which are from models with the same V_p value, but with different V_s/V_p ratio. For a given P-wave velocity V_p, one V_s/V_p ratio can be selected from the model which has the closest synthetic AVA trend. To repeat this procedure by varying the P-wave velocity V_p can yield a number of V_s/V_p ratio such that each pair of V_p and V_s/V_p ratio generates a petrophysical parameter fit to the extracted AVA data. The V_p and V_s/V_p ratio pairs are then crossplotted into a so-called 'petrophysics-fit' curve. The intersection point of this petrophysics-fit curve and the classic lithology-related (V_p V_s relationship) curves (Castagna, et. al., 1993) indicates reasonable values of V_p and V_s for the reservoir.

8.3 Observations

For limiting the search range for the petrophysical parameters, model tests are first designed to find out a reasonable range of P-wave velocity (V_{p2}) of the reservoir. Assuming $V_s/V_p \approx 0.5$, a variation of V_{p2} is allowed between 80% - 120% of V_{p1} (P-wave velocity of the overlying shale layer). Then, the theoretical AVA trend for each model can be obtained by using exact reflection coefficient calculations. After normalizing each curve with its own normal-incident-reflection amplitudes, Figure 8.5

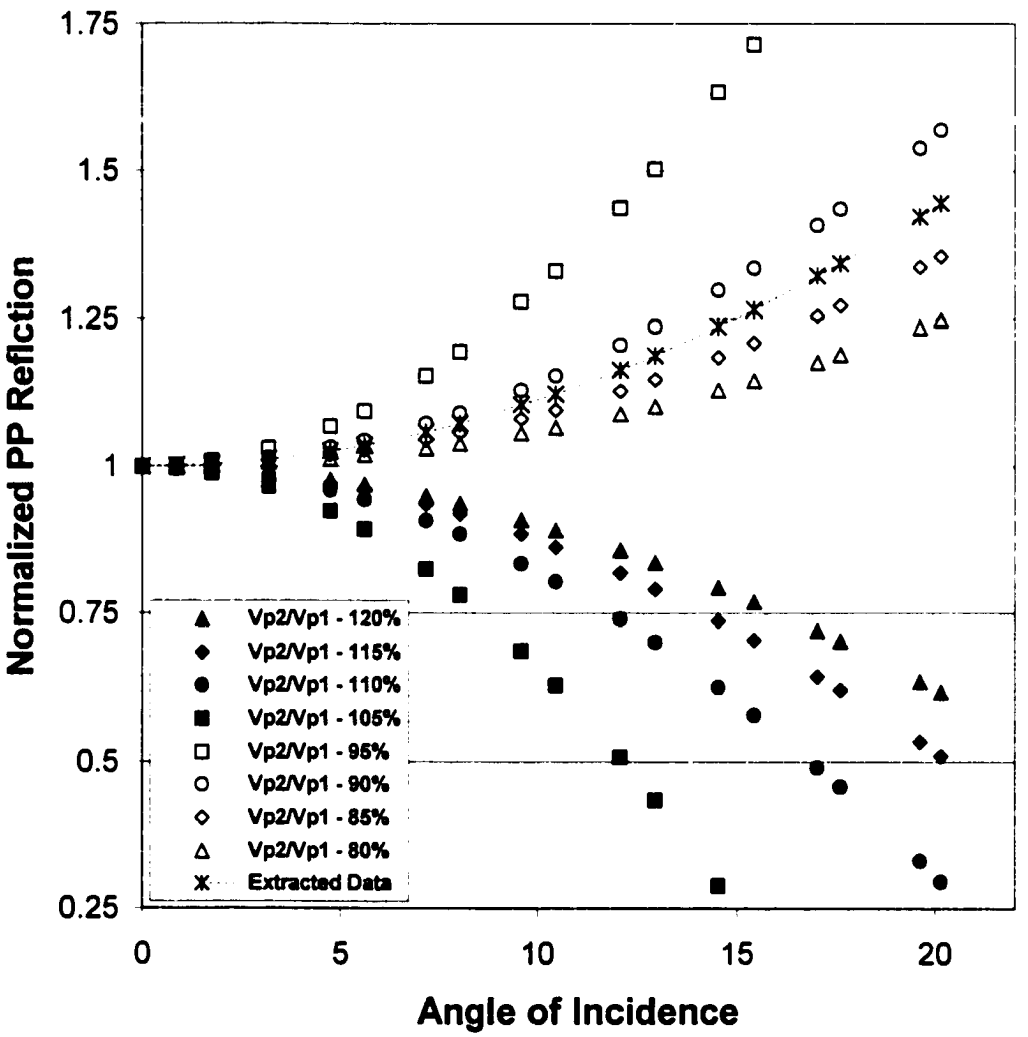

Figure 8.5 Synthetic AVA curves obtained from the exact reflection coefficient procedure. Models uses different value for V_{p2}, while keep $V_{s2}/V_{p2} = 0.5$

shows a group of synthetic model AVA trends (each V_{p2} with a difference of 5% V_{p1}) compared with the extracted data. It shows clearly that, when $V_{p2} < V_{p1}$, the synthetic amplitude increases with angle of incidence which agrees with the extracted data AVA trend. As the first result in this case study the P-wave velocity of reservoir should be smaller than the overlying shale layer.

With a knowledge of V_{p2} variation range, model tests can be applied for searching the value pairs of V_{p2} and V_{s2}/V_{p2} using iterative procedure as described in section (8.2.3). Setting $V_{p2} = .9\ V_{p1}$ as an example, Figure 8.6 compares the synthetic models (with different V_s/V_p ratio) to the extracted data, and presents a good curve fit when $V_{s2}/V_{p2} = .45$. The value pair ($V_{p2} = .9\ V_{p1}$ and $V_{s2}/V_{p2} = .45$) is then selected for setting up a possible petrophysical relationship. All the value pairs of V_{p2} and V_{s2}/V_{p2} can be crossplotted into a petrophysical-fit curve as shown in Figure 8.7. The values of V_{p2} and V_{s2}/V_{p2} can be determined by reading the intersection point of this petrophysics-fit curve and an empirical V_p -V_s trend for sand (Castagna, et. al., 1993) in Figure 8.7. If the overlying shale layer is isotropic, the petrophysics parameter extraction result in this case study is: $V_{p2} = 1742$ m/s, $V_{s2} = 557$ m/s.

Under the assumption that shales are usually anisotropic, more model tests are conducted by adding anisotropic parameters to the overlying shale layer. To simplify the discussion, elliptical anisotropy is assumed in this model study. By varying only anisotopic parameters, Figures 8.8 – 8.10 show distinct anisotropic effects on the synthetic AVA trends. In this case study, it happens that incrementally adding 10% anisotropy to the overlying shale causes a 5% drop in V_s/V_p ratio inverted target interval.. Figure 8.11 shows the anisotropic effects (from the overlying shale) on the

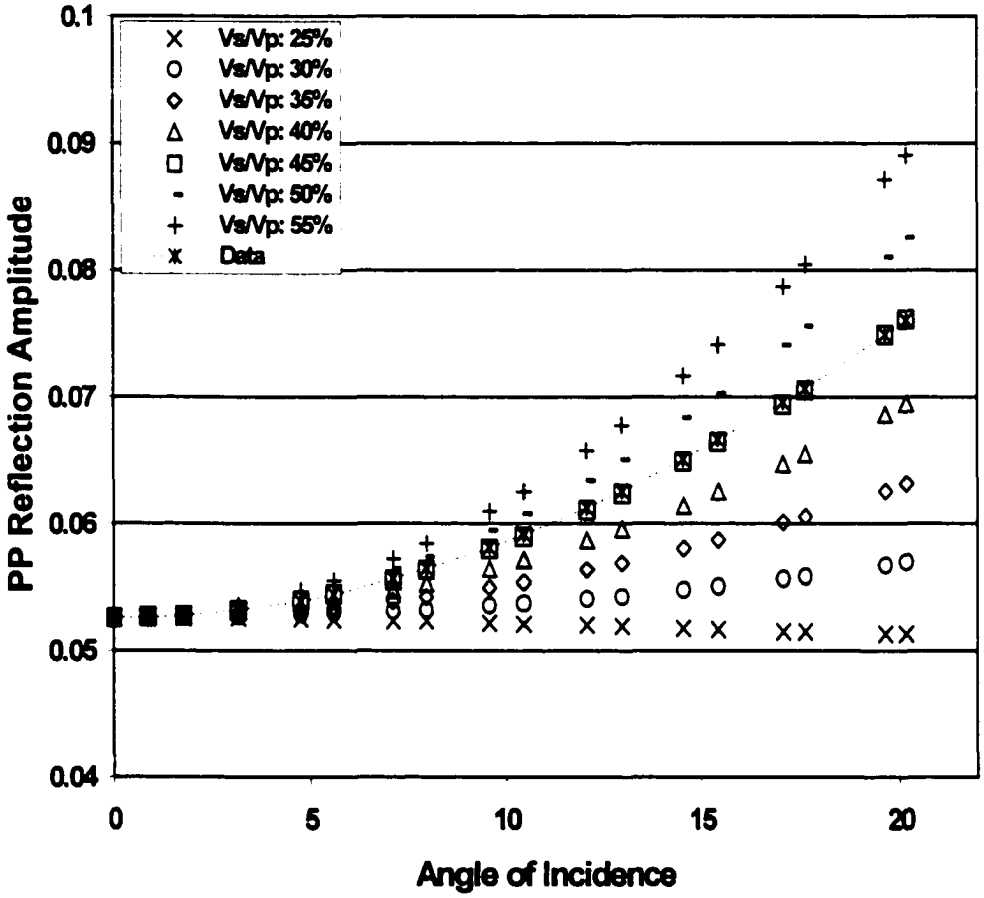

Figure 8.6 Comparison between synthetic AVA curves and the data. The synthetic models use same P-wave velocity $V_{p2} = 90\%V_{p1}$, with varying different ratio of V_{s2}/V_{p2}. The overlaid shale is assumed to be isotropic.

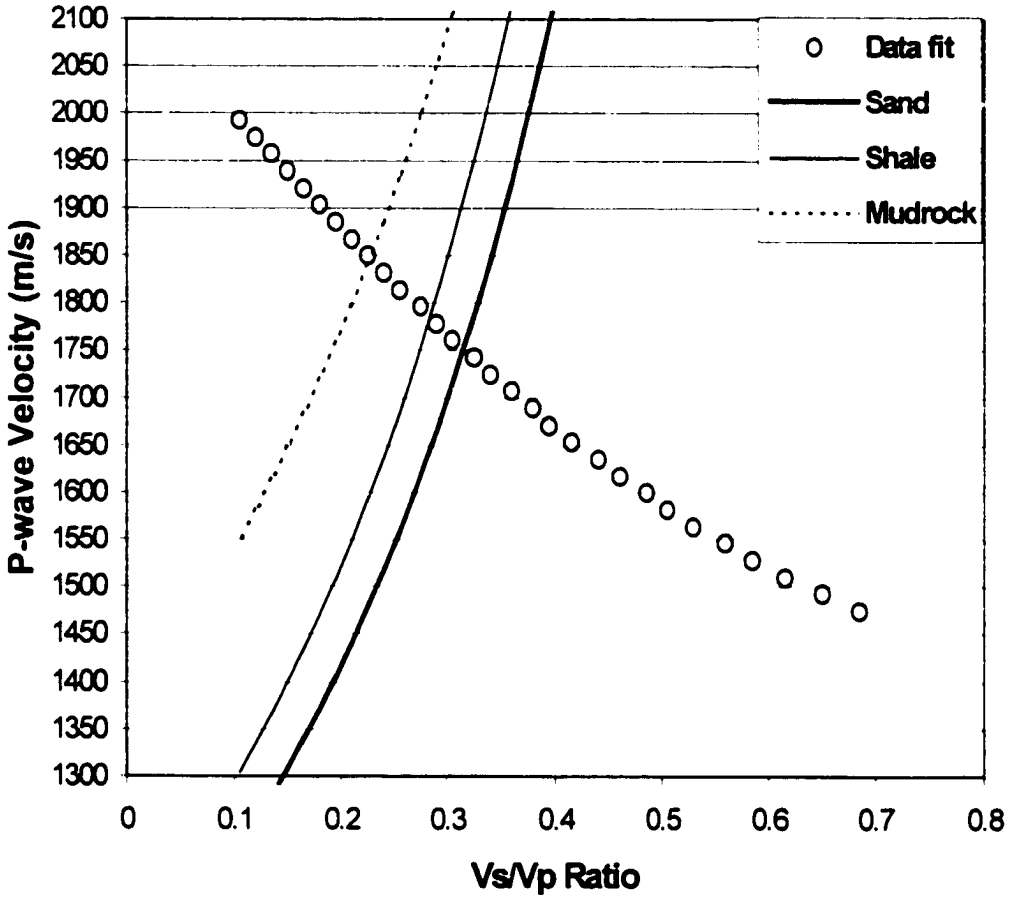

Figure 8.7 V_p versus V_s/V_p crossplot: each pair of V_p and V_s/V_p values means a curve fit between the synthetic model and the data. The overlaid shale is assumed to be isotropic.

petrophysical-fit result. For example, assuming the overlying shale has 20% anisotropy, the result of petrophysical parameter extraction changes to: V_{p2} = 1671 m/s, V_{s2} = 485 m/s. Compared with parameter extraction result from Figure 8.7, this result is a 4% drop in V_p and 13% drop in V_s. Thus, the anisotropy from the overlying shale may have a larger effect on the V_s extraction than the V_p extraction.

Compared with the isotropic curve, the three anisotropic ones in Figure 8.11 also indicate an increasing influence from the degree of anisotropy of the overlying shale.

8.4 Conclusions

Due to the close relationship between the rock petrophysical properties and its seismic response, it is possible to derive the petrophysical parameters from the AVO analysis. The strategy described in this chapter is sensitive in extracting P-wave and S-wave velocities. This method is believed applicable in the exploration practice, particularly in the case where only seismic data is available.

The first group of model tests should be designed to find out a reasonable range of P-wave velocities of the reservoir for the purpose of limiting the search scope of the petrophysics parameters. This will constrain the inversion for V_s and V_p pairs.

The computation procedure for exact reflection coefficients is a necessary and powerful tool in this strategy. Exact synthetic models provide a solid basis for comparison and may be extended to a wider range of incidence angle.

Anisotropy from overlying shale or underlying sand has an effect on the extraction of reservoir parameters. The effect increases with increasing degree of anisotropy. It is also noticed that the anisotropic effect on V_s extraction of the reservoir

can be much stronger than the extraction of V_p. However, anisotropy is usually weak, especially in shallow, deep-water shale. An estimation of local anisotropic parameter (of shale) may be enough for extraction of the reservoir's petrophysical parameters.

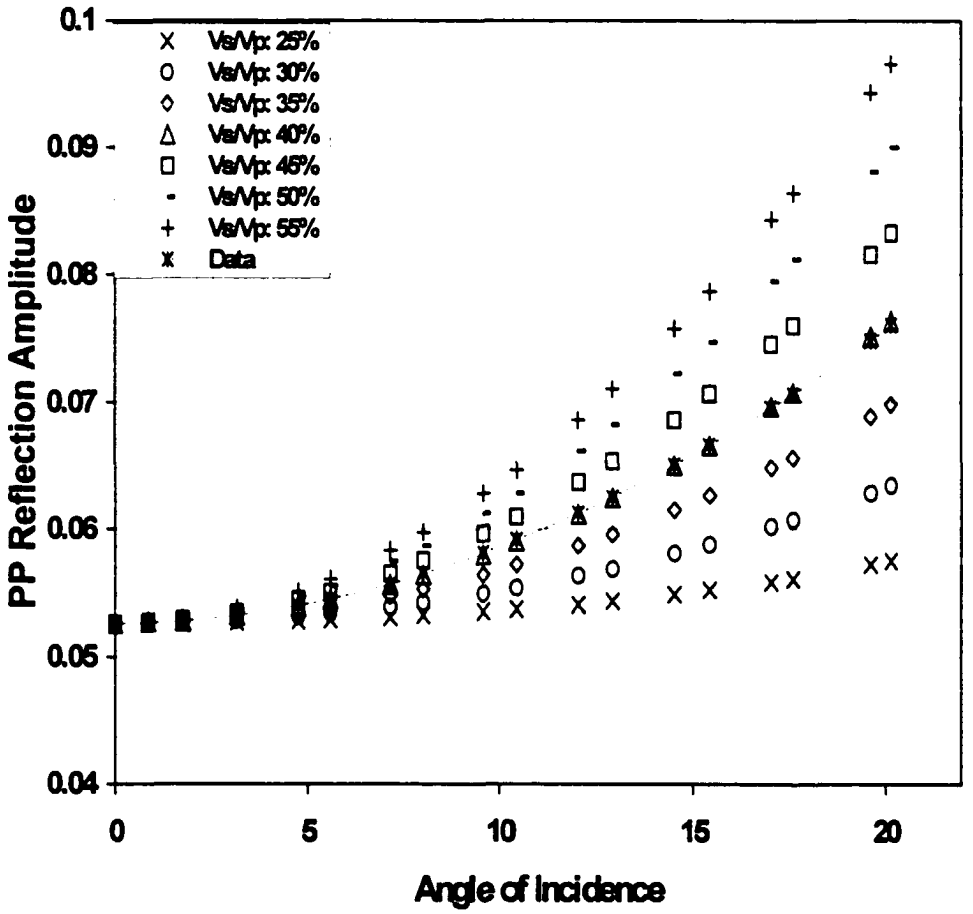

Figure 8.8 Comparison between synthetic AVA curves (with 10% anisotropy) and the data.

The isotropic parameters of the models are exactly the same as Figure 8.6. The overlaid shale is assumed to have 10% anisotropy.

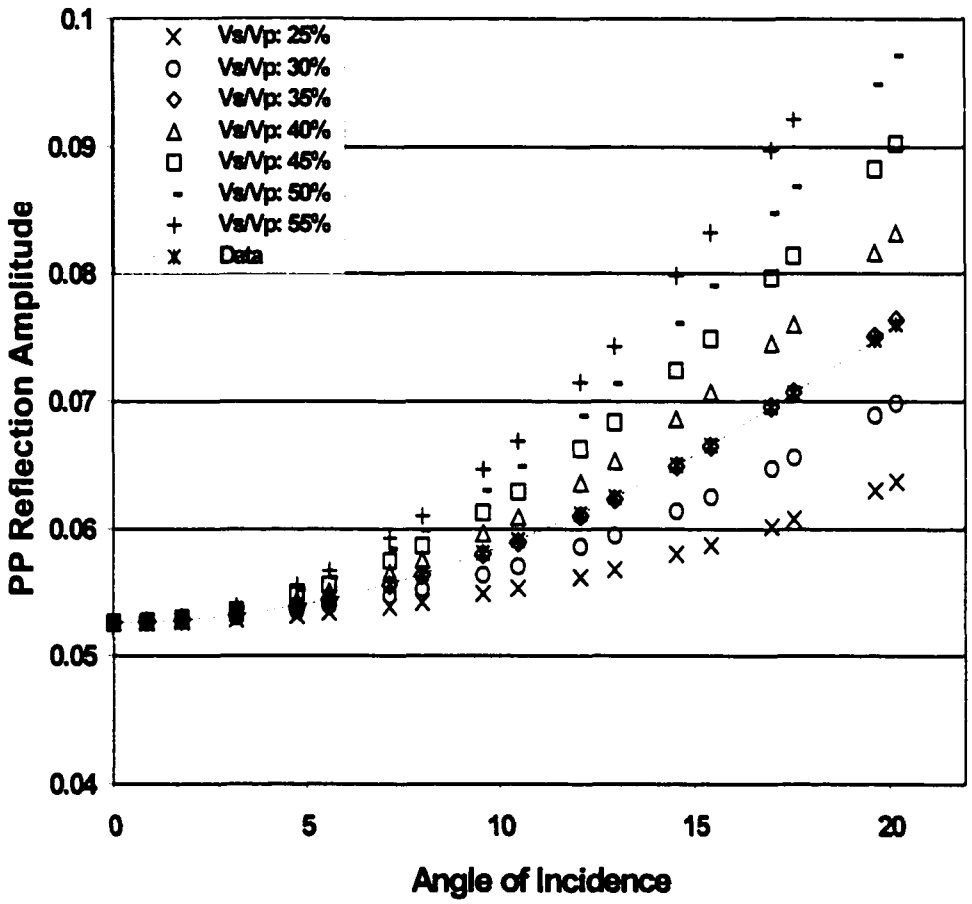

Figure 8.9 Comparison between synthetic AVA curves (with 20% anisotropy) and the data.

The isotropic parameters of the models are the same as Figure 8.6. The overlaid shale is assumed to have 20% anisotropy.

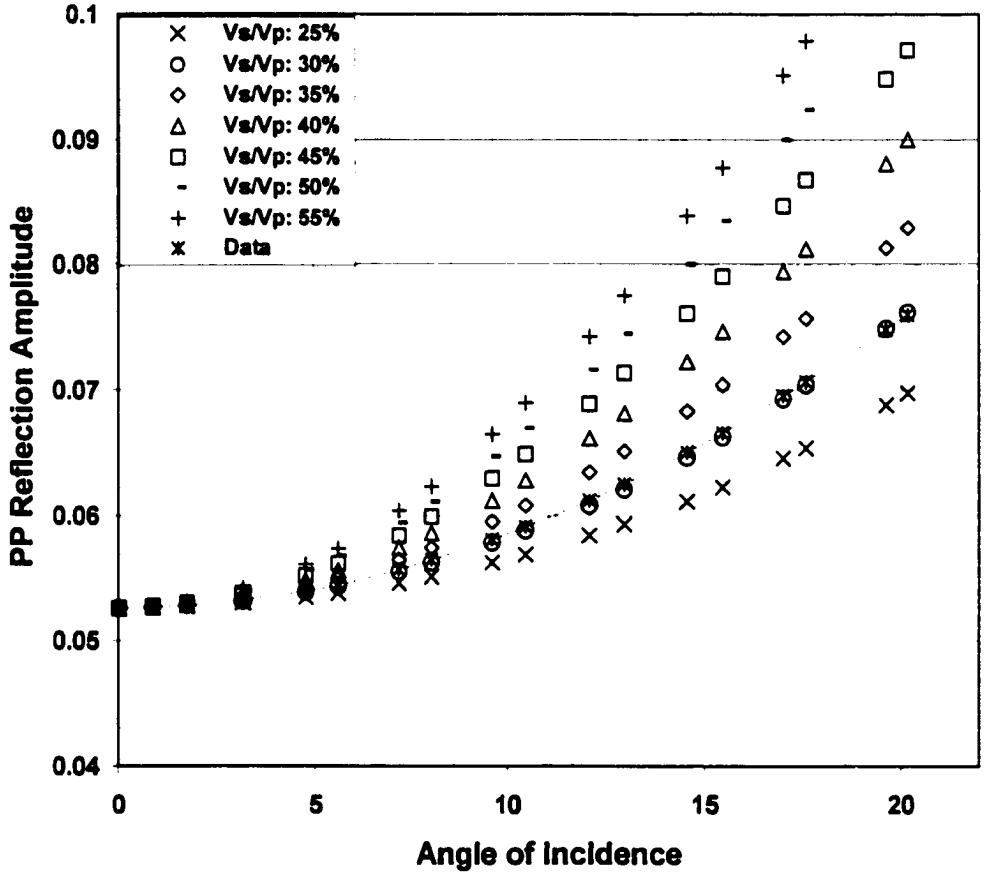

Figure 8.10 Comparison between synthetic AVA curves (with 30% anisotropy) and the data.

The isotropic parameters of the models are the same as Figure 8.6. The overlaid shale is assumed to have 30% anisotropy.

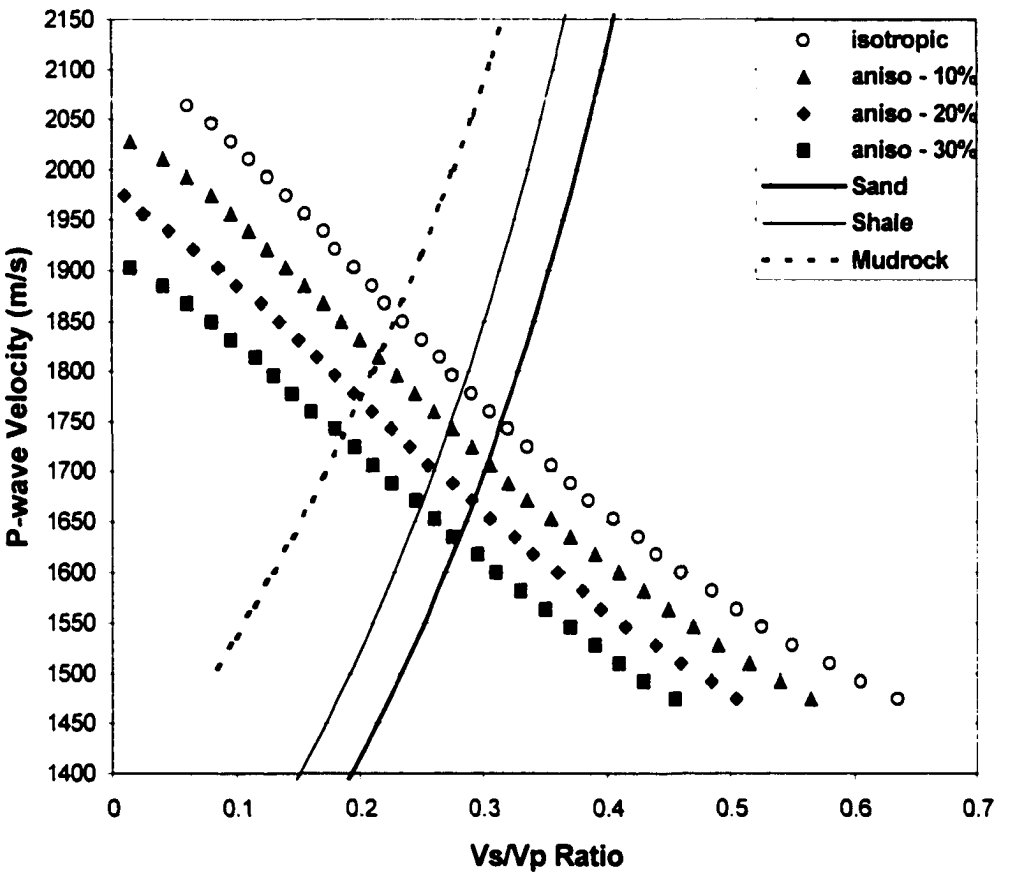

Figure 8.11 V_p versus V_s/V_p crossplot showing the anisotropic effects: each pair of V_p and V_s/V_p values means a curve fit between the synthetic model and the data.
The anisotropy of the overlaid shale is assumed to vary from 0 – 30%.

Chapter 9

Conclusions and Discussions

The results of this thesis represent a contribution to the present understanding of the effects of anisotropy on AVO analysis. The exact reflection coefficient results derived in his thesis make AVO modeling more realistic in complex fracture system.

Daley's exact reflection coefficient in VTI media is rederived in this thesis. A number of typographical errors are corrected in the solutions published by Daley and Hron (1997 & 1979). Under the condition that all of the elastic constants (a total of ten considering both media) and densities of the VTI media are known, the exact reflection coefficients can be obtained in straightforward manner from a series of algebraic expressions.

A unified algorithm for solving the exact reflection coefficients in general anisotropic media is developed. Consideration of wave propagation in the acoustic-axis directions is also included in the general algorithm. This algorithm is a numerical solution, and many numerical problems have to be handled properly during the computation. Some discussions on solving the problems are included in this thesis.

Separate computer programs have been completed, for both VTI (using corrected Daley's solution) and general anisotropic media, to calculate the exact reflection coefficients for reflected quasi-P wave and quasi-S waves when the incident angle (with the wave mode) is specified upon a boundary between two anisotropic

media. These algorithms provide basic tools for most of the research work accomplished in this thesis.

Approximate equations have been applied widely for modeling of VTI media under the assumption that the elastic contrast across the reflection interface is small and the anisotropy is weak. These approximate equations are important because they simplify the dependence of the reflection response upon the parameters. Four published P-wave reflection approximations in VTI media (Baniks, 1986, Ruger, 1995, Thomson, 1993, Wei, 1995) have been analyzed by comparing them to the corrected exact Daley's solution. Some interesting results are: 1) Under isotropic conditions, all four approximations perform the same for any incidence angle, and they are only good approximations when the incidence angle is small. 2) Under anisotropic situations, different approximations work better for different categories of isotropic base models. Banik's approximation over a wider range of incidence angles seem to be superior to the others for many models. Ruger's approximation is more accurate at small incidence angles.

It has been widely accepted that , under isotropic conditions in the Earth's crust, crossplotting of AVO intercept (A) and gradient (B) can be a useful seismic lithologic analysis tool. However, anisotropy exists in the real world. Using a synthetic model study, this research work shows that anisotropy can complicate the application of the powerful AVO technique.

It is well known that anisotropy above and below an interface effects the AVO gradient (B) and curvature (C): 1) On an A versus B crossplot, anisotropy may cause large changes in the B-intercept (which can be mistaken for Poisson's ratio deviations)

and may also cause minor changes in slope. 2) On an A versus C crossplot, large differences may occur in both C-intercept (which can be mistaken for density contrasts), slope, and curve shape. According to Shuey's equation, an A versus C crossplot should be linear with a slope of one. 3) Even in the isotropic case, distinct curvature appears in the A versus C crossplot, which is not predicted by Shuey's equation. An A^2 term must be added to the C-term to obtain linearity in the isotropic case. Deviation from this slope can be a direct indication of anisotropy.

Through the study of anisotropic effects on AVO crossplotting, an empirical correction to Ruger's approximation is introduced. This empirical approximation results in a more accurate crossplot interpretation, and thus provides insight into anisotropic effects on AVO.

Anisotropic effects on seismic stacked sections are often ignored during conventional processing that assumes hyperbolic moveout. This can create pitfalls for interpreters on stacked and partially stacked sections due to improper removal of NMO. These pitfalls include pseudo faults, anticlines, channels, amplitude anomalies, and flat spots. There are quality control methods (eg. inspecting NMO corrected gathers) to mute the improperly flattened events. However, when far offset information is important, muting is not a viable solution. Even higher-order moveout corrections may not entirely correct these problems and complete anisotropic processing may be necessary. As a suggestion from this work, the interpreter should be particularly suspicious of structures evident on full or far-offset stacks that do not appear on near-offset stacks.

A synthetic AVO study over fractured reservoir models reveals that the azimuthal variation of the converted PS reflections is more sensitive to fractures than PP reflections. Assuming background material is isotropic, fractures can be 'seen' from azimuthal converted PS AVO even under small incidence angle conditions.

AVO modeling using the exact reflection coefficient approach developed in this thesis is a useful tool for detecting fracture properties. It is found that a model containing a single fracture set presents the largest variation on azimuthal AVO while multiple fracture sets with different azimuths and the same total crack density has a reduced azimuthal response. Multiple fracture sets tend to weaken the azimuthal anisotropic effects. It is also realized that the out-of-plane S-wave azimuthal AVO can be theoretically used to find any vertical symmetry planes that may be an indication of the orientation direction of one fracture set.

Petrophysical parameters, such as the P-wave velocity, S-wave velocity, and density, etc., are important information for hydrocarbon exploration. Here, a strategy is completed to extract from the AVO analysis the P-wave (V_p) and S-wave (V_s) velocity of the reservoir. The theoretical basis of this work is that there exists a tight relationship between the rock petrophysical properties and its seismic response (Castagna, et al., 1993). Anisotropy from overlying shale has an effect on the extraction of reservoir parameters. It is noticed that the effect on extraction of V_s can be much stronger than the effect upon extraction of V_p.

Finally, from the experience gained during this thesis research, it is suggested that anisotropic effects should be included in any AVO analysis of field data. The exact

reflection coefficients in either VTI or general anisotropic conditions are powerful and efficient tools for making these AVO studies.

References

Aki, K., and Richards, P. G., 1980, Quantitative seismology: Theory and methods: Vol. 1 W. M. Freeman & Co.

Allen, J. L., and Peddy, C. P., 1993, Amplitude variation with offset: Gulf Coast Case Studies: Geophysical Developments Series, Volume 4, SEG.

Auld, B.A., 1973, Acoustic fields and waves in solids, vol.1: John Wiley and Sons.

Babuska, V., Cara, M., 1991, Seismic anisotropy in the earth: Kluwer Academic Publication.

Backus, G. E., 1962, Long-wave elastic anisotropy produced by horizontal layering: J. Geophys. Res. 67, 4427-4440.

Banik, N. C., 1987, An effective anisotropy parameter in transversely isotropic media: Geophysics, 52, 1654-1664

Berryman, J. G., 1979, An effective anisotropy in transversely isotropic media: Geophysics, 44, 896-917.

Blangy, J.P., 1994, AVO in transversely isotropic media – An overview: Geophysics, 59, 775-781.

Carcione, J. M., 1990, Wave propagation in anisotropic linear viscoelastic media: theory and simulated wavefields: Geophys. J. Int., 101, 739-750.

Castagna, J. P., Swan, H. W., Foster, D. J., 1998, Framework for AVO gradient and intercept interpretation: Geophysics, 63, 948-956

Castagna, J. P., Swan, H. W., 1997, Principles of AVO crossplotting: The Leading Edge, 16, 337-342.

Castagna, J. P., Backus, G. E., 1993, Offset dependent reflectivity: Theory and Methods. SEG.

Castagna, J. P., Batzle, M. L., Kan, T. K., 1993, Rock physics – The link between rock properties and AVO response: Theory and Methods. SEG.

Castagna, J. P., Batzle, M. L., Eastwood, R. L., 1985, Relationships between compressional-wave velocities in clatic silicate rocks, Geophysics, 50, 571-581.

Cheadle, S. P., Brown, R. J., Lawton, D. C., 1991, Orthorhombic anisotropy: a physical seismic modeling study: Geophysics, 56, 1603-1613.

Chen, H., Castagna, J. P., 2000, Tutorial: Model study of anisotropic effects on full and partial stacks: Geophysics, 65, 4, 1028-1031.

Chen, H., Castagna, J. P., 1999, Model study of anisotropic effects on full and partial stacks: 1999 SEG Expended Abstract, 1892-1895

Chen, H., Castagna, J. P., Brown, R. L., Ramos A. C. B., 1999, Three-parameter AVO crossplotting in anisotropic media: 1999 SEG Expended Abstract, 73-76

Chen, H., Castagna, J. P., Brown, R. L., Ramos A. C. B., 2000, Three-parameter AVO crossplotting in anisotropic media: Geophysics, in press

Chen, W., 1995, AVO in Azimuthally anisotropic media fracture detection using P-wave data and a seismic study of naturally fractured tight gas reservoirs: Ph.D. dissertation, Stanford University, Stanford, California

Cheng, C. H., Toksoz, M. N., 1979, Inversion of seismic velocities for the pore aspect ratio spectrum of a rock: Journal of Geophysical Research, 84, 7533-7543

Daley, P. F., and Hron, F., 1977, Reflection and transmission coefficients for transversely isotropic media: BSSA, 67, 661-675

Daley, P.F., and Hron, F., 1979, Reflection and transmission coefficients for seismic waves in ellipsoidally anisotropic media: Geophysics, 44, 25-38

Dix C.H., 1955, Seismic velocities from surface measurements, Geophysics, 20, 68-86

Edmund, G., Henneke, II, 1971, Reflection-refraction of stress wave at a plane boundary between anisotropic media: The Journal of the Acoustical Society of America, 51, 210-217

Fagin, S. W., 1991, Seismic modeling of geologic structures: Applications to exploration problems, SEG.

Fatti, j. L., Smith, G. C., Vail, P. J., Strauss, P. J. and Levitt, P. R., 1994, Detection of gas in sandstone reservoirs using AVO analysis: A 3-D seismic case history using the Geostack technique: Geophysics, 59, 1362-1376.

Gardner, G. H. F., Gardner, L. W., Gregory, A. R., 1974, Formation velocity and density - the diagnostic basics for stratigraphic traps, Geophysics, 39, 770-780.

Gibson, Jr. R.L., Toksoz, M. N., 1990, Permeability estimation from velocity anisotropy in fractured rock: Journal of Geophysical Research, 95, 15634-15655.

Helbig, K., and Schoenberg, M., 1987, Anomalous polarization of elastic waves in transversely isotropic media: J. Acoust. Soc. Am., 81, 1235-1245.

Hilterman, F., 1989, Is AVO the seismic signature of rock properties: 59th Ann. Int. Mtg., SEG., Expended Abstracts, 559.

Hoenig A. 1979, Elastic moduli of a non-randomly cracked body: International Journal Solids Structures, 15, 137-154.

Hoenig A. 1978, The behavior of a flat elliptical crack in an anisotropic elastic body: International Journal Solids Structures, 14, 925-934.

Hornby, B. E., 1995, Experimental determination of the anisotropic elastic properties of shales: Seismic Anisotropy, SEG, 238-296.

Hudson, J. A., Liu, E. 1999, Effective elastic properties of heavily faulted structures: Geophysics, 64, 479-485.

Hudson, J. A., 1991, Crack distdributions which account for a given seismic anisotropy: Geophysical Journal Institute, 104, 517-521.

Hudson, J. A. 1990, Overall elastic properties of isotropic materials with arbitrary distribution of circular cracks: Geophysical Journal Institute, 102, 465-469.

Hudson, J. A. 1981, Wave speeds and attenuation of elastic waves in material containing cracks: Geophysical J. R. astr. Soc., 64, 133-150.

Hudson, J. A. 1980, Overall properties of a crack solid: Math. Proc. Camb. Phil. Soc., 88, 371-384.

Hudson, J. A. 1975, Overall properties of a cracked solid: Mathematical Proceedings Cambridge Philosophy Society, 88, 371-384.

Keith, C. M., and Crampin, S., 1977, Seismic body waves in anisotropic media: Reflection and refraction at a plane interface: Geophs. J. Roy. Astr. Soc., 49, 181-208.

Kim, K. Y., Wrolstad, K. H., Aminzadeh, F., 1993, Effects of transverse isotropy on P-wave AVO for gas sands: geophysics, 58, 883-888.

Koefoed, O., 1955, On the effect of Poisson's ratio of rock strata on the reflection coefficients of plane waveGeophsi. Prosp., 3, 381-387.

Levin, F. K., 1979, Seismic velocities in transversely isotropic media; Geophysics, 44, 918-936

Love, A. E. H., 1934, A treatise on the mathematical theory of elasticity: Cambridge University Press

Lorenz, J. C., Teufel, L. W., Warpinski, N. R., 1991, Regional fractures I: a mechanism for the formation of regional fractures at depth in flat-lying reservoirs: The American Association of Petroleum Geologists Bulletin, 75, No. 11, 1714-1737.

Mavko, G. M., Nur, A., 1978, The effect of nonelliptical cracks on compressibility of rocks: Journal of Geophysical Research, 83, 4459-4468

Mueller, M., 1992, Using shear waves to predict lateral variability in vertical fracture intensity: The Leading Edge, 11, No. 2, 29-35

Nur, A., 1971, Effects of stress on velocity anisotrpy in rocks: J. geophys. Res., 76, 2022-2034.

O'connell, R. J., 1977, Viscoelatic properties of fluid-saturated cracked solids: Journal of Geophysical Research, 82, 5719-5735.

O'connell, R. J., 1974, Seismic velocities in dry and saturated cracked solids: Journal of Geophysical Research, 79, 5412-5425.

Ostrander, W.J., 1984, Plane-wave reflection coefficients for gas sands at nonnormal angles of incidence: Geophsics, 49, 1637-1648.

Ostrander, W.J., 1984, Plane-wave reflection coefficients for gas sands at nonnormal angles of incidence: 52nd Ann. Int. Mtg., SEG, Expanded Abstracts, 216-218.

Robertson, J. D., Corrigan D., 1983, Radiation patterns of shear-wave vibrator in near-surface shale: Geophysics, 48, 19-26.

Rokhlin, S. I., Bolland, T.K., and Adler, L., 1986, Reflection and refraction of elastic waves on a plane interface between two generally anisotopic media: J. Acoust. Soc. Am., 79, 4, 906-918.

Ruger, A., 1997, P-wave reflection coefficients for transversely isotropic models with vertical and horizontal axis of symmetry: Geophysics, 62, 713-722.

Rutherford, S. R., and Williams, M. W., 1989, Amplitude-versus-offset variations in gas sands: Geophysics, 54, 680-688.

Schoenberg, M., Helbig, K., 1997, Orthorhombic media: Modeling elastic wave behavior in a vertically fractured earth: Geophysics, 62, 1954-1974.

Schoenberg, M., Sagers, C., 1995, Seismic anisotropy of fractured rock: Geophysics, 60, 204-211

Schoenberg, M., Douma, J., 1988, Elastic wave propagation in media with parallel fractures and aligned cracks: Geophysical Prospecting, 36, 571-590.

Shuey, R. T., 1985, A simplification of the Zoeppritz equations: Geophysics, 50, 609-614.

Sheriff, R. E., 1991, Encyclopedic dictionary of exploration geophysics, Third edition, Society of Exploration Geophysicists

Smith, G. C., 1996, 3-parameter geostack, 1996 SEG Expended Abstract, 1747-1750

Swan, H.W., 1993, Properties of direct AVO hydrocarbon indicators: Offset-dependent reflectivity-Theory and practice of AVO analysis: Soc. Expl. Geophys. 78-92

Thomsen, L., 1993, Weak anisotropic refection: Offset-dependent reflectivity-theory and practice of AVO analysis, IG-8, 103-111, SEG

Thomsen, L., 1988, Reflection seismology over azimuthally anisotropic media: Geophysics, 53, 304-313.

Thomsen, L., 1986, Weak elastic anisotropy: Geophysics, 51, 1954-1966.

Thomsen, L., 1985, Biot-consistent elastic moduli of porous rocks: Geophysics, 50, 2797-2807.

Toksoz, M. N., Cheng, C. H., Timur, A., 1976, Velocities of seismic waves in porous rocks: geophysics, 41, 621-643

Tsvankin, I., Thomsen, L., 1994, Nonhyperbolic reflection moveout in anisotropic media: Geophysics, 59,1290-1304

Tsvankin, I., 1995, Body-wave radiation patterns and AVO in transversely isotropic media: Geophysics, 60, 1409-1425

Tsvankin, I., 1996, P-wave signatures and notation for transversely isotropic media: An overview: Geophysics, 61, 467-483

Vernik, L., Nur, A., 1992, Ultrasonic velocity and anisotropy of hydrocarbon source rocks: Geophysics, 57, 727-735

Vernik, L., Liu, X., 1997, Velocity anisotropy in shales: A petrophysical study: Geophysics, 62, 521-532

Walsh, J. B., 1966, Seismic wave attenuation in rock due to friction, Journal of Geophysical Research, 71, 2591-2599

Walsh, J. B., 1965, The effect of cracks on the compressibility of rock, Journal of Geophysical Research, 70, 381-389

Wright, J., 1984, The effects of anisotropy on reflectivity-offset: 54 th Ann. Internat. Mtg., Soc. Expl. Geophys. Expanded Abstracts, 670-672.

Wright, J., 1987, The effects of tansverse isotropy on reflection amplitude versus offset: Geophysics, 52, 564-567.

Zoeppritz, K., 1919, Erdbebenwellen, on the refleciton and penetration of seismic waves through unstable layers. Gottinger Nachichten, 1(VII(VII B), 66-84

Appendix I: FORTRAN90 Subroutine for Calculation of Exact P-wave and Reflection and Transmission Coefficients

```
!*************************************************************
! Name:         Daley_coefficient
! Description:  This subroutine is to calculate the exact P-
!               wave reflection and transmission
!               coefficients in TI media assuming P-wave
!               incidence. Given the incident and reflecting
!               TI media, it takes the incidence angle (Ib)
!               as input. Then, it use Daley's equations to
!               compute the reflection and transmission
!               coefficients of P- and AV-wave. SH waves are
!               not considered in this program.
!               During the computation, two other
!               subroutines, "compute_L_M" and
!               "compute_Velocity_Angle", are called.
! Input:        Ib    - P-wave incidence phase angle
! Output:       R11   - P-wave reflection coefficient
!               R12   - P-wave transmission coefficient
!               R13   - SV-wave reflection coefficient
!               R14   - SV-wave transmission coefficient
! Global Variables:
!               VPv1  - Vetical P-wave velocity of incident
!                       medium (α1)
!               VSv1  - Vertical S-wave velocity of incident
!                       medium (β1)
!               Ep1   - Thomsen anisotropic parameter ε of
!                       incident medium
!               Es1   - Thomsen anisotropic paramter γ of
!                       incident medium
!               Dlt1  - Thomsen anisotropic parameter δ of
!                       incident medium
!               de1   - density of incident medium (ρ1)
!               VPv2  - Vertical P-wave velocityof reflecting
!                       medium (α2)
!               VSv2  - Vertical S-wave velocity of
!                       reflecting medium (β2)
!               Ep2   - Thomsen anisotropic parameter ε of
!                       reflecting medium
!               Es2   - Thomsen anisotropic paramter γ of
!                       reflecting medium
```

```
!              Dlt2 - Thomsen anisotropic parameter δ of
!                     reflecting medium
!              de2  - density of reflecting medium (ρ2)
!              pi   = 3.1415926
!*************************************************************


Subroutine Daley_coefficient(Ib,R11,R12,R13,R14)
Implicit None

   Real, Intent(INOUT) :: Ib
   Complex, Intent(OUT) :: R11,R12,R13,R14

   Real :: Vp1,Vp2,Vs3,Vs4
!   Vp1 - P-wave reflection velocity
!   Vp2 - P-wave transmission velocity
!   Vs3 - SV-wave reflection velocity
!   Vs4 - SV-wave transmission velocity

   Complex :: R1,R2,R3,R4
!   R1 - Sine of P-wave reflection angle
!   R2 - Sine of P-wave transmission angle
!   R3 - Sine of SV-wave reflection angle
!   R4 - Sine of SV-wave transmission angle

   Real :: Ci11,Ci33,Ci13,Ci55
!   Ci11, Ci33, Ci13, Ci55: Elastic stiffness of incident
!                           media

   Real :: Cr11,Cr33,Cr13,Cr55
!   Cr11, Cr33, Cr13, Cr55: Elastic stiffness of
!                           reflecting media

!  All parameters below are same as in Daley Page666-667
   Complex :: l1,l2,l3,l4,m1,m2,m3,m4
   Real :: x,n,k1,k2
   Complex ::P,Q,S,R
   Complex :: b1,b2,d1,d2,w1,w2,eb1,eb2,l
   Complex :: T1,T2,T3,T4,T5,T6,T7,T8,T9,T10,T11,T12
   Complex :: E1,E2,E3,E4,E5,E6,E7,E8,E9,E10,E11,E12,D

   Call compute_Velocity_An(Ib,Vp1,Vp2,Vs3,Vs4,R1,R2,R3,R4)

   Call l_m_compute(VPv1,VSv1,Ep1,Dlt1,R1,l1,m1)
   Call l_m_compute(VPv2,VSv2,Ep2,Dlt2,R2,l2,m2)
   Call l_m_compute(VPv1,VSv1,Ep1,Dlt1,R3,l3,m3)
```

```
Call l_m_compute(VPv2,VSv2,Ep2,Dlt2,R4,l4,m4)

Ci33=del*VPv1**2
Cil1=(1+2*Ep1)*Ci33
Ci55=del*VSv1**2
Ci13=SQRT((Ci33-Ci55)*((1+2*Dlt1)*Ci33-Ci55))-Ci55

Cr33=de2*VPv2**2
Cr11=(1+2*Ep2)*Cr33
Cr55=de2*VSv2**2
Cr13=SQRT((Cr33-Cr55)*((1+2*Dlt2)*Cr33-Cr55))-Cr55

x =R1
n =Vp1/Vp2
k1=Vs3/Vp1
k2=Vs4/Vp2
P =Sqrt(1.-R1**2)
Q =Sqrt(1.-R2**2)
S =Sqrt(1.-R3**2)
R =Sqrt(1.-R4**2)

b1 = Ci55
b2 = Cr55
d1 = l3*Ci33-m3*Ci13
d2 = l4*Cr33-m4*Cr13
w1 = Vp1/(Vs3*(l1+m1))*((m3+l3)*S**2-l3)
w2 = Vp1/(Vs4*(l1+m1))*((m4+l4)*R**2-l4)
eb1= l1*Ci13+(m1*Ci33-l1*Ci13)*P**2
eb2= (l2*Cr13+(m2*Cr33-l2*Cr13)*Q**2)*(Vp1/Vp2)
l  = (l2+m2)/(l1+m1)

T1 =  eb2 - eb1*l2/(n*l1)
T2 =-(b2*w2*k1*l3/m1 - b1*w1*k2*l4/(n*m1))
T3 =  b2*w2 + b1*l4*k2*x**2/(n*m1)
T4 =-(eb2*m3/l1 + d1*l2*x**2/(n*l1))
T5 =  b1*(w1 + k1*l3*x**2/m1)
T6 =  eb2*m4/l1 + d2*l2*x**2/(n*l1)
T7 =  b2*l - b1*m2/m1
T8 =-(d2*m3/l1 - d1*m4/l1)
T9 =  b2*(w2*m2/m1 + l*l4*k2*x**2/(n*m1))
T10=  eb1*m3/l1 + d1*x**2
T11=-(eb1*m4/l1 + d2*x**2)
T12=  b1*w1*m2/m1 + b2*l*l3*k1*x**2/m1

E1 =  T1*T2*x**2
E2 =  T3*T4*P*S
E3 =  T5*T6*P*R
```

```
      E4 =  T7*T8*P*Q*R*S*x**2
      E5 =  T9*T10*Q*S
      E6 =  T11*T12*R*Q
      E7 =2*T5*T11*P*R
      E8 =2*T3*T10*P*S
      E9 =2*T7*T11*P*Q*R*x
      E10=2*T1*T3*P*x
      E11=2*T7*T10*S*Q*P*x
      E12=2*T1*T5*P*x

      D = E1+E2-E3+E4-E5+E6

      R11 = (-E1+E2-E3+E4+E5-E6)/D
         If (Real(R2)>=1.) Then
         R12=0
         Else
      R12 = (E7-E8)/D
         End If
      R13 = (E10-E9)/D
         If (Real(R4)>=1.) Then
         R14=0
         Else
      R14 = (E11-E12)/D
         End If

End Subroutine Daley_coef
```

```
!*************************************************************
!Name:         compute_L_M
!Description: This subroutine calculates the l and m
!              values which define the polarization
!              direction of particle displacement. The
!              values of l and m are different corresponding
!              to reflected P-wave, reflected SV-wave,
!              transmitted P-wave and transmitted SV-wave.
!Input:        Vp      - Vertical P-wave velocity
!              Vs      - Vertical S-wave velocity
!              epsilon - Anisotropic parameter
!                        (Thomsen, 1986)
!              delta   - Anisotropic parameter
!                        (Thomsen, 1986)
!              Rr      - Sine of wave propagation angle
!Output:       values of l and m
!*************************************************************

Subroutine l_m_compute(Vp,Vs,epsilon,delta,Rr,l,m)
Implicit None

   Real, Intent(IN) :: Vp,Vs,epsilon,delta
   Complex, Intent(IN) :: Rr
   Complex, Intent(OUT) :: l,m
   Complex :: A11,A33,A13,A55,A1,A2,Q

   A33=Vp**2
   A11=(1+2*epsilon)*A33
   A55=Vs**2
   A13=SQRT((A33-A55)*((1+2*delta)*A33-A55))-A55
   A1=2*(A13+A55)**2-(A33-A55)*(A11+A33-2*A55)
   A2=(A11+A33-2*A55)**2-4*(A13+A55)**2
   Q=SQRT((A33-A55)**2+2*A1*Rr**2+A2*Rr**4)

   If (Rr==0.) Then
      l=SQRT(((Q-A33+A55)/0.000001+(A11+A33-2*A55))/(2*Q))
   Else
      l=SQRT(((Q-A33+A55)/Rr**2+(A11+A33-2*A55))/(2*Q))
   End If

   If (Rr==(1.0,0.0)) Then
      m=SQRT(((Q-A11+A55)/0.000001+(A11+A33-2*A55))/(2*Q))
   Else
      m=SQRT(((Q-A11+A55)/(1-Rr**2)+(A11+A33-2*A55))/(2*Q))
   End If

End Subroutine l_m_compute
```

```
!*************************************************************
! Name:         compute_Velocity_Angle
! Description: This subroutine calculates the 4 velocities
!               (reflected P, transmitted P, reflected SV,
!               and transmitted SV) and 4 corresponding sine
!               values of the wave propagation angles.
!Input:         Ip     - P-wave incident phase angle
!Output:        V1     - P-wave reflection velocity
!               V2     - P-wave transmission velocity
!               V3     - SV-wave reflection velocity
!               V4     - SV-wave transmission velocity
!               sinR1  - Sine of P-wave reflection angle
!               SinR2  - Sine of P-wave transmission angle
!               SinR3  - Sine of SV-wave reflection angle
!               SinR4  - Sine of SV-wave transmission angle
!*************************************************************

Subroutine compute_Velocity_Angle(Ip,V1,V2,V3,V4,&
                    sinR1,sinR2,sinR3,sinR4)
Implicit None

   Real, Intent(INOUT) :: Ip
   Real, Intent(OUT) :: V1,V2,V3,V4
   Complex, Intent(OUT) :: sinR1,sinR2,sinR3,sinR4

   Real, Dimension(4) :: Vr,Rr,U,V
   Real :: VH,VV
   Real :: Vi !phase vel
   Real :: z,z1,E
   Integer :: j
   Real :: fi1,fi2,Ai1,Ai2,Ai11,Ai33,Ai55,Ai13
   Real :: fr1,fr2,Ar1,Ar2,Ar11,Ar33,Ar55,Ar13,Vrph

   U(1)=VPv1
   U(2)=VPv2
   U(3)=VSv1
   U(4)=VSv2
   V(1)=Sqrt(1+2*Ep1)*VPv1
   V(2)=Sqrt(1+2*Ep2)*VPv2
   V(3)=Sqrt(1+2*Es1)*VSv1
   V(4)=Sqrt(1+2*Es2)*VSv2

   Ai33=Vpv1**2
   Ai11=(1+2*Ep1)*Ai33
   Ai55=VSv1**2
   Ai13=SQRT((Ai33-Ai55)*((1+2*Dlt1)*Ai33-Ai55))-Ai55
```

```
Ar33=Vpv2**2
Ar11=(1+2*Ep2)*Ar33
Ar55=VSv2**2
Ar13=SQRT((Ar33-Ar55)*((1+2*Dlt2)*Ar33-Ar55))-Ar55

Ai1=2*(Ai13+Ai55)**2-(Ai33-Ai55)*(Ai11+Ai33-2*Ai55)
Ai2=(Ai11+Ai33-2*Ai55)**2-4*(Ai13+Ai55)**2
Ar1=2*(Ar13+Ar55)**2-(Ar33-Ar55)*(Ar11+Ar33-2*Ar55)
Ar2=(Ar11+Ar33-2*Ar55)**2-4*(Ar13+Ar55)**2

fi1=Ai33+Ai55+(Ai11-Ai33)*Sin(Ia)**2
fi2=Sqrt((Ai33-Ai55)**2+2*Ai1*Sin(Ia)**2+Ai2*Sin(Ia)**4)
Vi=Sqrt((fi1+fi2)/2.)

Do j=1,4
   VH=V(j)
   VV=U(j)

   If(j==1) Then
      Rr(j)=Sin(Ip)
      Vr(j)=Vi

   Else If (j==2) Then

      z=0
      Do
         fr1=Ar33+Ar55+(Ar11-Ar33)*z**2
         fr2=Sqrt((Ar33-Ar55)**2+2*Ar1*z**2+Ar2*z**4)
         Vrph=Sqrt((fr1+fr2)/2.)
         z1=(1./Vi*SIN(Ip))*Vrph
         E=ABS(z1-z)

         If (E<0.000001) Then
            Rr(j)=z
            Vr(j)=Vrph
            Exit
         Else
            z=z1
         End If
      End Do

   Else If (j==3) Then

      z=0
      Do
         fr1=Ai33+Ai55+(Ai11-Ai33)*z**2
         fr2=Sqrt((Ai33-Ai55)**2+2*Ai1*z**2+Ai2*z**4)
```

```
            Vrph=Sqrt((fr1-fr2)/2.)
            z1=(1./Vi*SIN(Ip))*Vrph
            E=ABS(z1-z)

            If (E<0.000001) Then
               Rr(j)=z
               Vr(j)=Vrph
               Exit
            Else
               z=z1
            End If
         End Do

      Else If (j==4) Then

         z=0
         Do
            fr1=Ar33+Ar55+(Ar11-Ar33)*z**2
            fr2=Sqrt((Ar33-Ar55)**2+2*Ar1*z**2+Ar2*z**4)
            Vrph=Sqrt((fr1-fr2)/2.)
            z1=(1./Vi*SIN(Ip))*Vrph
            E=ABS(z1-z)

            If (E<0.000001) Then
               Rr(j)=z
               Vr(j)=Vrph
               Exit
            Else
               z=z1
            End If
         End Do

      End If
   End Do

   V1 =Vr(1)
   V2 =Vr(2)
   V3 =Vr(3)
   V4 =Vr(4)

   sinR1=Rr(1)
   sinR2=Rr(2)
   sinR3=Rr(3)
   sinR4=Rr(4)

End Subroutine compute_Velocity_Angle
```

Appendix II: FORTRAN90 Subroutines for Calculation of Approximate P-wave Reflection coefficient

```
!*************************************************************
!Name:          Banik_coef / Thomsen_coef / Ruger_coef
!               / Wei_coef
!Description:   Each individual subroutine calculates the
!               approximate P-wave reflection coefficient in
!               TI media. Given the incident and reflecting
!               TI media, it takes the incidence angle and
!               the acoustic parameters of the two TI media
!               as input, and get the reflection coefficient
!               as output
!Input:         Ib        - P-wave incidence phsse angle
!               a01       - P-wave velocity of incident
!                           medium (α1)
!               b01       - Vertical S-wave velocity of
!                           incident medium (β1)
!               de1       - density of incident medium (ρ1)
!               epsilon1  - P-wave anisotropic parameter of
!                           incident medium (εp1)
!               delta1    - anisotropic parameter of incident
!                           medium (δ1)
!               a02       - Vertical P-wave velocity of
!                           reflecting medium (α2)
!               b02       - Vertical S-wave velocity of
!                           reflecting medium (β2)
!               epsilon2  - P-wave anisotropic parameter of
!                           reflecting medium (εp2)
!               delta2    - anisotropic parameter of
!                           reflecting medium (δ2)
!               de2       - density of reflecting medium (ρ2)
!Output:        Rpp       - Approximate P-wave reflection
!                           coefficient
!*************************************************************

Subroutine Banik(Ip,a01,b01,delta1,a02,b02,delta2 Rpp)

   Real, Intent(IN) :: Ip
   Real, Intent(IN) :: a01,b01,delta1
   Real, Intent(IN) :: a02,b02,delta2
   Real, Intent(OUT) :: Rpp
```

```
   Real :: da, db, dde,ddelta
!   da=a02-a01, db=b02-b01, dde=de2-de1,dd=d2-d1

   Real :: I, a0,b0,de
!   a0=(a01+a02)/2,b0=(b01+b02)/2,de=(de1+de2)/2

   a01=Vpv1
   b01=Vsv1
   delta1=Dlt1

   a02=Vpv2
   b02=Vsv2
   delta2=Dlt2

   da =a02-a01
   db =b02-b01
   dde=de2-de1
   ddelta=delta2-delta1

   a0 =(a01+a02)/2
   b0 =(b01+b02)/2
   de =(de1+de2)/2

   Rpp=0.5*(1-4*(b0/a0*Sin(Ip))**2)*dde/de+da/&
          (2*Cos(Ip)**2*a0)+4*(b0/a0*Sin(Ip))**2*db/b0+&
          ddelta/2*Sin(Ip)**2

End Subroutine Banik


!-------------------------------------------------------
Subroutine Thomsen(Ip, a01,b01,epsilon1,delta1,&
               a02,b02,epsilon2,delta2,Rpp)

   Real, Intent(IN) :: Ip
   Real, Intent(IN) :: a01,b01,epsilon1,delta1
   Real, Intent(IN) :: a02,b02,epsilon2,delta2
   Real, Intent(OUT) :: Rpp

   Real :: da, db, dde,dea,ddelta
!   da=a02-a01, db=b02-b01, dde=de2-de1,dd=d2-d1,
!   dea=epsilon2-epsilon1

   Real :: a0,b0,de
!   a0=(a01+a02)/2,b0=(b01+b02)/2,de=(de1+de2)/2

   Real :: Z0,G0,dZ,dG
```

```
   a01=Vpv1
   b01=Vsv1
   epsilon1=Ep1
   delta1=Dlt1

   a02=Vpv2
   b02=Vsv2
   epsilon2=Ep2
   delta2=Dlt2

   da =a02-a01
   db =b02-b01
   dde=de2-de1
   dea=epsilon2-epsilon1
   ddelta=delta2-delta1

   a0 =(a01+a02)/2
   b0 =(b01+b02)/2
   de =(de1+de2)/2

   Z0 =de*a0
   G0 =de*b0**2
   dZ =de2*a02-de1*a01
   dG =de2*b02**2-de1*b01**2

   Rpp=dZ/(2*Z0)+0.5*(da/a0-(2*b0/a0)**2*(dG/G0)+&
          ddelta)*Sin(Ip)**2+0.5*(da/a0-(ddelta-&
          dea))*(Tan(Ip)*Sin(Ip))**2

End Subroutine Thomsen


!-----------------------------------------------------
Subroutine Ruger(Ip, a01,b01,epsilon1,delta1,&
               a02,b02,epsilon2,delta2,Rpp)

   Real, Intent(IN) :: Ip
   Real, Intent(IN) :: a01,b01,epsilon1,delta1
   Real, Intent(IN) :: a02,b02,epsilon2,delta2
   Real, Intent(OUT) :: Rpp

   Real :: da, db, dde,dea,ddelta
!   da=a02-a01, db=b02-b01, dde=de2-de1,
!   dd=d2-d1,dea=epsilon2-epsilon1

   Real :: a0,b0,de
```

```
   !a0=(a01+a02)/2,b0=(b01+b02)/2,de=(de1+de2)/2

   Real :: Z0,G0,dZ,dG

   a01=Vpv1
   b01=Vsv1
   epsilon1=Ep1
   delta1=Dlt1

   a02=Vpv2
   b02=Vsv2
   epsilon2=Ep2
   delta2=Dlt2

   da =a02-a01
   db =b02-b01
   dde=de2-de1
   dea=epsilon2-epsilon1
   ddelta=delta2-delta1

   a0 =(a01+a02)/2
   b0 =(b01+b02)/2
   de =(de1+de2)/2

   Z0 =de*a0
   G0 =de*b0**2
   dZ =de2*a02-de1*a01
   dG =de2*b02**2-de1*b01**2

   Rpp=dZ/(2*Z0)+0.5*(da/a0-(2*b0/a0)**2*(dG/G0)+&
          ddelta)*Sin(Ip)**2+0.5*(da/a0+dea)*&
          (Tan(Ip)*Sin(Ip))**2

End Subroutine Ruger


!-----------------------------------------------------
Subroutine Wei(Ip, a01,b01,epsilon1,delta1,&
               a02,b02,epsilon2,delta2,Rpp)

   Real, Intent(IN) :: Ip
   Real, Intent(IN) :: a01,b01,epsilon1,delta1
   Real, Intent(IN) :: a02,b02,epsilon2,delta2
   Real, Intent(OUT) :: Rpp

   Real :: da, db, dde,ddelta,dea
!   da=a02-a01, db=b02-b01, dde=de2-de1,dd=d2-d1
```

```
    Real :: I, a0,b0,de
    !a0=(a01+a02)/2,b0=(b01+b02)/2,de=(de1+de2)/2

    a01=Vpv1
    b01=Vsv1
    epsilon1=Ep1
    delta1=Dlt1

    a02=Vpv2
    b02=Vsv2
    epsilon2=Ep2
    delta2=Dlt2

    da =a02-a01
    db =b02-b01
    dde=de2-de1
    dea=epsilon2-epsilon1
    ddelta=delta2-delta1

    a0 =(a01+a02)/2
    b0 =(b01+b02)/2
    de =(de1+de2)/2

    Rpp=(dde/de+da/a0)/2.-2*(b0/a0)**2*(dde/de+&
           2*db/b0)*Sin(Ip)**2+da/a0*Tan(Ip)**2/2+&
           (ddelta-2*dea)/2*Sin(Ip)**2

End Subroutine Wei
```

Appendix III. Error Correction for Daley and Hron's Papers

Error correction in Daley and Hron's 1977 paper

Error	Correction
Page 663, last line	
$Q^{(v)} = \{\left(A_{33}^{(v)} - A_{55}^{(v)}\right)^2 + 2A_1^{(v)}\sin\theta_v + A_2^{(v)}\sin^2\theta_v\}^{1/2}$	$Q^{(v)} = \{\left(A_{33}^{(v)} - A_{55}^{(v)}\right)^2 + 2A_1^{(v)}\sin^2\theta_v + A_2^{(v)}\sin^4\theta_v\}^{1/2}$
Page 667, line 1	
$\cos\theta_2 = Q = \left(1 - k_1^2 x^2\right)^{1/2}$	$\cos\theta_2 = Q = \left(1 - \frac{x^2}{n^2}\right)^{1/2}$
Page 667, line 2	
$\cos\theta_3 = S = \left(1 - \frac{x^2}{n^2}\right)^{1/2}$	$\cos\theta_3 = S = \left(1 - k_1^2 x^2\right)^{1/2}$
Page674, line 31	
$\lambda_1 = \frac{1}{2}\left\{K + \sqrt{K^2 - L^2}\right\}$	$\lambda_1 = \frac{1}{2}\left\{K + \sqrt{K^2 - 4L}\right\}$
Page 674, line 31	
$\lambda_2 = \frac{1}{2}\left\{K - \sqrt{K^2 - L^2}\right\}$	$\lambda_2 = \frac{1}{2}\left\{K - \sqrt{K^2 - 4L}\right\}$
Page 675, line 14	
$A_1 = 2\left(A_{13} + A_{55}\right)^2 - \left(A_{33} + A_{55}\right)\left(A_{11} + A_{33} - 2A_{55}\right)$	$A_1 = 2\left(A_{13} + A_{55}\right)^2 - \left(A_{33} - A_{55}\right)\left(A_{11} + A_{33} - 2A_{55}\right)$
Page 675, line 33	
$E_8 = 2T_2T_{10}PQ$	$E_8 = 2T_3T_{10}PQ$

Error correction in Daley and Hron's 1979 paper

Error	Correction
Page 31, line 32	
$\alpha_i = \rho_i\left[(ax_i^2 - b_i^2)(az_i^2 - b_i^2)\right]^{1/2}$	$\alpha_i = \rho_i\left\{\left[(ax_i^2 - b_i^2)(az_i^2 - b_i^2)\right]^{1/2} - b_i^2\right\}$
Page 32, line 12	
$\delta_i = \rho_i(az_i^2 l_{i+2} - \alpha_i m_{i+2})$	$\delta_i = \rho_i az_i^2 l_{i+2} - \alpha_i m_{i+2}$
Page 32, line 24	
$T_7 = \beta_2 l - \beta_1 \frac{m_2}{l_1}$	$T_7 = \beta_2 l - \beta_1 \frac{m_2}{m_1}$

Appendix IV. FORTRAN 90 Subroutine for Calculation of Exact Quasi-P and Quasi-S Reflection and Transmission Coefficients

```
!*************************************************************
!Name:         BndryRefletion
!Description: Given the incident and reflecting general
!              anisotropic media, this subroutine takes the
!              incidence wave normal as input, and computes
!              the exact P-wave, fast SV-wave, slow SV-wave
!              reflection and transmission coefficients.
!              The computation takes the following five
!              steps:
!                Step1: Calculate slowness of incident wave
!                         -- Subroutine "PhaseVelocity" is
!                            called
!                Step2: Calculate 3 reflected and 3
!                       transmitted slowness vectors
!                         -- Subroutine "SlownessOnZ" is
!                            called
!                Step3: Calculate polarizations for each
!                       waves
!                         -- Subroutine "Polarization" is
!                            called
!                Step4: Select signs for polarizations
!                         -- Subroutine "Polar_Sign" is
!                            called
!                Step5: Calculate reflection coefficients
!                         -- Subroutine "BndryCondition" is
!                            called
!Input:       Aij - elastic stiffness tensor of incident
!                   medium
!             Bij - elastic stiffness tensor of reflecting
!                   medium
!             Nij - unit vector of incident wave normal
!Output:      Rj  - one dimensional array of 6 coefficients.
!                      1-3:  Refl. Coef. of P,F,S
!                      4-6:  Tran. Coef. of P,F,S
!*************************************************************

Subroutine BndryRefletion (Aik, Bik, Nij, Rj)
Implicit None

   Real(8), intent(IN), Dimension (3,3,3,3) :: Aik,Bik
   Complex(8), Intent(IN), Dimension (3) :: Nij
```

```
   Complex(8), Intent(OUT), Dimension (6) :: Rj

   Real(8), Dimension (3) :: Minc
   Complex(8), Dimension (3) :: Min,Mpl,Mfl,Msl,Mp2,Mf2,Ms2
         !incidence slowness and 3 Refl. and tran. slowness
   Complex(8), Dimension (3) :: Pinc,Ppl,Pfl,Psl
   Complex(8), Dimension (3) :: Pp2,Pf2,Ps2
         !inc. polarization and 3 refl. and tran. Polar.
   Complex(8), Dimension (3) :: Mpt,Mft,Mst,Ppt,Pft,Pst
   Complex(8), Dimension (3) :: Nijt,AvgS
         !for F=S (slowness) case
   Complex(8), Dimension (3,3) :: Ml,Mm,Pl,Pm,Pju,pjb
         !for Polar Sign
   Complex(8), Dimension (7,3) :: Pk,Mk
         !P: polarization M: slowness
         !1-3: Refl. P,F,S 4-6: Tran. P,F,S 7: inc
   Complex(8) :: diff    !for F=S: meagure diff. Sf-Ss
   Real(8) :: adiff
   Complex(8) :: V1,V2,V3 ! for P, F, S
   Real :: tick
   integer :: i,j,k,l

!-------------------------------------------------------
!Step1: Calculate the slowness of incident wave

   Call PhaseVelocity (Aik,Nij,V1,V2,V3)

   !assuming P incidence
   Minc(1)=Real(Nij(1)/V1)
   Minc(2)=Real(Nij(2)/V1)
   Minc(3)=Real(Nij(3)/V1)

!Print *, "V123",V1

!-------------------------------------------------------
!Step2: Calculate the 3 reflected and 3 transmitted
!       slowness

   tick=1.
!    tick=1: incident medium
   Call SlownessOnZ(Aik,Minc,tick,Mpl,Mfl,Msl)

   tick=0.
!    tick=0: transmitting medium
   Call SlownessOnZ(Bik,Minc,tick,Mp2,Mf2,Ms2)
```

```
!-------------------------------------------------------------
!Step3: Calculate polarizations for each waves

! Compute polarization for incident wave
   Call Polarization(Aik,Mp1,Pp1)
   Call Polarization(Bik,Mp2,Pp2)

!Calculate the 2 S polarizations under 2 conditions:
! 1) 2 S have diffrent slownesses;
! 2) 2 S have the same slowness value

! Compute polarizations for 3 reflected waves
   diff=Mf1(3)-Ms1(3)
   adiff=Sqrt(Real(diff)**2+Imag(diff)**2)
   If (adiff<1.E-010) Then
      Do i=1,3
         AvgS(i)=(Mf1(i)+Ms1(i))/2._8
         Mf1(i)=AvgS(i)
         Ms1(i)=AvgS(i)
      End Do

      Do i=1,3
         Nijt(i)=AvgS(i)/Sqrt(AvgS(1)**2+AvgS(2)**2+&
                 AvgS(3)**2)
      End Do

      Call PhaseVelocity (Aik,Nijt,V1,V2,V3)
      Do i=1,3
         Mpt(i)=Nijt(i)/V1
      End Do

      Call Polarization(Aik,Mpt,Ppt)
      Call Polarization_FeqS(Ppt,Pf1,Ps1)

   Else
      Call Polarization(Aik,Mf1,Pf1)
      Call Polarization(Aik,Ms1,Ps1)
   End If

! Compute polarizations for 3 transmitted waves
   diff=Mf2(3)-Ms2(3)
   adiff=Sqrt(Real(diff)**2+Imag(diff)**2)
   If (adiff<1.E-010) Then

      Do i=1,3
         AvgS(i)=(Mf2(i)+Ms2(i))/2._8
         Mf2(i)=AvgS(i)
```

```
            Ms2(i)=AvgS(i)
         End Do

         Do i=1,3
             Nijt(i)=AvgS(i)/Sqrt(AvgS(1)**2+AvgS(2)**2+&
                     AvgS(3)**2)
         End Do

         Call PhaseVelocity (Bik,Nijt,V1,V2,V3)
         Do i=1,3
            Mpt(i)=Nijt(i)/V1
         End Do

         Call Polarization(Bik,Mpt,Ppt)
         Call Polarization_FeqS(Ppt,Pf2,Ps2)

      Else
         Call Polarization(Bik,Mf2,Pf2)
         Call Polarization(Bik,Ms2,Ps2)
      End If

      !change to complex slowness for incident wave
      Do i=1,3
         Min(i)=Minc(i)
      End Do
      Call Polarization(Aik,Min,Pinc)

!-------------------------------------------------------
!Step4: Select signs for polarizations

! Save upgoing and downgoing slowness vectors and
! polarization vectors in different matrices
      Do i=1,3
         Ml(1,i)=Mp1(i)
         Ml(2,i)=Mf1(i)
         Ml(3,i)=Ms1(i)
         Mm(1,i)=Mp2(i)
         Mm(2,i)=Mf2(i)
         Mm(3,i)=Ms2(i)
         Pl(1,i)=Pp1(i)
         Pl(2,i)=Pf1(i)
         Pl(3,i)=Ps1(i)
         Pm(1,i)=Pp2(i)
         Pm(2,i)=Pf2(i)
         Pm(3,i)=Ps2(i)
      End Do
```

```
! Choose polarization signs
   Call Polar_Sign(Ml,Pl,Pju)
   Call Polar_Sign(Mm,Pm,Pjb)

!-------------------------------------------------------
!Step5: Calculate reflection coefficients

   Do i=1,3
      Mk(1,i)=Mp1(i)
      Mk(2,i)=Mf1(i)
      Mk(3,i)=Ms1(i)
      Mk(4,i)=Mp2(i)
      Mk(5,i)=Mf2(i)
      Mk(6,i)=Ms2(i)
      Mk(7,i)=Minc(i)
   End Do

   Do i=1,3
      Pk(1,i)=Pju(1,i)
      Pk(2,i)=Pju(2,i)
      Pk(3,i)=Pju(3,i)
      Pk(4,i)=Pjb(1,i)
      Pk(5,i)=Pjb(2,i)
      Pk(6,i)=Pjb(3,i)
      Pk(7,i)=Pinc(i)
   End Do

   Call  BndryCondition(Aik,Bik,Mk,Pk,Rj)

End Subroutine BndryRefletion
```

```
!*************************************************************
!Name:         PhaseVelocity
!Description: Given the incident wave normal, this
!             subroutine calculates the phase velocities
!             of quasi-Pwave, fast quasi-S wave, and
!             slow quasi-S wave along the direction
!Input:        A   - elastic stiffness matrix
!             Ni   - unit vector of incident wave normal
!Output:       Vp   - P wave phase velocity
!             Vfs  - Fast SV wave phase velocity
!             Vss  - Slow SV wave phase velocity
!*************************************************************


Subroutine PhaseVelocity (A,Ni,Vp,Vsf,Vss)
Use MATH_UTIL, ONLY: CUBIC
   !CUBIC: Subroutine to solve cubic polynomial
Implicit None

   Real(8), Intent(IN), Dimension (3,3,3,3) :: A
   Complex(8), Intent(IN), Dimension (3) :: Ni
   Complex(8), Intent(OUT) :: Vp,Vsf,Vss

   Complex(8), Dimension (3,3) :: B
   Complex(8) :: C0,C1,C2,C3
   Complex(8) :: R1,R2,R3
   Real(8), Dimension(3) :: Vtemp
   Real(8) :: MaxV,MidV,MinV
   Integer :: i,j,k,l

   Do i=1,3
      Do k=1,3

         B(i,k)=0
         Do j=1,3
            Do l=1,3
               B(i,k)=B(i,k)+A(i,j,k,l)*Ni(j)*Ni(l)
            End Do
         End Do

      End Do
   End Do

   C3=(-1._8,0._8)
```

```
   C2=B(1,1)+B(2,2)+B(3,3)

   C1=B(3,1)*B(1,3)+B(2,3)*B(3,2)+B(2,1)*B(1,2)- &
      B(1,1)*B(3,3)-B(3,3)*B(2,2)-B(2,2)*B(1,1)

   C0=B(1,1)*B(2,2)*B(3,3)+B(1,2)*B(2,3)*B(3,1)+&
      B(1,3)*B(2,1)*B(3,2)-B(3,1)*B(1,3)*B(2,2)-&
      B(2,3)*B(3,2)*B(1,1)-B(2,1)*B(1,2)*B(3,3)

   Call CUBIC(C3,C2,C1,C0,R1,R2,R3)

   Vtemp(1)=Real(R1)
   Vtemp(2)=Real(R2)
   Vtemp(3)=Real(R3)

   MaxV=Vtemp(1)
   MinV=Vtemp(1)
   MidV=0

   Do i=1,3
      If (MaxV<Vtemp(i)) Then
         MaxV=Vtemp(i)
      End If

      If (MinV>Vtemp(i)) Then
         MinV=Vtemp(i)
      End If
   End Do

   j=0
   Do i=1,3
      If (Vtemp(i)<MaxV .and. Vtemp(i)>MinV) Then
         MidV=Vtemp(i)
      Else If (Vtemp(i)==MinV) Then
         j=j+1
      End If
   End Do

   If (Vsf==0 .and. j==2) MidV=MinV

   Vp=Sqrt(MaxV)
   Vsf=Sqrt(MidV)
   Vss=Sqrt(MinV)

End Subroutine PhaseVelocity
```

```
!*************************************************************
!Name:         ABCcompute
!Description:  This subroutine calculates the A, B, C (3X3)
!              matrices, which collect the parameters of
!              different powers of m3 (Z component of
!              slowness). The A, B and C matrices are used
!              to build the 6th order polynomial for the
!              slowness vectors.
!Input:        Cij - elastic stiffness matrix
!              m1  - X component of incident slowness
!              m2  - Y component of incident slowness
!Output:       A   - parameter of square of m3
!              B   - parameter of m3
!              C   - parameter of constant
!*************************************************************

Subroutine ABCcompute (Cij,m1,m2,A,B,C)
Implicit None

   Real(8), Intent(IN), Dimension(3,3,3,3) :: Cij
   Real(8), Intent(IN) :: m1,m2
   Real(8), Intent(OUT), Dimension(3,3) :: A,B,C

   Integer :: i,j,k,l

   Do i=1,3
      Do k=1,3

         A(i,k)=Cij(i,3,k,3)

         B(i,k)=Cij(i,1,k,3)*m1+Cij(i,2,k,3)*m2+&
                Cij(i,3,k,1)*m1+Cij(i,3,k,2)*m2

         C(i,k)=Cij(i,1,k,2)*m1*m2+Cij(i,1,k,1)*m1**2+&
                Cij(i,2,k,2)*m2**2+Cij(i,2,k,1)*m1*m2

         If (i==k) C(i,k)=C(i,k)-1._8

      End Do
   End Do

End Subroutine ABCcompute
```

```
!*************************************************************
!Name:         Diagonal
!Description:  This subroutine takes one set of m3's
!              parameters with diagonal expressions as
!              input, and calculates the coefficients in
!              front of different powers of m3. (see equ.
!              (6.15) - (6.17) in thesis)
!Input:        G  - 3X3 matrix collected m3's parameters of
!                   diagonal expression
!Output:       EE - one-dimensional array parameters in
!                   front of different powers (from 6 to 0)
!                   of m3
!*************************************************************

Subroutine Diagonal(G,EE)
Implicit None

   Real(8), Intent(IN), Dimension(3,3) :: G
   Real(8), Intent(OUT), Dimension(7) :: EE

! 1st equ. in (6.17)
   EE(1)=G(1,1)*G(2,1)*G(3,1)

! 2nd equ. in (6.17)
   EE(2)=G(1,1)*G(2,2)*G(3,1)+G(1,2)*G(2,1)*G(3,1)+&
         G(1,1)*G(2,1)*G(3,2)

! 3rd equ. in (6.17)
   EE(3)=G(1,1)*G(2,3)*G(3,1)+G(1,3)*G(2,1)*G(3,1)+&
         G(1,2)*G(2,2)*G(3,1)+G(1,1)*G(2,2)*G(3,2)+&
         G(1,2)*G(2,1)*G(3,2)+G(1,1)*G(2,1)*G(3,3)

! 4th equ. in (6.17)
   EE(4)=G(1,3)*G(2,2)*G(3,1)+G(1,2)*G(2,3)*G(3,1)+&
         G(1,1)*G(2,3)*G(3,2)+G(1,3)*G(2,1)*G(3,2)+&
         G(1,2)*G(2,2)*G(3,2)+G(1,1)*G(2,2)*G(3,3)+&
         G(1,2)*G(2,1)*G(3,3)

! 5th equ. in (6.17)
   EE(5)=G(1,3)*G(2,3)*G(3,1)+G(1,3)*G(2,2)*G(3,2)+&
         G(1,2)*G(2,3)*G(3,2)+G(1,1)*G(2,3)*G(3,3)+&
         G(1,3)*G(2,1)*G(3,3)+G(1,2)*G(2,2)*G(3,3)

! 6th equ. in (6.17)
   EE(6)=G(1,3)*G(2,3)*G(3,2)+G(1,3)*G(2,2)*G(3,3)+&
```

```
          G(1,2)*G(2,3)*G(3,3)

! 7th equ. in (6.17)
   EE(7)=G(1,3)*G(2,3)*G(3,3)

End Subroutine Diagonal
```

```
!*************************************************************
!Name:         SlownessOnZ
!Description:  Given an incident slowness and the reflected
!              (or transmitted)medium parameters, this
!              subroutine calculates the three reflected (or
!              transmitted) slownesses (P, FS, and SS).
!              During the computation, three other
!              subroutines, ABCcompute, Diagonal, and Cubic,
!              are called.
!Input:        AIJ - elastic stiffness matrix
!              Mi  - slowness of incident wave
!              tic - flag to indicate incident or reflecting
!                    medium
!Output:       Sp  - slowness of P-wave
!              Sf  - slowness of fast SV-wave
!              Ss  - slowness of slow SV-wave
!*************************************************************

Subroutine SlownessOnZ(AIJ,Mi,tic,Sp,Sf,Ss)
Use MATH_UTIL, ONLY: CUBIC
Implicit None

   Real(8), Dimension (3,3,3,3),Intent(IN) :: AIJ
   Real(8), Dimension (3),Intent(IN) :: Mi
   Real, Intent(IN) :: tic
   Complex(8), Dimension (3),Intent(OUT) :: Sp,Sf,Ss

   Real(8) :: PP,Fsv,Ssv
   Real(8), Dimension (3,3) :: Aa,Bb,Cc
   Real(8), Dimension (3,3) :: D1,D2,D3,D4,D5,D6
   Real(8), Dimension (7)   :: E1,E2,E3,E4,E5,E6,E7
   Complex(8) :: S1,S2,S3
   Real(8), Dimension(3) :: Stmp
   Real(8) :: MaxS,MidS,MinS
   Integer :: i,j,k,l,flag,z
   Logical :: tf

   Call ABCcompute(AIJ,Mi(1),Mi(2),Aa,Bb,Cc)

   Do i=1,3
      D1(i,1)=Aa(i,i)
      D1(i,2)=Bb(i,i)
      D1(i,3)=Cc(i,i)
   End Do

   D2(1,1)=Aa(1,2)
```

```
D2(2,1)=Aa(2,3)
D2(3,1)=Aa(1,3)
D2(1,2)=Bb(1,2)
D2(2,2)=Bb(2,3)
D2(3,2)=Bb(1,3)
D2(1,3)=Cc(1,2)
D2(2,3)=Cc(2,3)
D2(3,3)=Cc(1,3)

D3(1,1)=Aa(1,3)
D3(2,1)=Aa(1,2)
D3(3,1)=Aa(2,3)
D3(1,2)=Bb(1,3)
D3(2,2)=Bb(1,2)
D3(3,2)=Bb(2,3)
D3(1,3)=Cc(1,3)
D3(2,3)=Cc(1,2)
D3(3,3)=Cc(2,3)

D4(1,1)=Aa(1,3)
D4(2,1)=Aa(2,2)
D4(3,1)=Aa(1,3)
D4(1,2)=Bb(1,3)
D4(2,2)=Bb(2,2)
D4(3,2)=Bb(1,3)
D4(1,3)=Cc(1,3)
D4(2,3)=Cc(2,2)
D4(3,3)=Cc(1,3)

D5(1,1)=Aa(1,2)
D5(2,1)=Aa(1,2)
D5(3,1)=Aa(3,3)
D5(1,2)=Bb(1,2)
D5(2,2)=Bb(1,2)
D5(3,2)=Bb(3,3)
D5(1,3)=Cc(1,2)
D5(2,3)=Cc(1,2)
D5(3,3)=Cc(3,3)

D6(1,1)=Aa(1,1)
D6(2,1)=Aa(2,3)
D6(3,1)=Aa(2,3)
D6(1,2)=Bb(1,1)
D6(2,2)=Bb(2,3)
D6(3,2)=Bb(2,3)
D6(1,3)=Cc(1,1)
D6(2,3)=Cc(2,3)
```

```
   D6(3,3)=Cc(2,3)

   Call Diagonal(D1,E1)
   Call Diagonal(D2,E2)
   Call Diagonal(D3,E3)
   Call Diagonal(D4,E4)
   Call Diagonal(D5,E5)
   Call Diagonal(D6,E6)

! Building coefficients for 6th order polynomial
   Do i=1,7
      E7(8-i)=E1(i)+E2(i)+E3(i)-E4(i)-E5(i)-E6(i)
   End Do

! Solve 6th order using cubic
   Call CUBIC(E7(7),E7(5),E7(3),E7(1),S1,S2,S3)

! Identify 3 slowness types
   Stmp(1)=Real(S1)
   Stmp(2)=Real(S2)
   Stmp(3)=Real(S3)

   MinS=Stmp(1)
   MaxS=Stmp(1)
   MidS=0

   Do i=1,3
      If (MinS>Stmp(i)) Then
         MinS=Stmp(i)
      End If

      If (MaxS<Stmp(i)) Then
         MaxS=Stmp(i)
      End If
   End Do

   j=0
   Do i=1,3
      If (Stmp(i)>MinS .And. Stmp(i)<MaxS) Then
         MidS=Stmp(i)
      Else If (Stmp(i)==MaxS) Then
         j=j+1
      End If
   End Do

   If (MidS==0 .and. j==2) MidS=MaxS
```

```
    S1=MinS
    S2=MidS
    S3=MaxS

    Sp(1)=Mi(1)
    Sp(2)=Mi(2)
    Sp(3)=Sqrt(S1)
    Sf(1)=Mi(1)
    Sf(2)=Mi(2)
    Sf(3)=Sqrt(S2)
    Ss(1)=Mi(1)
    Ss(2)=Mi(2)
    Ss(3)=Sqrt(S3)

    If (tic==1) Then
       Sp(3)=-Sp(3)
       Sf(3)=-Sf(3)
       Ss(3)=-Ss(3)
    End If

End Subroutine SlownessOnZ
```

```
!************************************************************
!Name:         PolarizationRoots
!Description: This subroutine solves MX =0; and
!              X1**2 + X2**2 +X3**2 =1
!              To minimize error in the solution, it
!              automatically picks the two non-linear
!              equations. It also selects the biggest root
!              and solves it first, and then solves the
!              other two.
!Input:        M - 3X3 matrix
!Output:       X - 3 unknowns
!************************************************************

Subroutine PolarizationRoots (M,X)
Implicit None

   Complex(8), Intent(IN), Dimension(3,3) :: M
   Complex(8), Intent(OUT), Dimension(3) :: X

   Complex(8), Dimension(9,2,3) :: D !
   Complex(8), Dimension(9) :: DD
   Complex(8) :: A1,A2,B
   Integer :: i,j,k,l

!-----------------------------------------
! columm do not change, in the order of M

! No. 1 & 2 equitions
   Do i=1,2
      Do j=1,3
         D(1,i,j)=M(i,j)
      End Do
   End Do

! No. 2 & 3 equitions
   Do i=1,2
      Do j=1,3
         D(2,i,j)=M(i+1,j)
      End Do
   End Do

! No. 1 & 3 equitions
   Do i=1,2
      Do j=1,3
         D(3,i,j)=M(2*i-1,j)
      End Do
```

```
   End Do

!-------------------------------
! columm change from 123 to 312

! No. 1 & 2 equitions
   Do i=1,2
      D(4,i,1)=M(i,3)
      D(4,i,2)=M(i,1)
      D(4,i,3)=M(i,2)
   End Do

! No. 2 & 3 equitions
   Do i=1,2
      D(5,i,1)=M(i+1,3)
      D(5,i,2)=M(i+1,1)
      D(5,i,3)=M(i+1,2)
   End Do

! No. 1 & 3 equitions
   Do i=1,2
      D(6,i,1)=M(2*i-1,3)
      D(6,i,2)=M(2*i-1,1)
      D(6,i,3)=M(2*i-1,2)
   End Do

!-------------------------------
! columm change from 123 to 231

! No. 1 & 2 equitions
   Do i=1,2
      D(7,i,1)=M(i,2)
      D(7,i,2)=M(i,3)
      D(7,i,3)=M(i,1)
   End Do

! No. 2 & 3 equitions
   Do i=1,2
      D(8,i,1)=M(i+1,2)
      D(8,i,2)=M(i+1,3)
      D(8,i,3)=M(i+1,1)
   End Do

! No. 1 & 3 equitions
   Do i=1,2
      D(9,i,1)=M(2*i-1,2)
      D(9,i,2)=M(2*i-1,3)
```

```
      D(9,i,3)=M(2*i-1,1)
   End Do

   B=0
   Do, i=1,9

      DD(i)=(D(i,2,3)*D(i,1,2)-D(i,1,3)*D(i,2,2))

      If (Abs(DD(i))>Abs(B)) Then
         B=DD(i)
         k=i
      End If

   End Do

   A1 = (D(k,1,1)*D(k,2,2)-D(k,1,2)*D(k,2,1))/B
   A2 = -(D(k,1,1)*D(k,2,3)-D(k,2,1)*D(k,1,3))/B

   If (k<=3) Then
      X(1) = Sqrt(1/(1+A1**2+A2**2))
      X(2) = A2*X(1)
      X(3) = A1*X(1)
   Else If (k>3 .and. k<=6) Then
      X(3) = Sqrt(1/(1+A1**2+A2**2))
      X(1) = A2*X(3)
      X(2) = A1*X(3)
   Else If (k>6 .and. k<=9) Then
      X(2) = Sqrt(1/(1+A1**2+A2**2))
      X(3) = A2*X(2)
      X(1) = A1*X(2)
   End If

End Subroutine PolarizationRoots
```

```
!************************************************************
!Name:         Polarization
!Description: Given a wave slowness and the medium
!              parameters, this subroutine calculates the
!              corresponding polarization.
!              During the computation, another subroutine,
!              PolarizationRoots, is called
!Input:        Aij - elastic stiffness matrix
!              Mi  - wave slowness vector
!Output:       Pi  - wave polarization vector
!************************************************************

Subroutine Polarization(Aij,Mi,Pi)
Implicit None

   Real(8), Intent(IN), Dimension(3,3,3,3) :: Aij
   Complex(8), Intent(IN), Dimension(3) :: Mi
   Complex(8), Intent(OUT), Dimension(3) :: Pi

   Complex(8), Dimension(3,3) :: D
   Integer :: i,j,k,l

   Do i=1,3
      Do k=1,3

         D(i,k)=(0._8,0._8)
         Do j=1,3
            Do l=1,3
               D(i,k)=D(i,k)+Aij(i,j,k,l)*Mi(j)*Mi(l)
! D(i,k) is equivalent to Hik in equ. (6.20) of the thesis
            End Do
         End Do

      End Do
   End Do

   D(1,1)=D(1,1)-1._8
   D(2,2)=D(2,2)-1._8
   D(3,3)=D(3,3)-1._8

   Call PolarizationRoots(D,Pi)

End Subroutine Polarization
```

```
!************************************************************
!Name:         Polarization_FeqS
!Description: This subroutine sets the two orthogonal SV
!              polarization when a P polarization is given.
!              This subroutine is called only when fast S
!              slowness is equal to slow S. The three
!              polarizations are orthogonal to each other.
!Input:        Pp  - polarization of P-wave
!Output:       Ps1 - polarization of one SV
!              Ps2 - polarization of the other SV
!************************************************************

Subroutine Polarization_FeqS(Pp,Ps1,Ps2)
Implicit None

   Complex(8), Intent(IN), Dimension(3) :: Pp
   Complex(8), Intent(OUT), Dimension(3) :: Ps1,Ps2

   Complex(8), Dimension(3) :: Ptmp
   Real(8) :: P

   P=Abs(Real(Pp(3)))
   If (Abs(P-1)<1.E-007) Then
      Ps1(1)=1._8
      Ps1(2)=0._8
      Ps1(3)=0._8
      Ps2(1)=0._8
      Ps2(2)=1._8
      Ps2(3)=0._8
   Else
      Ps1(1)=-Pp(2)/Sqrt(Pp(1)**2+Pp(2)**2)
      Ps1(2)=Pp(1)/Sqrt(Pp(1)**2+Pp(2)**2)
      Ps1(3)=0

      Ptmp(1)=Ps1(2)*Pp(3)
      Ptmp(2)=-Ps1(1)*Pp(3)
      Ptmp(3)=Ps1(1)*Pp(2)-Ps1(2)*Pp(1)

      Ps2(1)=Ptmp(1)/Sqrt(Ptmp(1)**2+Ptmp(2)**2+Ptmp(3)**2)
      Ps2(2)=Ptmp(2)/Sqrt(Ptmp(1)**2+Ptmp(2)**2+Ptmp(3)**2)
      Ps2(3)=Ptmp(3)/Sqrt(Ptmp(1)**2+Ptmp(2)**2+Ptmp(3)**2)
   End If

End Subroutine Polarization_FeqS
```

```
!*************************************************************
!Name:         Polar_Sign
!Description: This subroutine selects the right sign for
!              each input polarization.
!Input:        Mic - slowness vector
!              Pic - polarization vector
!Output:       Pjc - corrected polarization vector
!*************************************************************

Subroutine Polar_Sign(Mic,Pic,Pjc)
Implicit None


   Complex(8), Intent(IN), Dimension(3,3) :: Mic,Pic
   Complex(8), Intent(OUT), Dimension(3,3) :: Pjc

   Real(8), Dimension(3,3) :: Mi,Pi !Real part of Mic,Pic
   Real(8), Dimension(2,3) :: Nrml !1: fast S; 2: slow S
   Real(8), Dimension(3) :: dotP
   Real(8) :: dot2,dot3
   Integer :: i,j

   Do i=1,3
      Do j=1,3
         Mi(i,j)=Real(Mic(i,j))
         Pi(i,j)=Real(Pic(i,j))
      End Do
   End Do

   dotP(1)=Mi(1,1)*Pi(1,1)+Mi(1,2)*Pi(1,2)+Mi(1,3)*Pi(1,3)

   If (dotP(1)>=0) Then
      Do i=1,3
         Pjc(1,i)=Pic(1,i)
      End Do
   Else If (dotP(1)<0) Then
      Do i=1,3
         Pjc(1,i)=-Pic(1,i)
      End Do
   End If

   If (Mi(2,1)==0._8 .And. Mi(2,2)==0._8) Then
      Nrml(1,1)=0._8
      Nrml(1,2)=0._8
      Nrml(1,3)=1._8
   Else
```

```
   Nrml(1,1)=-Mi(2,2)/Sqrt(Mi(2,1)**2+Mi(2,2)**2)
   Nrml(1,2)=Mi(2,1)/Sqrt(Mi(2,1)**2+Mi(2,2)**2)
   Nrml(1,3)=0._8
End If

If (Mi(3,1)==0._8 .And. Mi(3,2)==0._8) Then
   Nrml(2,1)=0._8
   Nrml(2,2)=0._8
   Nrml(2,3)=1._8
Else
   Nrml(2,1)=-Mi(3,2)/Sqrt(Mi(3,1)**2+Mi(3,2)**2)
   Nrml(2,2)=Mi(3,1)/Sqrt(Mi(3,1)**2+Mi(3,2)**2)
   Nrml(2,3)=0._8
End If

dotP(2)=Nrml(1,1)*Pi(2,1)+Nrml(1,2)*Pi(2,2)+&
        Nrml(1,3)*Pi(2,3)

dotP(3)=Nrml(2,1)*Pi(3,1)+Nrml(2,2)*Pi(3,2)+&
         Nrml(2,3)*Pi(3,3)

dot2=Abs(dotP(2))
dot3=Abs(dotP(3))

If (dot2==0._8 .And. dot3==0._8) Then
   Do i=2,3
      Do j=1,3
         Pjc(i,j)=Pic(i,j)
      End Do
   End Do
Else
   If (dot2<=dot3) Then

      If (Pi(2,2)>=0) Then
         Do i=1,3
            Pjc(2,i)=Pic(2,i)
         End Do
      Else If (Pi(2,2)<0) Then
        Do i=1,3
           Pjc(2,i)=-Pic(2,i)
        End Do
      End If

      If (Pi(3,3)<=0) Then
         Do i=1,3
            Pjc(3,i)=Pic(3,i)
         End Do
```

```
         Else If (Pi(3,3)>0) Then
            Do i=1,3
               Pjc(3,i)=-Pic(3,i)
            End Do
         End If

      Else If (dot2>dot3) Then

         If (Pi(2,3)<=0) Then
            Do i=1,3
               Pjc(2,i)=Pic(2,i)
            End Do
         Else If (Pi(2,3)>0) Then
            Do i=1,3
               Pjc(2,i)=-Pic(2,i)
            End Do
         End If

         If (Pi(3,2)>=0) Then
            Do i=1,3
               Pjc(3,i)=Pic(3,i)
            End Do
         Else If (Pi(3,2)<0) Then
            Do i=1,3
               Pjc(3,i)=-Pic(3,i)
            End Do
         End If

      End If

   End If

End Subroutine Polar_Sign
```

```
!*************************************************************
!Name:         LinearSolution
!Description:  This subroutine calculates the roots of 6
!              linearized equations with six unknowns in the
!              following form:
!                Ai1X1+Ai2X2+Ai3X3+Ai4X4+Ai5X5+Ai6X6+Ai7=0
!                (i=1,2,...6)
!              This routine is used to solve for reflection/
!              transmission coefficients from boundary
!              conditions.
!Input:        A - 6X7 matrix parameters
!Output:       X - one dimension array of 6 unknowns
!*************************************************************

Subroutine LinearSolution(A,X)
Implicit None

   Complex(8), Intent(IN), Dimension(6,7) :: A
   Complex(8), Intent(OUT), Dimension(6) :: X

   Complex(8), Dimension(6,7) :: B
   Complex(8), Dimension(7) :: Btmp
   Complex(8) :: C, D
   Integer :: i,j,k,l

   Do i=1,6
      Do j=1,7
         B(i,j)=A(i,j)
      End Do
   End Do

   If (B(1,7)==(0.,0.) .And. B(2,7)==(0.,0.) .And. &
               B(4,7)==(0.,0.) .And. B(5,7)==(0.,0.)) Then

      X(1)=(B(3,7)*B(6,4)-B(6,7)*B(3,4))/(B(3,4)*B(6,1)-&
            B(6,4)*B(3,1))
      X(2)=(0._8,0._8)
      X(3)=(0._8,0._8)
      X(4)=(B(6,7)*B(3,1)-B(3,7)*B(6,1))/(B(3,4)*B(6,1)-&
            B(6,4)*B(3,1))
      X(5)=(0._8,0._8)
      X(6)=(0._8,0._8)

   Else

      Do k=2,6
```

```
            Do i=k-1,6
               If (B(i,k-1)/=0._8) Then
                  Exit
               Else       !to avoid a '0' diagonal element
                  Do j=1,7
                     Do l=i,5
                        Btmp(j)=B(l,j)
                        B(l,j)=B(l+1,j)
                        B(l+1,j)=Btmp(j)
                     End Do
                  End Do
               End If
            End Do

            Do i=k,6
               C=B(i,k-1)/B(k-1,k-1)
               Do j=1,7
                  B(i,j)=B(i,j)-B(k-1,j)*C
               End Do
            End Do
         End Do

         X(6)=-B(6,7)/B(6,6)
         Do i=1,5
            D=-B(6-i,7)
            Do j=1,i
               D=D-B(6-i,7-j)*X(7-j)
            End Do
            X(6-i)=D/B(6-i,6-i)
         End Do
      End If

End Subroutine LinearSolution
```

```
!*************************************************************
!Name:         BndryCondition
!Description: By matching the boundary condition (of
!              horizontal displacement and normal stress)
!              between two general anisotropic media,this
!              subroutine calculates the 6 exact reflection
!              and transmission coefficients.
!              During the computation, another subroutine,
!              "LinearSolution", is called.
!Input:        Aij - elastic stiffness matrix of incident
!                    medium
!              Bij - elastic stiffness matrix of reflecting
!                    medium
!              Mi  - 7X3 two dimensional array of slowness
!                    vectors (inci. P, refl. P, FS, and SS,
!                    tran. P, FS, and SS.)
!              Pj  - 7X3 two dimensional array of
!                    polarization vectors (inci. P, refl. P,
!                    FS, and SS,  tran. P, FS, and SS.)
!Output:       Ri  - one dimensional array of 3 reflection
!                    and transmitted coefficients.
!                    1-3:  Refl. Coef. of P,F,S
!                    4-6:  Tran. Coef. of P,F,S
!*************************************************************

Subroutine BndryCondition(Aij,Bij,Mi,Pj,Ri)
Use math_util
Implicit None

   Real(8), Intent(IN), Dimension(3,3,3,3) :: Aij,Bij
   Complex(8), Intent(IN), Dimension(7,3) :: Mi
   Complex(8), Intent(IN), Dimension(7,3) :: Pj
   Complex(8), Intent(OUT), Dimension(6) :: Ri

   Complex(8), Dimension(6,7) :: Dij
   Integer :: i,j,k,l,m,n

   Do m=1,3
      Do n=1,7
         If(n>=4 .and. n<=6) Then
            Dij(m,n)=-Pj(n,m)
         Else
            Dij(m,n)=Pj(n,m)
         End If
      End Do
   End Do
```

```
    Do m=4,6
       Do n=1,7

          Dij(m,n)=0
          Do i=1,3
             Do k=1,3
                If (n<=3) Then                    ! refl P,F,S

                   Dij(m,n)=Dij(m,n)+Aij(m-3,3,k,i)*&
                            Mi(n,k)*Pj(n,i)

                Else If (n>3 .And. n<=6) Then ! tran P,F,S

                   Dij(m,n)=Dij(m,n)-Bij(m-3,3,k,i)*&
                            Mi(n,k)*Pj(n,i)

                Else If (n==7) Then          ! for inci. Wave

                   Dij(m,n)=Dij(m,n)+Aij(m-3,3,k,i)*&
                            Mi(n,k)*Pj(n,i)

                End If
             End Do
          End Do

       End Do
    End Do

    Call LinearSolution(Dij,Ri)

End Subroutine BndryCondition
```

Appendix V. FORTRAN 90 Subroutine for computing the elastic stiffness matrix of fractured medium and VTI overlying medium

```
!*****************************************************************
!Name:         MediaParameters
!Description: This subroutine determines the elastic
!              stiffness matrices of both the incident
!              medium (VTI) and the reflecting medium
!              (general anisotropy from multiple sets of
!              fractures). Values of medium parameters (like
!              velocity density, fracture porosity, etc)
!              are defined inside the subroutine. Calling
!              this subroutine will return the two stiffness
!              matrices without any input.
!              During the computation, three subroutines,
!              CrackCompliance, Linear6RealSlsn, and
!              Cij_Cijkl are called. Another subroutine,
!              Transformation_properties, can be called if
!              coordinate system rotation is needed.
!Output:       Ajk - 3X3X3X3 four dimensional array of
!                    elastic stiffness of incident medium
!              Bjk - 3X3X3X3 four dimensional array of
!                    elastic stiffness of reflecting medium
!*****************************************************************

Subroutine MediaParameters(Ajk,Bjk)
Implicit None

   Real(8), Intent(OUT), Dimension (3,3,3,3) :: Ajk,Bjk

   Real(8), Dimension (6,6) :: Ci,Cj,Sj
!   Cj: stiffness matrix; Sj: compliance matrix

   Real(8) :: PV1,SV1,epsln1,dlt1,gamma1,de1
!   incident medium parameters

   Real(8) :: PV2,SV2,epsln2,dlt2,gamma2,de2
!   reflecing medium background parameters

   Real(8) :: poro,Vpma,a,b,c
!   matrix parameters

  Real(8), Dimension (3,3,3,3) :: Ajkr, Bjkr
```

```
  Real(8), Dimension (3,3) :: V2H
  Logical :: Rotation
!  for coordinate  system rotation


!   parameters below are for fractured zone
   Integer :: K
!   k sets fracture

   Real(8), Allocatable, Dimension (:) :: cd,azi,dip
!   cd :  crack density
!   azi:  azimuthal angle
!   dip:  dip angle

   Real(8), Dimension (6,6) :: Sfk
!   6X6 compliance matrix for kth set of fracture

   Real(8), Dimension (6,6) :: Sb
!   6X6 compliance matrix for background medium

   Real(8), Dimension (6) :: Sbi,Cji
!   storing temp column vector of Sb and Cj

   Real(8), Dimension (6) :: UntI
!   column of unit matrix

   Real(8) :: c11,c33,c12,c13,c44,c66
   Real(8) :: d11,d33,d12,d13,d44,d66
   integer :: i,j,l


! Allocate space for crack set parameters
   K=2
   Allocate (cd(1:K))
   Allocate (azi(1:K))
   Allocate (dip(1:K))


! Define Thomsen (1986) parameters for incident medium
   PV1=2500._8                    ! in m/s
   SV1=1250._8
   de1=2600._8
   epsln1=0._8
   dlt1=0._8
   gamma1=0._8
```

```
! Define Thomsen (1986) parameters for transmitted medium
   Vpma=6530._8
   poro=0.1_8
   a=-0.05508_8
   b=1.01677_8
   c=-1.03049_8

   PV2=Vpma*(1._8-poro)                    ! in m/s
   SV2=(a*(PV2/1000._8)**2+b*(PV2/1000._8)+c)*1000._8
   de2=2.71_8*(1._8-poro)
   epsln2=0._8
   dlt2=0._8
   gamma2=0._8

   cd(1)=0.05_8
   azi(1)=0._8
   dip(1)=90._8
   cd(2)=0.05_8
   azi(2)=60._8
   dip(2)=90._8


! Compute stiffness components for incident medium
   c33=de1*PV1**2
   c11=(1+2*epsln1)*c33
   c44=de1*SV1**2
   c66=(1+2*gamma1)*c44
   c13=SQRT(2*dlt1*c33*(c33-c44)+(c33-c44)**2)-c44
   c12=c11-2*c66


! Compute stiffness components for transmitting medium
   d33=de2*PV2**2
   d11=(1+2*epsln2)*d33
   d44=de2*SV2**2
   d66=(1+2*gamma2)*d44
   d13=SQRT(2*dlt2*d33*(d33-d44)+(d33-d44)**2)-d44
   d12=d11-2*d66


!-------------------------------------------
!Calculate incident stiffness matrix

   Do i=1,6
      Do j=1,6
         If (i==j) Then
```

```
            If (i<=2) Then
               Ci(i,j)=c11/del
            Else If (i==3) Then
               Ci(i,j)=c33/del
            Else If (i>=4 .and. i<6) Then
               Ci(i,j)=c44/del
            Else
               Ci(i,j)=c66/del
            End If
         Else If (i/=j .and. i<=3 .and. j<=3) Then
            If (i==3 .or. j==3) Then
               Ci(i,j)=c13/del
            Else
               Ci(i,j)=c12/del
            End If
         Else
               Ci(i,j)=0._8
         End If
      End Do
   End Do


!-----------------------------------------------
!Calculate reflecting background stiffness matrix

   Do i=1,6
      Do j=1,6
         If (i==j) Then
            If (i<=2) Then
               Cj(i,j)=d11
            Else If (i==3) Then
               Cj(i,j)=d33
            Else If (i>=4 .and. i<6) Then
               Cj(i,j)=d44
            Else
               Cj(i,j)=d66
            End If
         Else If (i/=j .and. i<=3 .and. j<=3) Then
            If (i==3 .or. j==3) Then
               Cj(i,j)=d13
            Else
               Cj(i,j)=d12
            End If
         Else
               Cj(i,j)=0._8
      End If
    End Do
```

```
   End Do


!-----------------------------------------------------
!convert background stiffness matrix to compliance matrix

! Creat a unit vector
   Do i=1,6

      Do j=1,6
         If (j==i) Then
            UntI(j)=1._8
         Else
            UntI(j)=0._8
         End If
      End Do

! Find column of matrix
      Call Linear6RealSlsn(Cj,UntI,Sbi)

! Build column of compliance matrix for background
      Do j=1,6
         Sb(i,j)=Sbi(j)
      End Do

  End Do


!-----------------------------------------------------
!Compute the total compliance matrix of reflecting medium

   Sj=Sb
   Do i=1,K
      Call CrackCompliance(PV2,SV2,de2, cd(i),&
                     azi(i),dip(i),Sfk)
      Sj=Sj+Sfk
   End Do

!-----------------------------------------------
!convert the total compliance matrix back to total
!stiffness matrix

   Do i=1,6

      Do j=1,6
         If (j==i) Then
            UntI(j)=1._8
```

```
         Else
            UntI(j)=0._8
         End If
      End Do

      Call Linear6RealSlsn(Sj,UntI,Cji)

      Do j=1,6
         Cj(i,j)=Cji(j)/de2
      End Do

   End Do

!-------------------------------------------------
!Transform the 6X6 stiffness matrices into 3X3X3X3 Cijkl
!stiffness tensor

   Call Cij_Cijkl(Ci,Ajk)
   Call Cij_Cijkl(Cj,Bjk)

!-------------------------------------------------
! Make a coordinate system rotation if necessary

   Rotation = "F"
   If (Rotation=="T") Then
      V2H(1,1)=0._8
      V2H(1,2)=0._8
      V2H(1,3)=-1._8
      V2H(2,1)=0._8
      V2H(2,2)=1._8
      V2H(2,3)=0._8
      V2H(3,1)=1._8
      V2H(3,2)=0._8
      V2H(3,3)=0._8

      Call Transformation_properties (Ajk,V2H,Ajkr)
      Call Transformation_properties (Bjk,V2H,Bjkr)
      Ajk=Ajkr
      Bjk=Bjkr
      End If

End Subroutine MediaParameters
```

```
!*************************************************************
!Name:         ij_m
!Description: This subroutine transfers the subscripts (ij,
!              or kl) of 3X3X3X3 elastic tensor
!              Cijkl into the subscripts (m) or (n) of the
!              6X6 matrix form.
!Input:        i - the first or third subscribe of Cijkl
!              j - the second or fourth subscribe of Cijkl
!Output:       m - ij's or kl's corresponding value of m or
!                  n in Cmn
!*************************************************************

Subroutine ij_m(ii,jj,mm)
Implicit None

   Integer, Intent(IN) :: ii,jj
   Integer, Intent(OUT) :: mm

   If (ii==1 .And. jj==1) Then
      mm=1
   Else If (ii==2 .And. jj==2) Then
      mm=2
   Else If (ii==3 .And. jj==3) Then
      mm=3
   Else If ((ii==2 .And. jj==3) .OR. &
                  (ii==3 .And. jj==2)) Then
      mm=4
   Else If ((ii==1 .And. jj==3) .OR. &
                  (ii==3 .And. jj==1)) Then
      mm=5
   Else If ((ii==1 .And. jj==2) .OR. &
                  (ii==2 .And. jj==1)) Then
      mm=6
   End If

End Subroutine ij_m
```

```
!*************************************************************
!Name:         CrackCompliance
!Description:  Given one set of fracture parameters, this
!              subroutine calculate the elastic compliance
!              matrix corresponding to the fracture set
!              according to Schoenberg and Sayers (1995)
!              model.
!Input:        Vp    - background P-wave velocity
!              Vs    - background S-wave velocity
!              dnsty - background density
!              crkde - crack density
!              azimu - azimuthal angle of fracture set
!              dipag - dip angle of fracture set (measured
!              from horizontal.
!Output:       Sk    - elastic compliance of the fracture
!                      set
!*************************************************************

Subroutine CrackCompliance(Vp,Vs,dnsty,&
                           crkde,azimu,dipag,Sk)
Implicit None

   Real(8), Intent(IN) :: Vp,Vs,dnsty,crkde,azimu,dipag
   Real(8), Intent(OUT), Dimension (6,6) :: Sk

   Real(8), Dimension (3) :: Ni
   Real(8), Dimension (3,3,3,3) :: Sij
   Real(8) :: g,pi,Zn,Zt,dtN,dtT,Mb,rb,lamda,mu
   Real(8) :: DTik,DTjk,DTil,DTjl
   Integer :: i,j,k,l,m,n

   pi=3.1415926_8
   Ni(1)=Sin(dipag*pi/180)*Cos(azimu*pi/180)
   Ni(2)=Sin(dipag*pi/180)*Sin(azimu*pi/180)
   Ni(3)=Cos(dipag*pi/180)

! Background elastic constants
   mu=dnsty*Vs**2
   lamda=dnsty*Vp**2-2*mu
   Mb=lamda+2*mu
   rb=lamda/Mb

   g=(Vs/Vp)**2
   dtN=4*crkde/(3*g*(1-g))
   dtT=16*crkde/(3*(3-2*g))
```

```
      Zn=dtN/(Mb*(1-dtN))
      Zt=dtT/(mu*(1-dtN))

      Do i=1,3
        Do j=1,3
          Do k=1,3
            Do l=1,3

              If (i==k) Then
                 DTik=1._8
              Else If (i/=k) Then
                 DTik=0._8
              End If

              If (j==k) Then
                 DTjk=1._8
              Else If (j/=k) Then
                 DTjk=0._8
              End If

              If (i==l) Then
                 DTil=1._8
              Else If (i/=l) Then
                 DTil=0._8
              End If

              If (j==l) Then
                 DTjl=1._8
              Else If (j/=l) Then
                 DTjl=0._8
              End If

              Sij(i,j,k,l)=(Zt/4)*(DTik*Ni(l)*Ni(j)+      &
                      DTjk*Ni(l)*Ni(i)+DTil*Ni(k)*Ni(j)+ &
                      DTjl*Ni(k)*Ni(i))+                  &
                      (Zn-Zt)*Ni(i)*Ni(j)*Ni(k)*Ni(l)

              Call ij_m(i,j,m)
              Call ij_m(k,l,n)
              Sk(m,n)=Sij(i,j,k,l)

            End Do
          End Do
        End Do
      End Do

End Subroutine CrackCompliance
```

```
!*************************************************************
!Name:         Linear6RealSlsn
!Description: This subroutine calculates the root of 6
!              linearized equations with six unknowns in the
!              following form:
!                Ai1X1+Ai2X2+Ai3X3+Ai4X4+Ai5X5+Ai6X6 = Yi
!                (i=1,2,...6)
!              The routine is used to find the inverse of
!              6X6 stiffness and compliance matrices.
!Input:        A - 6X6 matrix parameters
!              Y - one dimensional array of 6 values at the
!                  right side of the linearized equation
!Output:       X - one dimension array of 6 unknowns
!*************************************************************

Subroutine Linear6RealSlsn(A,Y,X)
Implicit None

   Real(8), Intent(IN), Dimension(6,6) :: A
   Real(8), Intent(IN), Dimension(6) :: Y
   Real(8), Intent(OUT), Dimension(6) :: X

   Real(8), Dimension(6,7) :: B
   Real(8), Dimension(7) :: Btmp
   Real(8) :: C, D
   Integer :: i,j,k,l

   Do i=1,6
      Do j=1,6
         B(i,j)=A(i,j)
      End Do
      B(i,7)=Y(i)
   End Do

   Do k=2,6
      Do i=k-1,6

         If (B(i,k-1)/=0._8) Then
            Exit

         Else      !to avoid a '0' diagonal element
            Do j=1,7
               Do l=i,5
                  Btmp(j)=B(l,j)
                  B(l,j)=B(l+1,j)
                  B(l+1,j)=Btmp(j)
```

```
            End Do
         End Do
      End If
   End Do

   Do i=k,6
      C=B(i,k-1)/B(k-1,k-1)
      Do j=1,7
         B(i,j)=B(i,j)-B(k-1,j)*C
      End Do
   End Do

End Do

X(6)=B(6,7)/B(6,6)
Do i=1,5

   D=B(6-i,7)
   Do j=1,i
      D=D-B(6-i,7-j)*X(7-j)
   End Do

   X(6-i)=D/B(6-i,6-i)

End Do

End Subroutine Linear6RealSlsn
```

```
!*************************************************************
!Name:         Cij_Cijkl
!Description: This subroutine transform a 6X6 Cij stiffness
!             matrix into a 3X3X3X3 Cijkl stiffness tensors
!Input:       Cij    - 6X6 two dimensional array of elastic
!                      stiffness
!Output:      Cijkl  - 3X3X3X3 four dimensional array of
!                      elastic stiffness
!*************************************************************

Subroutine Cij_Cijkl(C,AIJ)
Implicit None

   Real(8), Intent(IN), Dimension (6,6) :: C
   Real(8), Intent(OUT), Dimension (3,3,3,3) :: AIJ

      AIJ(1,1,1,1)=C(1,1)
      AIJ(1,1,1,2)=C(1,6)
      AIJ(1,1,1,3)=C(1,5)
      AIJ(1,1,2,1)=C(1,6)
      AIJ(1,1,2,2)=C(1,2)
      AIJ(1,1,2,3)=C(1,4)
      AIJ(1,1,3,1)=C(1,5)
      AIJ(1,1,3,2)=C(1,4)
      AIJ(1,1,3,3)=C(1,3)

      AIJ(1,2,1,1)=C(6,1)
      AIJ(1,2,1,2)=C(6,6)
      AIJ(1,2,1,3)=C(6,5)
      AIJ(1,2,2,1)=C(6,6)
      AIJ(1,2,2,2)=C(6,2)
      AIJ(1,2,2,3)=C(6,4)
      AIJ(1,2,3,1)=C(6,5)
      AIJ(1,2,3,2)=C(6,4)
      AIJ(1,2,3,3)=C(6,3)

      AIJ(1,3,1,1)=C(5,1)
      AIJ(1,3,1,2)=C(5,6)
      AIJ(1,3,1,3)=C(5,5)
      AIJ(1,3,2,1)=C(5,6)
      AIJ(1,3,2,2)=C(5,2)
      AIJ(1,3,2,3)=C(5,4)
      AIJ(1,3,3,1)=C(5,5)
      AIJ(1,3,3,2)=C(5,4)
      AIJ(1,3,3,3)=C(5,3)
```

```
AIJ(2,1,1,1)=C(6,1)
AIJ(2,1,1,2)=C(6,6)
AIJ(2,1,1,3)=C(6,5)
AIJ(2,1,2,1)=C(6,6)
AIJ(2,1,2,2)=C(6,2)
AIJ(2,1,2,3)=C(6,4)
AIJ(2,1,3,1)=C(6,5)
AIJ(2,1,3,2)=C(6,4)
AIJ(2,1,3,3)=C(6,3)

AIJ(2,2,1,1)=C(2,1)
AIJ(2,2,1,2)=C(2,6)
AIJ(2,2,1,3)=C(2,5)
AIJ(2,2,2,1)=C(2,6)
AIJ(2,2,2,2)=C(2,2)
AIJ(2,2,2,3)=C(2,4)
AIJ(2,2,3,1)=C(2,5)
AIJ(2,2,3,2)=C(2,4)
AIJ(2,2,3,3)=C(2,3)

AIJ(2,3,1,1)=C(4,1)
AIJ(2,3,1,2)=C(4,6)
AIJ(2,3,1,3)=C(4,5)
AIJ(2,3,2,1)=C(4,6)
AIJ(2,3,2,2)=C(4,2)
AIJ(2,3,2,3)=C(4,4)
AIJ(2,3,3,1)=C(4,5)
AIJ(2,3,3,2)=C(4,4)
AIJ(2,3,3,3)=C(4,3)

AIJ(3,1,1,1)=C(5,1)
AIJ(3,1,1,2)=C(5,6)
AIJ(3,1,1,3)=C(5,5)
AIJ(3,1,2,1)=C(5,6)
AIJ(3,1,2,2)=C(5,2)
AIJ(3,1,2,3)=C(5,4)
AIJ(3,1,3,1)=C(5,5)
AIJ(3,1,3,2)=C(5,4)
AIJ(3,1,3,3)=C(5,3)

AIJ(3,2,1,1)=C(4,1)
AIJ(3,2,1,2)=C(4,6)
AIJ(3,2,1,3)=C(4,5)
AIJ(3,2,2,1)=C(4,6)
AIJ(3,2,2,2)=C(4,2)
AIJ(3,2,2,3)=C(4,4)
AIJ(3,2,3,1)=C(4,5)
```

```
      AIJ(3,2,3,2)=C(4,4)
      AIJ(3,2,3,3)=C(4,3)

      AIJ(3,3,1,1)=C(3,1)
      AIJ(3,3,1,2)=C(3,6)
      AIJ(3,3,1,3)=C(3,5)
      AIJ(3,3,2,1)=C(3,6)
      AIJ(3,3,2,2)=C(3,2)
      AIJ(3,3,2,3)=C(3,4)
      AIJ(3,3,3,1)=C(3,5)
      AIJ(3,3,3,2)=C(3,4)
      AIJ(3,3,3,3)=C(3,3)

End Subroutine Cij_Cijkl
```

```
!*************************************************************
!Name:         Transformation_properties
!Description:  This subroutine calculates the new elastic
!              stiffness matrix after a coordinate system
!              rotation
!Input:        C   - elastic stiffness matrix before system
!                    rotation
!              Aij - new coordinate rotation matrix
!Output:       Cp  - elastic stiffness matrix after system
!                    rotation
!*************************************************************

Subroutine Transformation_properties (C,Aij,Cp)
Implicit None

   Real(8), Intent(IN), Dimension (3,3,3,3) :: C
   Real(8), Intent(IN), Dimension (3,3) :: Aij
   Real(8), Intent(OUT), Dimension (3,3,3,3) :: Cp

   Integer :: m,n,o,p,i,j,k,l

   Do m=1,3
     Do n=1,3
       Do o=1,3
         Do p=1,3

           Cp(m,n,o,p)=0
           Do i=1,3
             Do j=1,3
               Do k=1,3
                 Do l=1,3

                   Cp(m,n,o,p)=Cp(m,n,o,p)+Aij(m,i)*&
                               Aij(n,j)*Aij(o,k)*Aij(p,l)*&
                               C(i,j,k,l)

                 End Do
               End Do
             End Do
           End Do

         End Do
       End Do
     End Do
   End Do

End Subroutine Transformation_properties
```